

1 **Transcriptional reprogramming of distinct peripheral sensory neuron subtypes**
2 **after axonal injury**

3
4 William Renthal^{1,2,5,7}, Ivan Tochitsky^{2,3,5}, Lite Yang^{1,2,3,6}, Yung-Chih Cheng^{3,6}, Emmy Li²,
5 Riki Kawaguchi⁴, Daniel H. Geschwind⁴, Clifford J. Woolf^{2,3}

6
7 ¹Department of Neurology, Brigham and Women's Hospital and Harvard Medical School,
8 60 Fenwood Rd. Boston, MA 02115

9 ²Department of Neurobiology, Harvard Medical School, 220 Longwood Ave. Boston, MA
10 02115

11 ³F.M. Kirby Neurobiology Center, Boston Children's Hospital, 3 Blackfan Cir. Boston, MA
12 02115

13 ⁴Program in Neurogenetics, Department of Neurology, David Geffen School of Medicine,
14 University of California, Los Angeles, Los Angeles, CA

15 ⁵co-first author

16 ⁶co-second author

17 ⁷Lead contact

18
19 Correspondence:

20 wrenthal@bwh.harvard.edu

21 clifford.woolf@childrens.harvard.edu

22

23

24 **Summary**

25 Primary somatosensory neurons are specialized to transmit specific types of sensory
26 information through differences in cell size, myelination, and the expression of distinct
27 receptors and ion channels, which together define their transcriptional and functional
28 identity. By transcriptionally profiling sensory ganglia at single-cell resolution, we find that
29 different somatosensory neuronal subtypes undergo a remarkably consistent and
30 dramatic transcriptional response to peripheral nerve injury that both promotes axonal
31 regeneration and suppresses cell identity. Successful axonal regeneration leads to a
32 restoration of neuronal cell identity and the deactivation of the growth program. This
33 injury-induced transcriptional reprogramming requires *Atf3*, a transcription factor which is
34 induced rapidly after injury and is necessary for axonal regeneration and functional
35 recovery. While *Atf3* and other injury-induced transcription factors are known for their role
36 in reprogramming cell fate, their function in mature neurons is likely to facilitate major
37 adaptive changes in cell function in response to damaging environmental stimuli.

38

39 **Keywords**

40 Nerve injury, regeneration, sensory neuron, single cell RNA-seq, gene expression,
41 dorsal root ganglion, reprogramming, cell identity, axon growth, *Atf3*

42

43

44

45

46

47 **Introduction**

48 Injury to peripheral axons of primary sensory neurons whose cell bodies reside in
49 dorsal root ganglia (DRG) leads to the induction of cell-intrinsic transcriptional programs
50 critical both for initiating axon growth and driving the pathological neuronal
51 hyperexcitability that underlies neuropathic pain (Chandran et al., 2016; Costigan et al.,
52 2002; He and Jin, 2016; Mahar and Cavalli, 2018; Scheib and Höke, 2013; Serra et al.,
53 2012; Tuszynski and Steward, 2012). Axon regeneration involves both the regrowth of
54 the injured axon and the correct reinnervation of its target, but this process is often
55 incomplete and can lead both to a loss of sensation and disabling chronic painful
56 neuropathies, such as phantom limb pain, diabetic neuropathy or chemotherapy-induced
57 neuropathy (Chapman and Vierck, 2017; Collins et al., 2018; Xie et al., 2017). The
58 molecular changes provoked by peripheral axonal injury have been the focus of intense
59 study (Chandran et al., 2016; Costigan et al., 2002; He and Jin, 2016; Mahar and Cavalli,
60 2018; Scheib and Höke, 2013; Serra et al., 2012; Tuszynski and Steward, 2012) since
61 the identification of the molecular drivers of regeneration has the potential to promote the
62 regeneration of injured central nervous system neurons, which, unlike neurons with axons
63 in the PNS, lack an intrinsic regeneration capacity (He and Jin, 2016; Mahar and Cavalli,
64 2018; Tuszynski and Steward, 2012). Additionally, a better understanding of the
65 mechanisms by which neuronal hyperexcitability develops after axonal injury may reveal
66 novel targets for analgesic development.

67 Previous molecular studies using bulk DRG tissue have identified transcriptional
68 networks regulated in the DRG in response to injury (Abe and Cavalli, 2008; Chandran et
69 al., 2016; Costigan et al., 2002; LaCroix-Fralish et al., 2011; Michaelievski et al., 2010;

70 Perkins et al., 2014; Xiao et al., 2002). However, the extensive cellular heterogeneity of
71 DRG cell types (Usoskin et al., 2015; Zeisel et al., 2018; Zheng et al., 2019) has made it
72 difficult to establish in which cell types these changes occur and whether these changes
73 are uniform or distinct across different neuronal subtypes. This challenge is underscored
74 by the fact that non-neuronal cells, including satellite glia, Schwann cells, dural cells and
75 endothelial cells, are collectively more abundant than sensory neurons in the DRG.
76 Moreover, peripheral sensory neurons themselves vary dramatically in size, conduction
77 velocity, gene expression patterns and the sensory transduction receptors present on
78 nerve terminals (Gatto et al., 2019; Le Pichon and Chesler, 2014; Usoskin et al., 2015;
79 Zeisel et al., 2018). In addition to the cellular heterogeneity within the DRG, in most nerve
80 injury models, only a fraction of DRG neurons are injured and bulk analyses cannot
81 differentiate between changes in injured or non-injured neurons (Berta et al., 2017;
82 Gosselin et al., 2010; Jessen and Mirsky, 2016; Laedermann et al., 2014; Rigaud et al.,
83 2008).

84 High-throughput single-nucleus genomics enables the characterization of axonal
85 injury response programs within distinct cell types of the DRG, without use of cell
86 dissociation procedures that themselves induce injury-like/immediate early gene
87 responses (Chiu et al., 2014; Frey et al., 2015; Lindwall et al., 2004; Nguyen et al., 2019).
88 Using droplet-based single-nucleus RNA sequencing (snRNA-seq) we mapped the
89 transcriptomes of 107,541 individual mouse DRG cells across a range of nerve injury
90 models. Remarkably, we find that axonal injury induces a common transcriptional
91 program across all neuronal subtypes that largely replaces the expression of their
92 subtype-specific genes. Non-neuronal cells exhibit a much smaller, distinct,

93 transcriptional response to injury. The response of sensory neurons to injury involves the
94 rapid induction of many of the transcription factors associated with reprogramming
95 fibroblasts into either pluripotent stem cells or differentiated cell types (Brouwer et al.,
96 2016), raising the possibility that neurons may invoke an analogous intrinsic
97 transcriptional reprogramming for generating their response to axonal injury. We further
98 demonstrate that *Atf3*, an axonal injury-induced transcription factor (Hunt et al., 2012;
99 Parsadanian et al., 2006; Tsujino et al., 2000) also implicated in cellular reprogramming
100 (Duan et al., 2019; Ronquist et al., 2017), is necessary for axotomy-induced neuronal
101 transcriptional reprogramming and for axonal regeneration and sensory recovery after
102 injury. Finally, we present a web-based resource for exploring changes in gene
103 expression across DRG cell types (www.painseq.com) to aid fundamental studies of
104 sensory neuron biology and development of novel therapeutics for pain and regeneration.

105

106 **Results**

107 **Single-nucleus RNA-seq of naive and injured DRG cell types**

108 To characterize transcriptional responses induced by peripheral axonal injury, we
109 performed snRNA-seq on lumbar DRGs from adult naive mice and compared their
110 transcriptional profiles to DRGs from mice after spinal nerve transection (SpNT) (the
111 segmental nerve that emerges directly from each DRG), sciatic nerve transection (ScNT)
112 or sciatic nerve crush (crush), over multiple time points, ranging from hours to months
113 after injury (Figure 1A). Full axonal regeneration with target reinnervation and functional
114 recovery is only observed in the sciatic crush model (Navarro et al., 1994). To determine
115 whether nerve injury response is distinct from other pain-producing insults, we also

116 characterized gene expression changes in lumbar DRGs from two models that do not
117 involve physical axotomy: a model of acute (1 week) chemotherapy-induced allodynia
118 (4mg/kg paclitaxel) (Velasco and Bruna, 2015) and a model of peripheral inflammation,
119 hindpaw injection of Complete Freund's Adjuvant (CFA, 20 μ L, 2 days) (Jaggi et al.,
120 2011).

121 In total, we obtained 107,541 DRG nuclei that passed quality control (see
122 methods). Sequenced nuclei had an average of 2,918 transcripts per nucleus
123 representing 1,478 unique genes per nucleus (Figure S1A). For the purposes of cell type
124 identification, DRG nuclei from naive and all experimental injury conditions were initially
125 clustered together based on their gene expression patterns. Dimensionality reduction
126 (uniform manifold approximation and projection [UMAP]) revealed 16 distinct groups of
127 cells. Nuclei in clusters expressing high levels of *Rbfox3*, which encodes the pan-neuronal
128 marker NeuN (Kim et al., 2009), were classified as neurons, and clusters expressing high
129 levels of known non-neuronal marker genes, such as *Sparc*, were classified as non-
130 neuronal nuclei (Figure S1B-C). We re-clustered neuronal and non-neuronal nuclei
131 separately to better visualize their distinct subtypes and used this separate visualization
132 in all subsequent analyses.

133 Focusing initially on naive DRG nuclei, the neuronal subtypes we observed include
134 *Tac1*⁺ peptidergic nociceptors (PEP), *Mrgprd*⁺ non-peptidergic nociceptors (NP), *Sst*⁺
135 pruriceptors, *Fam19a4*⁺/*Th*⁺ low threshold mechano-receptive neurons with C-fibers
136 (cLTMR), *Nefh*⁺ A fibers including A-LTMRs and proprioceptors (NF), (Figures 1B, S1C).
137 Non-neuronal cells include *Apoe*⁺ satellite glia, *Mpz*⁺ Schwann cells and *Cldn5*⁺
138 endothelial cells (Figures 1C, S1C-D). The distinct neuronal and non-neuronal subtypes

139 we identified in DRGs from naive animals were also observed in all injury models and are
140 similar to those previously reported (Figure S1C-D) (Usoskin et al., 2015; Zeisel et al.,
141 2018; Zheng et al., 2019). We also observed a neuronal cluster that expresses *Fam19a4*,
142 but very low levels of *Th*, which we termed putative-cLTMR2 (p_cLTMR2). A subset of
143 the cell type selective marker genes (Figures S1E-G), including those of p_cLTMR2
144 (Figure S1H), were studied by *in situ* hybridization and found largely to label distinct, non-
145 overlapping cell populations (Usoskin et al., 2015; Zeisel et al., 2018; Zheng et al., 2019).

146 In addition to the cell-type-specific gene expression patterns of known marker
147 genes, we also observed distinct expression patterns of ion channels, G-protein coupled
148 receptors (GPCRs), neuropeptides, and transcription factors (Figure S2A, Table S1, see
149 methods). For example, we observed that PEP1 and PEP2 neurons express the ion
150 channels *Trpv1* and *Atp2b4* and the GPCRs *Sstr2* (PEP1 only) and *Gpr26* (PEP2 only),
151 as well as multiple neuropeptides including *Tac1*, *Adcyap1*, and *Calca* (PEP1 only),
152 whereas NF1-3 neurons express the ion channels *Scn1b* and *Scn4b* and the GPCR
153 *Adgrg2* (NF2,3 only), highlighting the molecular and functional differences between
154 distinct subtypes of DRG neurons.

155

156 **Axonal injury induces a new transcriptional state in DRG neurons.**

157 To characterize the transcriptional programs activated in response to axonal injury,
158 we first compared DRG nuclei from naive mice to DRG nuclei from mice 6 hours (h), 12h,
159 1day (d), 1.5d, 2d, 3d and 7d after transection of the spinal nerves from the respective
160 ganglia, which results in the axotomy of >90% of DRG neurons in the affected ganglia
161 (Shortland et al., 2006; Tsujino et al., 2000). Strikingly, we observed that new neuronal

162 clusters emerge by 1d after SpNT, which are essentially absent in naive mice and which
163 contain neurons that express very high levels of known injury-induced genes such as
164 *Sprr1a* (Figure 1D). By 3 days after injury, few nuclei cluster with naive neurons,
165 consistent with an axotomy of most DRG neurons. New injury-induced clusters of nuclei
166 were not observed in non-neuronal cells (Figure S2B). To quantify the extent of injury
167 among all neurons after SpNT, we defined the new neuronal clusters that emerged after
168 the injury as an “injured state” if the cluster was comprised of greater than 95% SpNT
169 nuclei and had a median normalized expression of *Atf3* greater than 2 (Figures 1E-F,
170 S2C). *Atf3* is a major injury-induced gene in axon-damaged neurons (Hunt et al., 2012;
171 Parsadanian et al., 2006; Tsujino et al., 2000). All other clusters were classified as being
172 in a transcriptionally “naive state,” and were comprised primarily of nuclei from naive mice
173 (~93% of nuclei in these clusters were from naive mice) with a median *Atf3* expression of
174 0. “Injured state” neurons express higher levels of all canonical DRG axonal injury-
175 induced genes such as *Atf3*, *Sox11*, *Sprr1a*, *Flrt3* (Chandran et al., 2016; Costigan et al.,
176 2002; LaCroix-Fralish et al., 2011; Perkins et al., 2014; Xiao et al., 2002) than “naive
177 state” neurons (Figures 1E, 1G, two-tailed Student’s t-test, $P < 0.001$) and overlap with
178 injury gene modules previously identified from bulk microarray studies (Chandran et al.,
179 2016) (Figure S2D). It is notable that we still observe a small number of “naive state”
180 neurons in mice who underwent SpNT (Figure 1D), consistent with the 5-10% of neurons
181 not axotomized in this model. Several of the canonical injury-induced transcription factors
182 are expressed within hours after injury, well before the full emergence of the “injured
183 state,” raising the possibility that these transcription factors are involved in establishing
184 the later transcriptional transformation of the neurons after injury (Figure 1G).

185 To test the accuracy of our injured versus non-injured neuron classification, we
186 compared the percentage of neurons classified as injured in SpNT, a proximal injury
187 model that causes axotomy of >90% of DRG neurons in the affected DRG (Shortland et
188 al., 2006; Tsujino et al., 2000) and in ScNT, a more distal injury model that results in
189 axotomy of ~50% of the affected DRGs (Laedermann et al., 2014; Rigaud et al., 2008).
190 Three days after axotomy, the injury classification identified 93.8% of neurons sequenced
191 as “injured” after SpNT and 53.3% after ScNT (Figure 1H, S2E). Therefore, there is good
192 agreement between the detection of axotomized neurons from the snRNA-seq analyses
193 and those measured by *in vivo* anatomical labeling/tracing (Rigaud et al., 2008; Shortland
194 et al., 2006). Interestingly, a few DRG neuronal nuclei from naive mice (mean 0.34%)
195 were classified as being in an “injured state,” which may be explained by neurons injured
196 from occult fight wounds that often occur in group-housed mice, and is consistent with the
197 rare detection by *in situ* hybridization of *Atf3*⁺ neurons in naive mice (see Figure 2).

198

199 **Classification of neuronal subtypes after axotomy**

200 A primary goal of this study was to determine whether the intrinsic axonal injury
201 transcriptional program differs between the distinct sensory neuronal subtypes and if
202 these differences could inform differential phenotypes after injury. Efforts to address this
203 question are complicated by the downregulation of the neuronal subtype-specific marker
204 genes that classify neuronal subtypes that begins less than a day after axotomy (Figure
205 2A). Three to seven days after injury, expression of the marker genes used to classify
206 neuronal subtypes was reduced by 65-97% compared to levels in naive DRGs, with a
207 more pronounced downregulation of small diameter neuron marker genes (*e.g.* *Tac1*,

208 *Mrgprd*) than those in large diameter neurons (e.g. *Nefh*, *Hapln4*) (Figure 2B). *In situ*
209 hybridization for several neuronal subtype marker genes, including *Th*, *Tac1*, *Mrgprd*,
210 *Hapln4*, *Sst* (Figures 2C-G) confirmed the significantly reduced marker gene expression.
211 The coupling of marker gene downregulation with the profound changes in cluster identity
212 after injury makes it difficult to classify injured neuronal subtypes, even if injury-induced
213 genes are omitted when clustering (Figure S3A). To overcome this, we used multiple
214 consecutive timepoints after SpNT to capture the transition between “naive” and “injured”
215 states for each neuronal subtype. When neighboring time points after injury were co-
216 clustered, residual cell-type-specific transcriptional signatures in injured nuclei led them
217 to co-cluster with nuclei classified prior to marker gene downregulation. The defined
218 subtypes were then projected onto the “unknown” injured nuclei with which they co-
219 clustered (Figures 3A-B, S3B) (see methods). As a complementary informatic approach
220 for classifying injured neuronal subtypes, we used a vector of injury-induced genes as a
221 measurement of injury progression (see methods), and removed the variation in each
222 gene that can be explained by the injury signal prior to clustering. Cell type assignments
223 from the two approaches had 99% concordance for naive cell types and 91% for injured
224 cell types (Figure S3C). To test the accuracy of the bioinformatic classification of neuronal
225 subtypes after injury we performed lineage tracing of non-peptidergic (*Mrgprd*+)
226 nociceptors after injury using *Mrgprd-Cre^{ERT2};Gcamp6f* reporter mice. SnRNA-seq of
227 DRGs from injured and naive reporter mice identified reporter-positive nuclei in the same
228 clusters as those classified informatically by pair-wise clustering and projection (estimated
229 error = 2.93% in “injured state” nuclei and 1.88% in “naive state” nuclei, Figure S3D). The
230 ability to classify neuronal subtypes at each time point after axonal injury (Figures 3B,

231 S3E) provides an opportunity to characterize cell-type-specific molecular adaptations to
232 axonal injury.

233

234 **Characterization of cell-type-specific transcriptional responses to injury reveals a**
235 **common program**

236 After classifying the neuronal subtypes of axotomized neurons following SpNT, we
237 performed differential gene expression analyses (defined as $FDR < 0.01$ and $\log_2FC > |1|$)
238 for each cell type and time point. For all DRG cell types except p_cLTMR2, the total
239 number of genes significantly regulated by axotomy increased over time until 3 to 7 days
240 after injury (Figure 4A), an effect that is observed when keeping the number of nuclei or
241 UMI constant over time (Figure S4A). However, the rate of gene induction after injury
242 varied across cell types (Figures 4A, S4B, Table S2). Small diameter neurons (e.g. NP
243 and PEP) induce more genes at earlier time points than large diameter neurons (e.g.
244 *Nefh*⁺ A-LTMRs) (Figures 4A, S4B), while Schwann cells induce very few genes after
245 injury. The genes upregulated in each neuronal subtype in response to injury significantly
246 overlap with those induced by injury in other neuronal subtypes, indicating a largely
247 common neuronal response to injury (Figures 4B, S4C). Indeed, between 74-94% of
248 genes induced in neuronal subtypes after injury are induced across multiple neuronal
249 subtypes (Figure 4C). The genes that are upregulated in response to injury in p_cLTMR2
250 or glial subtypes are notably distinct from those that are commonly upregulated in the
251 other neuronal subtypes (Figures 4B, S4C).

252 The common gene program induced after neuronal axotomy is enriched for genes
253 involved in axon guidance, axonogenesis and regulation of cell migration (Figure S4D),

254 and significantly overlaps ($p = 8 \times 10^{-33}$, hypergeometric test) with the injury-induced
255 magenta gene module identified from a gene co-expression network analysis of bulk DRG
256 microarray data (Chandran et al., 2016). This common neuronal transcriptional program
257 includes genes previously identified in studies of axonal injury from bulk DRG tissue, such
258 as *Atf3*, *Gal*, *Jun*, *Npy*, *Sox11* and *Sprr1a* (Figure 4D, Table S3) (Chandran et al., 2016;
259 Costigan et al., 2002; LaCroix-Fralish et al., 2011; Perkins et al., 2014; Xiao et al., 2002).
260 In addition to the common neuronal regeneration-associated program, there were also
261 common changes in the expression of genes that impact neuronal excitability in all
262 neuronal subtypes, including downregulation of multiple potassium channels and
263 upregulation of the calcium channel, *Cacna2d1* (Figure S4E). These ion channel gene
264 expression changes may contribute to the ectopic activity observed in injured neurons
265 after axotomy (Liu et al., 2000; Patel et al., 2018; Serra et al., 2012; Tsantoulas and
266 McMahon, 2014).

267 Single-nucleus profiling provides an opportunity to quantify the fraction of neurons
268 within a DRG that induce the common transcriptional response to injury. We found that
269 ~50% percent of the neurons in each neuronal subtype show induction of the common
270 injury gene program within hours after SpNT and this population increases to >90% 3-7
271 days after injury (Figure 4E), closely approximating the fraction of neurons physically
272 axotomized in this model.

273 We also identified a smaller population of genes selectively induced only in specific
274 neuronal subtypes after injury (Figures 4C-D, Table S4-5). These include genes involved
275 in chloride homeostasis, cGMP signaling and integrin signaling pathways, some of which
276 may contribute to cell-type-specific forms of axonal regeneration. For example, cLTMR1

277 neurons selectively induce *Serpinf1*, which has a pro-regenerative function in DRG
278 neurons (Stevens et al., 2019) and NP neurons selectively induce *Vat1*, which also
279 enhances DRG axon growth (Jia et al., 2018). Other cell-type-specific gene alterations
280 may contribute to the neuropathic pain phenotype, as NF1 neurons selectively induce
281 *Wipi2*, which is involved in autophagy in DRG neurons (Stavoe et al., 2019), a process
282 argued to reduce the pain associated with sciatic nerve injury (Chen et al., 2018). PEP1
283 neurons selectively induce *Ano1*, which promotes pain hypersensitivity (Lee et al., 2014).
284 These cell-type-specific gene expression changes in response to injury may also
285 contribute to differences in axonal regeneration and/or excitability between distinct cell
286 types.

287 Axonal regeneration and neuropathic pain appear to involve the participation of
288 non-neuronal cells, such as the satellite glia which surround the somata of DRG neurons
289 and the Schwann cells found around DRG axons (Gosselin et al., 2010; Jessen and
290 Mirsky, 2016; Ji et al., 2016), but it has been difficult to isolate these cells and analyze
291 their injury-induced gene expression changes (Jager et al., 2018). We find that while
292 satellite glia induce a large number of genes in response to axonal injury, Schwann cells
293 induce comparatively few genes (Figures 4A, 4D, Table S5). Several neuronal
294 regeneration-associated genes, including *Atf3* and *Sox11*, are upregulated after axotomy
295 in satellite glia and Schwann cells, but the induction is smaller in magnitude and more
296 transient compared to neurons. A number of genes are selectively induced in glia but not
297 in axotomized neurons. Satellite glia specifically induce tenascin C (*Tnc*) and fibronectin
298 1 (*Fn1*), both major components of the extracellular matrix, raising questions about the
299 functional consequences of a potential change in the extracellular matrix in the immediate

300 vicinity of neuronal cell bodies and their axons. Schwann cells uniquely induce
301 complement C1q-like protein 3 (*C1ql3*) and *Tmem130*, a poorly characterized gene,
302 although again the consequences of these changes require further study.

303 While many of the genes induced in sensory neurons after injury may promote
304 regeneration-associated regrowth, the reprogramming of the injured neurons'
305 transcriptome extends beyond regeneration-associated genes and includes the
306 downregulation of genes that define the identity and functional specialization of the
307 neuron (Figure S4B).

308

309 **Profound transcriptional reprogramming after axotomy**

310 To determine how cell-type-specific genes are regulated after axonal injury, we
311 first compared gene expression in each neuronal cell type to that of all other neuronal
312 subtypes to identify the cell-type-specific genes that are preferentially expressed in
313 specific DRG cell types (FDR<0.01, log₂FC>1, Table S6). More than 73% of the “cell-
314 type-specific genes” in each DRG neuronal subtype were downregulated after axotomy
315 (Figure 4F) and this downregulation occurred over the same time frame as the induction
316 of the common neuronal injury genes (Figure 4G). By contrast, cell-type-specific markers
317 in satellite glia, and Schwann cells were less affected by injury (Figure 4G). To determine
318 whether the downregulation of cell-type-specific genes in neurons was specific to these
319 genes or more broadly observed across the transcriptome, we compared the expression
320 of cell-type-specific genes after injury to a set of randomly selected, expression-matched
321 genes. We found that cell-type-specific genes were significantly more downregulated
322 after injury than a set of randomly selected expression-matched genes in each neuronal

323 subtype, except p_cLTMR2 (Figure S4F), indicating that there is a preferential
324 downregulation of cell-type-specific genes in neurons after injury rather than a global
325 redirection of transcriptional activators from all genes to injury response genes or a
326 computational artifact of normalization. To quantify the extent of transcriptional
327 reprogramming within each neuron, we generated scores using the average counts of
328 common injury genes (injury score) or cell-type-specific genes (cell-type-specificity
329 score). Projecting these scores onto each neuron in the UMAP plot accurately labeled the
330 neurons as injured, with high injury scores and low cell-type-specificity scores (Figure
331 4H).

332

333 **Time course of injury-induced transcriptional reprogramming**

334 To investigate the kinetics of injury-induced transcriptional reprogramming from
335 initial injury through complete axonal regeneration, we turned to the sciatic nerve crush
336 model in which full axonal regeneration, target reinnervation, and functional recovery
337 occur within weeks to months after injury (Navarro et al., 1994; Vogelaar et al., 2004).

338 Similar to SpNT and ScNT, nuclei from mice who underwent sciatic crush injury
339 began to adopt a transcriptional profile consistent with nerve injury within a day after
340 sciatic crush, with injured nuclei displaying maximal injury scores and minimal cell-type-
341 specificity scores 3-7 days after injury (Figure 5A). Similar injury-induced transcriptional
342 changes were observed in both male and female DRG neurons after sciatic crush (Figure
343 S5A). Between 2 weeks and 3 months following sciatic crush injury, the injured clusters
344 of neurons gradually disappear (Figures 5A-B) in parallel with functional recovery (Figure
345 S5B).

346 The reduction in the number of “injured state” neurons 2-3 months after crush injury
347 could be explained either by the reversal of their transcriptional reprogramming due to
348 successful regeneration, or by the selective cell death of this neuronal population, both of
349 which have been suggested as possibilities in the literature (Hart et al., 2002; Kataoka et
350 al., 2007; Tandrup et al., 2000). To test the latter possibility, we generated an injury
351 reporter mouse (*Atf3-Cre^{ERT2};Gcamp6f*) in which *Atf3* induction drives Cre-dependent
352 expression of the *Gcamp6f* reporter gene (Figure S5C). This reporter efficiently marks
353 injured *Atf3*+ DRG neurons 1 week after sciatic crush injury (Figure S5D-F). The
354 percentage of reporter positive neurons was unchanged from 1 week to two months after
355 crush, when the injury program has disappeared (Figures 5C-F), indicating that injured
356 neurons do not die but rather return to their naive transcriptional profiles. This result is
357 consistent with previous studies which reported minimal to no DRG neuron death after
358 sciatic crush in rodents (Swett et al., 1995). Therefore, injury-induced transcriptional
359 reprogramming reverses if axonal regeneration and reinnervation is complete.

360 Because sciatic crush, like ScNT, only results in the physical injury of ~50% of L3-
361 5 DRG axons (Chang and Namgung, 2013), there is a mixture of neurons with injured or
362 uninjured axons in these ganglia. This can be observed both in the UMAP plots 3 and 7
363 days after sciatic crush (Figure 5A) as well as in the percentage of nuclei within clusters
364 classified as injured (Figure 5B). To identify whether injury-induced gene expression also
365 occurs in unaxotomized neurons, we performed differential expression analysis between
366 neurons classified as uninjured in animals who underwent sciatic crush and the same cell
367 type in naive animals. We found a transient induction of some common injury-induced
368 genes in uninjured neurons after sciatic crush, but the magnitude of these changes was

369 very small in comparison to injured neurons from the same mice (Figures S5G-H). The
370 transient induction of common injury response genes like *Atf3* or *Nts* could be due to
371 surgical injury-induced inflammation and stress, or paracrine signaling between injured
372 and non-injured neurons (Berta et al., 2017; Fukuoka et al., 2012).

373 Cell-type-specific marker genes were downregulated in injured neurons after
374 sciatic crush (Figures 5A, S5I-N), but we could assign neuronal subtypes to all nuclei,
375 including those injured by crush or ScNT, because they co-clustered with the classified
376 SpNT injured neuronal subtypes (Figure S6A). Differential gene expression analysis
377 comparing injured neuronal subtypes after sciatic crush or ScNT at each time point after
378 injury with their respective naive subtypes, revealed a peak of gene induction 3-7 days
379 after injury, similar to that observed for SpNT (Figure 5G). Moreover, there is significant
380 overlap between the genes induced in a given cell type across all the axotomy models
381 (Figure 5H, Figure S6B-C), indicating that a common transcriptional program is induced
382 by axotomy in most peripheral sensory neuron subtypes regardless of injury location
383 (proximal or distal) or the fraction of injured DRG neurons. It should be noted that the
384 small number of gene expression changes in crush and ScNT compared to SpNT was
385 primarily a consequence of the smaller number of axotomized neurons in the distal injury
386 models than SpNT. The extent and composition of the gene expression changes were
387 quite similar across the distal and proximal axotomy models when specifically comparing
388 neurons in the “injured state” with their naive controls (Figure S6D).

389

390 **Inflammatory and chemotherapy-induced transcriptional changes**

391 The high correlation between the transcriptional programs induced by three
392 different physical axotomy models led us to test whether the same reprogramming is
393 engaged in a model of acute painful peripheral neuropathy caused by paclitaxel treatment
394 and an inflammatory pain model produced by intraplantar injection of Complete Freund's
395 Adjuvant (CFA). Paclitaxel treatment causes mechanical allodynia 1 week after treatment
396 (Figure S6E) and causes peripheral neuropathy by 4 weeks after treatment (Toma et al.,
397 2017; Velasco and Bruna, 2015), while injection of CFA into the hindpaw leads to
398 inflammation and mechanical allodynia within 24 hours after treatment (Figure S6F)
399 (Ghasemlou et al., 2015; Jaggi et al., 2011). SnRNAseq was performed on L3-5 DRGs
400 from mice treated with paclitaxel or CFA and compared with naive and axotomized mice.
401 Over 99% of neurons from paclitaxel-treated mice and CFA-treated mice clustered
402 together with naive nuclei (Figure 5I). Cell-type-specific differential expression analysis
403 between paclitaxel- or CFA-treated and naive-treated mice displayed few statistically
404 significant genes (Figure 5G, S6G) and those which were significantly regulated had little
405 overlap with axotomy models (Figure 5H, I). The presence of pain is thus independent of
406 injury-induced transcriptional reprogramming in DRG neurons.

407

408 **Transcriptional mechanisms underlying injury-induced transcriptional** 409 **reprogramming of sensory neurons**

410 Transcription factors that mediate the injury-induced transcriptional
411 reprogramming must be induced very rapidly (≤ 1 day) after injury and have consensus
412 DNA binding sites enriched in the set of genes that are induced several days after injury
413 when the injury score plateaus (Figure 6A). Within hours of injury, we identified 24

414 transcription factors commonly upregulated after SpNT across neuronal subtypes and
415 whose target gene regulation is enriched in DRG nuclei (Figure 6B, see methods). Over
416 half of these 24 transcription factors have been previously detected after axonal injury
417 (e.g. *Atf3*, *Jun*, *Jund*) (Chandran et al., 2016; Herdegen et al., 1992; Mahar and Cavalli,
418 2018; Patodia and Raivich, 2012; Tsujino et al., 2000). After identifying transcription factor
419 binding motifs that are significantly enriched compared to all motifs in the set of
420 commonly-induced injury genes, we ranked each early injury-induced transcription factor
421 by the number of these enriched motifs they bind. We observed that the activating protein
422 1 (AP-1) family members such *Jun*, *Jund*, and *Fosl2* as well as *Atf3* were associated with
423 the highest number of enriched motifs, an effect that was not observed for motifs identified
424 in random sets of genes (Figure 6C, permutation test, $P < 0.001$). We chose to focus on
425 *Atf3* because it is the transcription factor most strongly upregulated within hours after
426 injury across neuronal subtypes whose consensus binding motifs are also enriched in the
427 common set of genes that are upregulated after injury compared to naive neurons.
428 Indeed, there is a strong and significant correlation between the level of *Atf3* mRNA and
429 its predicted activity on its target genes in individual neurons (Figures 6D, S7A, Pearson's
430 $r = 0.48$, permutation test, $P < 0.001$), indicating that *Atf3* is likely to play an important role
431 in injury-induced transcriptional reprogramming.

432 While many of the injury-induced transcription factors are known to have both
433 transcriptional activating and repressing roles (Aguilera et al., 2011; Renthal et al., 2008),
434 the absence of their motif enrichment in the set of cell-type-specific genes compared to
435 random sets of genes (Figure 6E) suggests alternative mechanisms are likely to
436 contribute to the downregulation of cell-type-specific genes after injury (see Discussion).

437 To determine if *Atf3* in sensory neurons is necessary for injury-induced
438 transcriptional reprogramming and sensory neuronal regeneration after injury, we
439 generated a floxed *Atf3* mouse and crossed it with *Vglut2-Cre* mice (Figures 7A), resulting
440 in a conditional knockout (cKO) of *Atf3* from >95% of sensory neurons (*Atf3* WT: 89 ± 1%
441 of DRG neurons 1 week after SpNT are ATF3+ Nissl+; *Atf3* cKO: 4 ± 2% of DRG neurons
442 1 week after SpNT are ATF3+ Nissl+; n=4 DRG sections, p<0.001, two-tailed Student's
443 t-test) (Figure 7B). Consistent with a role for *Atf3* in axonal regeneration (Gey et al., 2016;
444 Jing et al., 2012; Seijffers et al., 2006), the deletion of *Atf3* in sensory neurons resulted in
445 a significant delay in functional sensory recovery after sciatic crush injury (Figure 7C), an
446 effect that we also observed using a tamoxifen-inducible cKO approach in the adult
447 mouse (Figures S7B-C).

448 To determine if *Atf3* is required for injury-induced transcriptional reprogramming,
449 we performed snRNA-seq on *Atf3^{fl/fl}* (WT) and *Vglut2-Cre;Atf3^{fl/fl}* cKO DRGs that are
450 either naive or 7 days after sciatic nerve crush. We clustered WT and *Atf3* cKO neuronal
451 nuclei together and found that the naive neuronal subtypes from these mice cluster
452 together and express the same subtype-specific marker genes (Figures 7D-E, S7D),
453 indicating a high degree of transcriptional similarity between naive WT and *Atf3* cKO DRG
454 neurons. To compare transcriptional responses between WT and *Atf3* cKO after sciatic
455 crush, we first identified the clusters of neurons from these mice that have high common
456 injury scores and exhibit the “injured” transcriptional state (Figures 7D, S7E). Consistent
457 with a central role of *Atf3* in driving injury-induced transcriptional reprogramming, we
458 observed significantly fewer *Atf3* cKO DRG neurons in the “injured” transcriptional state
459 7 days after sciatic nerve crush than WT neurons (Figures 7E-G), an effect that is not

460 explained by neuronal cell loss (Figure S7F). The attenuation of injury-induced
461 transcriptional reprogramming in *Atf3* cKO DRG neurons is associated with significantly
462 less putative *Atf3* target gene induction than is observed in WT neurons after injury
463 (Figures 7H, S7G). Moreover, the clusters of “injured state” *Atf3* cKO neurons express
464 most common injury genes at significantly lower levels than “injured state” WT neurons
465 (e.g. *Sprr1a*, *Gal*, *Gap43*) (Figures 7I-J), which likely contributes to the axonal
466 regeneration deficit in these mice (Schmid et al., 2014; Woolf et al., 1990). Together,
467 these findings implicate *Atf3*, and possibly other transcription factors that are induced
468 rapidly after injury, in the transcriptional reprogramming and subsequent axonal
469 regeneration that occurs after nerve injury.

470

471 **Discussion**

472 Peripheral nerve injury initiates a cascade of events that result in the conversion
473 of sensory neurons from a non-growing to an active regenerating state. While previous
474 studies have generated a number of mechanistic insights into this process, they have
475 largely relied on bulk DRG gene expression studies which mask heterogeneous response
476 to axonal injury (Chandran et al., 2016; Costigan et al., 2002; Xiao et al., 2002) or the
477 dissociation or sorting of a small number of DRG neurons (Chiu et al., 2014; Sakuma et
478 al., 2016; Usoskin et al., 2015; Zeisel et al., 2018), a process which itself induces many
479 injury-related transcriptional changes (Hrvatin et al., 2018; Lacar et al., 2016; Wu et al.,
480 2017). To avoid these confounders, and to identify cell type specific changes, we used
481 snRNA-seq to generate a DRG cell atlas, with gene expression profiles of 107,541 DRG
482 nuclei derived from naive and injured mice. Using these data, we interrogated the

483 transcriptional mechanisms by which injury initiates axonal regeneration and may also
484 contribute to neuropathic pain (Cattin and Lloyd, 2016; Ji et al., 2016).

485 One of the most dramatic findings in our study is that peripheral axonal injury
486 results in a profound transcriptional reprogramming of DRG neurons, one involving both
487 the induction of a common set of injury-response genes across neuronal subtypes and
488 the coincident downregulation of their cell-type-specific genes. This transcriptional
489 reprogramming is reversible, as the transcriptional states of injured neuronal nuclei return
490 to their naive states within weeks, when the axons successfully reinnervate their targets,
491 (Figure S5B) (Navarro et al., 1994; Vogelaar et al., 2004). An analogous process also
492 occurs in the trigeminal ganglion after infraorbital nerve injury (Nguyen et al., 2019).
493 Injury-induced transcriptional reprogramming leads to a new transcriptional state in which
494 neuronal subtypes become difficult to distinguish because of the upregulation of a
495 common set of injury-response genes and the attenuation of cell-type-specific genes after
496 injury. However, we were able to classify each injured neuronal subtype by developing
497 an informatic approach, validated by lineage tracing, that extracted the subtle cell-type-
498 specific gene expression signatures that remained after injury. This ability to classify
499 injured neuronal subtypes then enabled us to determine which components of the nerve
500 injury response are common or cell-type-specific. While cell-type-specific gene
501 expression changes do manifest after axonal injury (e.g. p_cLTMR2) and may contribute
502 to distinct injury responses between cell types (Figure 4D, Table S4), the most striking
503 observation was that the majority of injury-induced gene expression changes are common
504 across neuronal subtypes and that the differences in gene expression between highly
505 specialized DRG neuronal subtypes are lost.

506 The profound transcriptional reprogramming that occurs after axotomy is
507 associated with the rapid induction of transcription factors within hours after injury. Many
508 of these transcription factors (e.g. *Atf3*, *Jun*, *Klf6*) have their consensus DNA binding sites
509 enriched in regions upstream of the genes induced days later after axotomy. *Atf3* has
510 previously been implicated in peripheral neuron regeneration (Gey et al., 2016; Seijffers
511 et al., 2007; Tsujino et al., 2000), but the mechanisms by which *Atf3* function have
512 remained unclear. Consistent with these prior reports, we observed that *Atf3* was one of
513 the most prominent neuronal injury-induced transcription factors identified in our study,
514 as defined by its rapid induction after injury and the extent of its motif enrichment in the
515 pool of injury-induced genes days after injury (Figure 6B). We also found that conditional
516 deletion of *Atf3* in sensory neurons resulted in a substantial impairment of sciatic nerve
517 regeneration and limited the ability of DRG neurons to activate the common neuronal
518 injury gene program (Figures 7C, 7G, 7I-J). *Atf3* is likely to act in concert with other injury-
519 induced transcription factors, such as *Jun* and *Klf6* (Chandran et al., 2016; Raivich et al.,
520 2004), to produce the transcriptional and functional metamorphosis from mature neurons
521 devoted to sensory transduction to injured neurons devoted to axonal growth and target
522 re-innervation, which is also accompanied by pain-producing ectopic neuronal activity.

523 It has been previously hypothesized that axonal injury may reactivate an
524 embryonic development program to drive regeneration (Harel and Strittmatter, 2006; Lisi
525 et al., 2017). We do observe a limited induction of genes after injury that are also
526 regulated during embryonic DRG development (Figure S7H, Table S8), but there is no
527 statistically significant overlap between these two programs. Rather, many of the injury-
528 induced transcription factors are related to the families of transcription factors capable of

529 reprogramming differentiated cells into induced pluripotent stem cells or in the
530 transdifferentiation of a mature cell into a distinct other cell type. This overlap suggests
531 that strong environmental stimuli, such as axonal injury, may invoke transcriptional
532 reprogramming mechanisms similar to those required to convert cells from one
533 transcriptional identity to another, in order to change the primary function of
534 somatosensory neurons from sensory transduction to axonal regeneration (Duan et al.,
535 2019; Ronquist et al., 2017). Unlike stem cell reprogramming, however, injury-induced
536 reprogramming is self-limited, only affecting the cell's transcriptional state until axonal
537 regeneration is complete. The mechanisms governing the timing and mechanisms of the
538 deactivation of injury-induced transcriptional reprogramming will be the subject of future
539 investigations.

540 While *Atf3* is a major driver of the common injury gene program and there are
541 fewer neurons in the “injured state” after axotomy in *Atf3* cKO compared to WT (Figure
542 7G), *Atf3* binding sites are not enriched in the cell-type-specific genes that are
543 downregulated after injury (Figure 6E). Thus, the downregulation of cell-type-specific
544 genes after injury may be an indirect consequence of *Atf3* or of another transcription factor
545 that is rapidly induced after injury and/or the redirection of RNA polymerase/co-activators
546 from cell-type-specific genes to the common injury response genes. The downregulation
547 of cell-type-specific genes after injury is likely to have functional implications, as many of
548 these downregulated genes are ion channels involved in maintaining neuronal excitability
549 (Figure S4E). For example, there is a broad downregulation of voltage-gated potassium
550 channels after peripheral axotomy, which has been reported previously in bulk gene
551 expression studies (Bangash et al., 2018; Chandran et al., 2016; Tsantoulas and

552 McMahon, 2014) and this is associated with the neuronal hyperexcitability linked to injury-
553 induced neuropathic pain (Colloca et al., 2017; Haroutounian et al., 2014; Serra et al.,
554 2012).

555 Non-neuronal cells such as satellite glia and Schwann cells do not exhibit the same
556 massive transcriptional reprogramming after nerve injury that sensory neurons do, but
557 several transcription factors (e.g. *Srebf1* and *Nr3c1*) are induced after injury and have
558 consensus binding sites enriched in the injury-induced genes in these cell types (Figure
559 S7I). Paracrine signaling from injured neurons must produce these changes but
560 interestingly our data indicate that non-injured neurons show only small and transient
561 alterations. Similarly, we did not observe the same magnitude of injury-induced
562 transcriptional reprogramming genes in non-axotomy models such as paclitaxel-induced
563 painful neuropathy or CFA-induced inflammatory pain, at least not at the time points we
564 investigated. These findings are consistent with observations from bulk gene expression
565 studies (Bangash et al., 2018; Zhang and Dougherty, 2014) and support the hypothesis
566 that distinct mechanisms are likely to drive nociceptor sensitization in these pain models.

567 We expect that single-cell sensory neuron atlases from both mice and humans will
568 catalyze the identification of novel therapeutic targets for nerve repair and/or pain.
569 Towards this goal, we have created an online resource at www.painseq.com which
570 enables facile access to and visualization of the snRNA-seq datasets presented and
571 analyzed in this study. This resource can be used to further explore the many gene
572 expression changes that occur in response to nerve injury, paclitaxel-induced neuropathy,
573 or inflammatory pain in animal models of these conditions.

574

575 **Acknowledgements**

576 We would like to thank Michael Tetreault, Daniel Taub, and Nick Andrews for assistance
577 with behavioral experiments; the Harvard Single Cell Core and Neurobiology Imaging
578 Facility for technical assistance; Sinisa Hrvatin, Aurel Nagy, Rory Kirshner, and Michael
579 Greenberg for analytic guidance and helpful discussions. W.R. is supported by NINDS
580 K08NS101064 and the Migraine Research Foundation. C.J.W. is supported by NINDS
581 R35NS105076 and the Bertarelli Foundation, Dr. Miriam and Sheldon G. Adelson Medical
582 Research Foundation, and the DARPA Panacea program (HR0011-19-2-0022)

583

584 **Author Contributions**

585 W.R. and I.T. designed, performed, and analyzed data for most experiments in this study.
586 L.Y. performed data analysis and designed the website. Y.C. performed and analyzed
587 experiments related to *Atf3* and generated the *Atf3-Cre^{ERT2}* mice. E.L. assisted with
588 experiments. R.K. and D.G. contributed to *Atf3KO* gene profiling. W.R., I.T., L.Y., and
589 C.J.W. wrote the manuscript. W.R., I.T. and C.J.W. supervised all aspects of the study.

590

591 **Declaration of Interests**

592 W.R. has received research grants from Teva Pharmaceuticals and Amgen for unrelated
593 studies. C.J.W. is a founder of Nocion Therapeutics and QurAlis.

594

595

596

597

598 **Figure Legends**

599 **Figure 1. Single-nucleus RNA sequencing of DRG neurons in mouse models of**
600 **peripheral axonal injury.**

601 (A) Diagram of mouse axotomy models. Spinal nerve transection (SpNT) is a proximal
602 injury resulting in axotomy of 90+% of all neurons in a given DRG, whereas sciatic nerve
603 transection (ScNT) and sciatic crush are distal injury models resulting in ~50% of
604 axotomized neurons on average across L3-L5 DRGs.

605 (B) UMAP plot of 10,212 neuronal nuclei from naive mice. Clusters correspond to 9
606 neuronal subtypes and a small group of cells of unknown classification.

607 (C) UMAP plot of 2,470 non-neuronal nuclei from naive mice representing 6 cell types.

608 Satglia = satellite glia

609 (D) UMAP plots displaying DRG neuronal subtypes expressing the injury-induced gene
610 *Spr1a* at different times after spinal nerve transection. Each time point was downsampled
611 to display 900 nuclei. Color denotes log₂-normalized expression of *Spr1a*; nuclei not
612 expressing *Spr1a* are colored grey.

613 (E) Bar plot showing the percent of SpNT nuclei [$100 * \text{SpNT nuclei} / (\text{naive} + \text{SpNT}$
614 $\text{nuclei})$] within each neuronal cluster (top row) and violin plots showing log₂-normalized
615 expression of selected injury-induced genes in each cluster (second to fourth rows).
616 Fractions were calculated from a pool of 7,742 naive neuronal nuclei and 6,482 spinal
617 nerve transection neuronal nuclei (> 1d). Cluster ID (x-axis) corresponds to cluster
618 number assignment from Seurat (see Figure S1E, methods). Clusters are classified as
619 “injured state” (red) if they are comprised of > 95% nuclei from SpNT mice and have a

620 median normalized *Atf3* expression > 0.8 SD from mean (corresponding to $> \log_2$ -
621 normalized expression of 2). All other clusters are classified as “naive state” (green).

622 (F) UMAP plot showing 7,000 naive neuronal nuclei and 7,000 randomly sampled SpNT
623 neuronal nuclei. Nuclei classified as being in their “naive state” are colored by their
624 assigned neuronal subtypes. Nuclei classified as in the “injured state” are colored red.

625 (G) Scatter plot of the \log_2 -normalized expression of four injury-induced genes (*Sprr1a*,
626 *Atf3*, *Flrt3* and *Sox11*) in “naive state” (green) and “injured state” (red) nuclei. While there
627 is little expression of *Atf3* and *Sprr1a* in the naive condition, there is some expression of
628 *Flrt3* and *Sox11* in naive neurons. Within hours after injury, the expression of *Atf3*, *Flrt3*,
629 and *Sox11* dramatically increases in neurons that are still classified as in the “uninjured
630 state.” *Sprr1a* expression is largely absent in neurons until 1d after injury, the time point
631 at which the “injured” transcriptional state emerges. These injury-induced genes remain
632 increased for at least 7d. Each time point is downsampled to 900 nuclei for purposes of
633 visualization.

634 (H) Percentage of naive, SpNT, and ScNT neuronal nuclei that are classified as in the
635 “injured state” at each time point after the respective injury.

636 cLTMR = C-fiber low threshold mechanoreceptor; PEP = peptidergic nociceptor; NP =
637 non-peptidergic nociceptor; NF = *Nefh*+ A-fiber low threshold mechanoreceptors; SST =
638 *Sst*+ pruriceptors.

639

640 **Figure 2. Loss of neuronal marker gene expression after DRG axonal injury.**

641 **(A)** UMAP plots displaying DRG neuronal subtypes after spinal nerve transection (SpNT).
642 Nuclei are colored by *Atf3* (top) or by subtype-specific marker genes (bottom). For each

643 gene, the color of nuclei represents the percentile of gene expression within SpNT
644 neurons above the median (50th percentile) of nuclei with > 0 counts of the corresponding
645 gene; nuclei with expression below the median and no expression are colored gray. For
646 cell-type-specific marker genes, 4.5% of nuclei that had expression above the median for
647 multiple markers and their colors were overlaid. Time points were downsampled to the
648 number of nuclei at the time point with the fewest number of nuclei sequenced (900
649 neuronal nuclei). Marker genes: *Atf3* (injury), *Fam19a4* (C-fiber low threshold
650 mechanoreceptor), *Tac1* (peptidergic nociceptor), *Cd55* (non-peptidergic nociceptor),
651 *Nefh* (*Nefh*+ A-fiber low threshold mechanoreceptors), *Nppb* (*Sst*+ pruriceptors).

652 **(B)** Plot showing expression level of neuronal subtype-specific marker genes across
653 neuronal nuclei and the fraction of naive or SpNT nuclei that express each gene (rows)
654 over time. Fraction of nuclei is calculated as the number of nuclei expressing each gene
655 (>0 counts) divided by the total number of nuclei at each time point. Expression at each
656 time point is calculated as the mean scaled counts of a marker gene relative to the highest
657 mean-scaled counts of that gene across time points.

658 **(C-G)** Fluorescence *in situ* hybridization (FISH) images of L4 mouse DRGs stained with
659 probes against *Atf3* (I-M, injury marker, red), *Tubb3* (I-M, neuronal marker, blue) and cell
660 type markers: *Mrgprd* (C, green), *Hapl4* (D, green), *Tac1* (E, green), *Th* (F, green) or *Sst*
661 (G, green). Representative sections from naive DRGs (left), DRGs 6 hours (middle) and
662 1 week (right) after SpNT are shown.

663 **(H)** Quantification of *Atf3* and DRG neuronal subtype-specific marker gene expression
664 from naive DRGs, DRGs 6 hours and 7 days after SpNT as measured by *in situ*
665 hybridization (n = 3-6 L4 DRGs from different mice for each probe combination). Each dot

666 on the boxplot represents gene expression within an individual cell, boxes indicate
667 quartiles and whiskers are 1.5-times the interquartile range (Q1-Q3). The median is a
668 black line inside each box. Significance testing by 1-way ANOVAs were all $P < 0.001$: *Th*
669 ($n = 36$ [naive], 36 [6h] , 33 [7d]), $F(2, 102) = 74.70$, *Atf3*(on *Th* slides), $F(2, 102) = 52.87$;
670 *Tac1* ($n = 68$ [naive], 93 [6h] , 78 [7d]), $F(2, 236) = 332.33$, *Atf3*(on *Tac1* slides), $F(2,$
671 $236) = 112.56$; *Mrgprd* ($n = 100$ [naive], 102 [6h] , 308 [7d]), $F(2, 507) = 1210.87$, *Atf3*(on
672 *Mrgprd* slides), $F(2, 507) = 315.33$; *Hapln4* ($n = 80$ [naive], 114 [6h] , 64 [7d]), $F(2, 255)$
673 $= 85.52$, *Atf3*(on *Hapln4* slides), $F(2, 255) = 192.61$; *Sst* ($n = 26$ [naive], 31 [6h] , 37
674 [7d]), $F(2, 91) = 82.98$, *Atf3*(on *Sst* slides), $F(2, 91) = 110.91$; Tukey HSD post-hoc testing
675 (***: $p < 0.001$, **: $p < 0.01$, *: $p < 0.05$).

676

677 **Figure 3. Classification of DRG neuronal subtypes after axotomy.**

678 **(A)** Classification of injured neuronal subtypes after spinal nerve transection (SpNT) by
679 pair-wise clustering and projection. UMAP plots showing 7,000 naive and 7,000 SpNT
680 neurons that were randomly sampled for purposes of visualization. Prior to pair-wise
681 clustering and projection, neurons that are classified in the “naive state” are colored by
682 their respective neuronal subtype, and neurons in the “injured state” are gray (left). After
683 injured neuronal subtype classification by pair-wise clustering and projection, injured-
684 state neurons (bold) are colored by their subtype (right). Naive-state neurons are also
685 colored by their subtype (faint).

686 **(B)** UMAP plots displaying the progression from naive to injured-state for each neuronal
687 subtype after pair-wise projection and clustering. DRG neurons from naive and each time

688 point after SpNT are shown (900 randomly-sampled neuronal nuclei per time point). Color
689 represents neuronal subtype.

690 cLTMR = C-fiber low threshold mechanoreceptor; PEP = peptidergic nociceptor; NP =
691 non-peptidergic nociceptor; NF = *Nefh*+ A-fiber low threshold mechanoreceptors; SST =
692 *Sst*+ pruriceptors.

693

694 **Figure 4. Characterization of cell-type-specific transcriptional responses to**
695 **peripheral nerve injury.**

696 **(A)** Heatmap of the number of significant injury-induced genes for each cell type and time
697 point after spinal nerve transection (SpNT) compared to their respective cell types in naive
698 mice (FDR < 0.01, $\log_2FC > 1$).

699 **(B)** Pair-wise comparison of overlapping injury-induced genes (FDR < 0.01, $\log_2FC > 1$;
700 3 and 7d after SpNT vs. naive) between the specified cell types after SpNT. Each square
701 is colored by the *P*-value for the overlap between each comparison (hypergeometric test).
702 Note that comparisons between the same gene list will always have 100% overlap but
703 will have different hypergeometric *p*-values depending on list size.

704 **(C)** Comparison of gene expression changes after SpNT compared to naive DRG
705 neurons. Significantly upregulated genes after SpNT (FDR < 0.01, $\log_2FC > 1$ SpNT vs.
706 naive) in each neuronal subtype were aggregated across time points and compared to
707 other neuronal subtypes to determine how many injury-induced genes are cell-type-
708 specific (red), shared between 2-4 neuronal subtypes (yellow), or commonly shared
709 between ≥ 5 other neuronal subtypes (green). Percentage of all significant injury-induced
710 genes that are cell-type-specific, shared between 2-4 subtypes, or shared commonly

711 across ≥ 5 subtypes are displayed on the bar plot. The total number of significantly-
712 induced genes by SpNT in each subtype is shown on top of each bar. See Tables S3-4
713 for gene lists.

714 **(D)** Heatmap displaying the change in expression over time after SpNT of regulated
715 common genes (significantly upregulated by SpNT in ≥ 5 neuronal subtypes) and cell-
716 type-specific genes (significantly upregulated by SpNT in 1 cell type) as defined in 4C.
717 Genes are rows and cell types at each time point after SpNT are columns. Log_2FC (SpNT
718 vs. naive) for each time point and cell type is displayed. Genes are colored gray if they
719 are not expressed in a cell type or at a certain time point. Select genes of interest are
720 labeled.

721 **(E)** Estimate of the fraction of nuclei that induce early injury-response genes (6h, 12h,
722 and 1d) or late injury-response genes (3 and 7 days) after SpNT. A nucleus was classified
723 as induced by injury if it expressed a threshold number of injury-response genes at the
724 respective time point. Nuclei at 6h/12h/1d were classified using injury-induced genes from
725 these time points, and 3d/7d nuclei were classified using a set of injury-induced genes at
726 these time points. The boxes are defined by the fraction of injury-induced nuclei using
727 different thresholds for the number of injury-response genes required for classification as
728 induced by injury. The upper bar is the fraction of injury-induced nuclei using 2 injury
729 genes/nucleus threshold, central line uses a 3 injury genes/nucleus threshold, and the
730 lower bar uses a 4 injury genes/nucleus threshold. Grey rectangles show the fraction of
731 nuclei from naive animals that are classified as induced by injury with the upper box
732 boundary corresponding to a 2 injury gene/nucleus threshold and the lower boundary
733 corresponding to a 4 injury gene/nucleus threshold. The set of injury-induced genes used

734 to classify nuclei as “injury-induced” was chosen from the 10 common injury genes from
735 Figure 4C with greatest fold-change between SpNT at 6h/12h/1d (early) or 3d/7d (late)
736 and naive. An injury gene was counted towards the injury induction threshold in each
737 nucleus if its Log₂-normalized expression was > 90th percentile of all nuclei of the same
738 cell type from naive animals.

739 **(F)** Regulation of cell-type-specific genes by SpNT in each cell type. Cell-type-specific
740 genes are genes that are expressed significantly higher in one naive cell type compared
741 to all other naive cell types (see methods). For each cell type, their respective cell-type-
742 specific genes are grouped by log₂FC after injury (SpNT at 3/7 days vs. naive within each
743 subtype). Pie charts show the fraction of cell-type-specific genes within each neuronal
744 subtype that are regulated by SpNT to the fold-change magnitude indicated. Total number
745 of cell-type-specific genes for each subtype are shown in the header.

746 **(G)** Line plots showing upregulation of common injury-induced genes (≥ 5 subtypes, from
747 C) and downregulation of cell-type-specific genes (from F) for each cell type after SpNT.
748 Each line represents the average log₂FC of common injury-induced genes (green) or cell-
749 type-specific genes (blue) over time. The ribbon represents standard deviation.

750 **(H)** UMAP plots of 19,184 naive and SpNT DRG neurons. Nuclei are colored by either an
751 aggregate injury score calculated from expression of 438 commonly induced genes after
752 axotomy (left, see methods) or an aggregate cell-type-specificity score (right see
753 methods). Aggregate cell-type-specificity scores are calculated for each neuronal type
754 separately based on their respective cell-type-specific genes (see F). Higher scores
755 indicate greater injury-induced or cell-type-specific gene expression.

756 cLTMR = C-fiber low threshold mechanoreceptor; PEP = peptidergic nociceptor; NP =
757 non-peptidergic nociceptor; NF = *Nefh*+ A-fiber low threshold mechanoreceptors; SST =
758 *Sst*+ pruriceptors.

759

760 **Figure 5. Transcriptional reprogramming of DRG neurons after axotomy.**

761 **(A)** UMAP plots displaying DRG neurons from either naive mice or mice who received
762 sciatic nerve crush followed by the indicated amount of time prior to harvesting. Each time
763 point down is sampled to the number of nuclei at which the fewest number of nuclei were
764 sequenced (1000 neuronal nuclei). Nuclei are colored by the common injury score (top)
765 or cell-type-specificity score (bottom) as in Fig 4H. Higher scores indicate greater injury-
766 induced or cell-type-specific gene expression.

767 **(B)** Percentage of naive, spinal nerve transection (SpNT), sciatic crush, sciatic nerve
768 transection (ScNT), paclitaxel-treated, Complete Freund's Adjuvant-treated (CFA)
769 neuronal nuclei that are classified as in the "injured state" at each time point after the
770 respective injury. Colors represent injury models; naive, crush, paclitaxel, and CFA are
771 bolded, SpNT and ScNT are faded.

772 **(C-E)** Fluorescence *in situ* hybridization (FISH) images of ipsilateral L4 *Atf3*-
773 *Cre*^{ERT2};*Gcamp6f* DRG sections from a naive mouse (C), 1 week after sciatic crush (D)
774 and 2 months after sciatic crush (E). Sections stained for the neuronal marker *Tubb3*
775 (magenta), DAPI (blue) and the reporter, *Gcamp6* (green). The *Atf3*-driven *Gcamp6*
776 reporter is upregulated after sciatic crush and persists for months after injury.

777 **(F)** Quantification of *Gcamp6* reporter gene expression in L4 *Atf3*-*Cre*^{ERT2};*Gcamp6f*
778 DRGs after sciatic crush measured by FISH. N = 3-4 DRG sections from different mice

779 per group, one-way ANOVA, $F(2, 8) = 37.4$, $P = 8.7 \times 10^{-5}$. Sciatic nerve crush injury
780 causes an increase in *Gcamp* reporter positive neurons 1 week after crush (Bonferroni
781 post-hoc, $P = 2.9 \times 10^{-4}$), which persists for two months after sciatic crush injury
782 (Bonferroni post-hoc, $P = 1.9 \times 10^{-4}$).

783 **(G)** Heatmap of the number of significant injury-induced genes for each cell type and time
784 point after SpNT, sciatic crush, ScNT, paclitaxel, or CFA compared to their respective cell
785 types in naive mice (FDR < 0.01, $\log_2FC > 1$).

786 **(H)** Pair-wise comparison of overlapping injury-induced genes between the specified cell
787 types 3/7 days after SpNT, sciatic crush, ScNT, or paclitaxel or 2 days after CFA (FDR <
788 0.01, $\log_2FC > 1$, compared to naive nuclei of the respective cell type). Each square is
789 colored by the *P*-value for the overlap between each comparison (hypergeometric test).
790 Note that comparisons between the same gene list will always have 100% overlap but
791 will have different hypergeometric *p*-values depending on list size.

792 **(I)** UMAP plots show neuronal nuclei after different injury models (left, 3,000 nuclei
793 randomly sampled equally from crush, SpNT, ScNT [total = 9,000 nuclei]; middle, 3000
794 nuclei randomly sampled from naive; right, 1,000 nuclei randomly sampled from paclitaxel
795 and CFA [total = 2,000 nuclei]). Each nucleus is colored by the injury model to which it
796 was exposed.

797 cLTMR = C-fiber low threshold mechanoreceptor; PEP = peptidergic nociceptor; NP =
798 non-peptidergic nociceptor; NF = *Nefh*+ A-fiber low threshold mechanoreceptors; SST =
799 *Sst*+ pruriceptors.

800

801 **Figure 6. Induction of a common set of transcription factors across sensory**
802 **neuronal subtypes after axotomy.**

803 **(A)** Mean common injury score for specific neuronal subtypes at each spinal nerve
804 transection (SpNT) time point. Dotted box highlights the time points at which transcription
805 factors that are significantly upregulated (FDR < 0.01, $\log_2FC > 0.5$, SpNT vs. naive) early
806 after injury were identified.

807 **(B)** Heatmap of 24 transcription factors (rows) that are significantly induced ≤ 1 day after
808 SpNT (FDR < 0.01, $\log_2FC > 0.5$) in ≥ 5 neuronal subtypes. Heatmap is colored by \log_2FC
809 (SpNT vs. naive) for each neuronal subtype and injury time point (columns).

810 **(C)** Bar graph showing the number of significantly-enriched transcription factor binding
811 motifs in 438 common injury-induced genes to which each early injury-induced
812 transcription factor binds. Gray bars show the average number of transcription factor
813 binding motifs enriched in 1000 sets of 438 randomly-selected expressed genes.

814 **(D)** UMAP of neuronal nuclei from naive and SpNT mice colored by their degree of ATF3
815 regulon enrichment (left, AUCell score, see methods) or \log_2 -normalized expression of
816 *Atf3* (right). Nuclei with no *Atf3* expression colored gray.

817 **(E)** Bar graph showing the number of significantly-enriched motifs in 1240 cell-type-
818 specific genes that each early injury-induced transcription factor binds (green bars). Gray
819 bars show the average number of transcription factor binding motifs enriched across 1000
820 sets of 1240 randomly-selected expressed genes.

821 cLTMR = C-fiber low threshold mechanoreceptor; PEP = peptidergic nociceptor; NP =
822 non-peptidergic nociceptor; NF = *Nefh*+ A-fiber low threshold mechanoreceptors; SST =
823 *Sst*+ pruriceptors.

824

825 **Figure 7. *Atf3* is required for axon regeneration.**

826 **(A)** Strategy used to create *Atf3* conditional knockout (cKO) mice. Transgenic mice
827 carrying a floxed allele of *Atf3*, where loxP sites surround exon 3 (nuclear localization
828 element) of *Atf3* were generated. These mice were crossed with *Vglut2-Cre* mice, which
829 express *Cre* in >95% of sensory neurons (Kupari et al., 2019).

830 **(B)** Representative images of *Vglut2-Cre;Atf3^{fl/fl}* (cKO, bottom) or *Atf3^{fl/fl}* (WT, top) 1 week
831 after SpNT injury. DRGs are stained with antibodies against ATF3 (green), DAPI (blue)
832 and neurons are counterstained with Nissl. There is a clear loss of ATF3 staining in the
833 cKO compared to the WT.

834 **(C)** Recovery of sensory function as measured by the pinprick assay in *Atf3^{fl/fl}* (WT) and
835 *Vglut2-Cre;Atf3^{fl/fl}* (*Atf3* cKO) mice after sciatic nerve crush. Sciatic nerve crush causes a
836 loss of sensory responses in the ipsilateral hindpaw, followed by a recovery over time
837 associated with sensory neuron regeneration. The pinprick responses of *Atf3^{fl/fl}* WT mice
838 (n=10, black line) recover to baseline within 15 days after sciatic nerve crush (1-way
839 repeated measures within subjects ANOVA, lower bound $F(1, 9) = 388$, $P = 1.0 \times 10^{-8}$).
840 The pinprick responses of *Atf3* cKO mice (n=14, red line) show a significant delay in the
841 time course of sensory function recovery (2-way repeated measures between subjects
842 ANOVA, $F(1, 22) = 33.7$, $P = 7.7 \times 10^{-6}$, Bonferroni post-hoc, * $P < 0.05$, *** $P < 0.001$),
843 suggesting a slower rate of sensory neuron regeneration.

844 **(D)** UMAP plot displaying 6,410 WT and 5,601 *Atf3* cKO DRG neurons from naive mice
845 and mice 7d after sciatic crush. Neurons are colored by their neuronal subtype.

846 **(E)** UMAP plot displaying 2,653 WT and 2,489 *Atf3* cKO DRG neurons from naive mice.
847 Neurons are colored by genotype.

848 **(F)** UMAP plot displaying 3,487 WT and 3,112 *Atf3* cKO DRG neurons from mice 7d after
849 sciatic crush. Neurons are colored by genotype. Arrows point to novel neuronal clusters
850 observed in the sciatic nerve crush samples.

851 **(G)** Bar plot indicating the percent of nuclei classified as in the “injured state” in each
852 condition (naive or 7d after crush) and genotype (WT or *Atf3* cKO). There is a significant
853 reduction in the number of “injured state” neurons in *Atf3* cKO compared to WT 7d after
854 sciatic crush (one-way ANOVA: $F(3, 4) = 192.96$, $P < 0.001$; Tukey HSD post-hoc testing
855 $P > 0.05$ for naive cKO vs. naive WT, $P < 0.01$ for naive cKO vs crush cKO, and naive
856 WT vs. crush cKO, $P < 0.001$ all other pair-wise comparisons).

857 **(H)** UMAP of WT (left) or *Atf3* cKO (right) DRG neuronal nuclei from naive mice and mice
858 7d after sciatic crush colored by their degree of ATF3 regulon enrichment (AUCell score,
859 see methods).

860 **(I)** Volcano plot displaying differential expression of 436 common injury-induced genes
861 between *Atf3* cKO and WT neuronal nuclei that are classified as in the “injured state.” The
862 common injury-induced genes are obtained from the 438 genes described in Figures 4C-
863 D; 2 genes were not expressed in *Atf3* WT and cKO mice.

864 **(J)** UMAP plots displaying 6,410 WT (left) and 5,601 *Atf3* cKO (right) neuronal nuclei from
865 naive mice and mice 7d after sciatic crush. Neurons are colored by the common injury
866 score (see methods).

867 cLTMR = C-fiber low threshold mechanoreceptor; PEP = peptidergic nociceptor; NP =
868 non-peptidergic nociceptor; NF = *Nefh*+ A-fiber low threshold mechanoreceptors; SST =
869 *Sst*+ pruriceptors.

870

871 **Figure S1, related to Figure 1. Single-nucleus RNA-seq of mouse DRG before and**
872 **after injury.**

873 **(A)** Sequencing and mapping metrics of 107,541 nuclei that passed quality control and
874 were analyzed in the study. Boxes indicate quartiles and whiskers are 1.5-times the
875 interquartile range (Q1-Q3). Data outside 1.5-times the interquartile range are labeled as
876 dots. The median is a white line inside each box. The distribution is aggregated across
877 all samples and displayed on the horizontal histogram. Number of nuclei collected by
878 sample (top), distribution of reads per sample (\log_{10} transformed, second), distribution of
879 uniquely mapped reads per sample (\log_{10} transformed, third), distribution of number of
880 unique molecular identifiers (UMI) per sample (\log_{10} transformed, bottom).

881 **(B)** UMAP plots of 10,000 randomly sampled nuclei from the 107,541 nuclei passing
882 quality control in the study. Color shows \log_2 -normalized expression of the neuronal
883 marker gene *Rbfox3* (top) and non-neuronal marker gene, *Sparc* (bottom).

884 **(C)** Dot plot of cell-type-specific marker genes (rows) in each cell type (columns) of nuclei
885 from naive DRGs. The fraction of nuclei expressing a marker gene is calculated as the
886 number of nuclei in each cell type that express a gene (> 0 counts) divided by the total
887 number of naive nuclei in the respective cell type. Expression in each cell type is
888 calculated as the mean scaled counts of the marker gene relative to the highest mean-
889 scaled counts of that gene across cell types.

890 **(D)** Percentage of nuclei from each biological sample (naive, spinal nerve transection
891 [SpNT], sciatic nerve transection [ScNT]) that were classified into the respective DRG cell
892 types. Neurons that were classified as in the “injured state” are shown in red. The number
893 on the right of each bar shows total number of nuclei that passed quality control for each
894 sample.

895 **(E-G)** Fluorescent *in situ* hybridization (FISH) images of naive L4 mouse DRGs stained
896 with DAPI (blue), *Mpz* (Schwann cell marker, green), *Tubb3* (neuronal marker, red) and
897 *ApoE* (satellite glia marker, magenta) (E); *Mrgprd* (NP [non-peptidergic] DRG neuronal
898 marker, green), *Tac1* (PEP [peptidergic] DRG neuronal marker, red) and *Nefh* (NF
899 [neurofilament+] DRG neuron marker, magenta) (F); *Mrgprd* (NP DRG neuron marker,
900 green), *Sst* (*Sst+* pruriceptive DRG neuron marker, red) and *Th* (cLTMR DRG neuron
901 marker, magenta) (G). There is minimal overlap between marker gene fluorescence,
902 suggesting these genes are expressed in distinct cell types.

903 **(H)** Representative FISH images of naive L4 mouse DRGs stained with DAPI (blue),
904 *Fam19a4* (cLTMR1 and p_cLTMR2 marker, green) and *Th* (c-LTMR1 marker, red). Some
905 cells express both *Th* and *Fam19a4* at high levels (cLTMR1), while others express
906 *Fam19a4* with little to no *Th* expression (p_cLTMR2).

907 cLTMR = C-fiber low threshold mechanoreceptor; PEP = peptidergic nociceptor; NP =
908 non-peptidergic nociceptor; NF = *Nefh+* A-fiber low threshold mechanoreceptors; SST =
909 *Sst+* pruriceptors.

910

911 **Figure S2, related to Figure 2. Characterization of DRG neuronal gene expression**
912 **before and after axonal injury.**

913 **(A)** Heatmaps of cell-type-specific gene expression patterns in naive DRG cell types.
914 Genes were included in the heatmap if they demonstrated significant cell type enrichment
915 (FDR < 0.01, $\log_2FC > 1$) using FindMarkers in Seurat and matched the displayed gene
916 ontology annotations. Heatmaps show scale.data from Seurat, which is the row-
917 normalized and centered mean expression of each gene in a given cell type.

918 **(B)** UMAP plots displaying DRG non-neuronal subtypes at different times after spinal
919 nerve transection. Each time point was randomly sampled to display 300 nuclei. Color
920 denotes \log_2 -normalized expression of *Sprr1a*, nuclei not expressing *Sprr1a* are colored
921 grey.

922 **(C)** UMAP plot of all 73,433 neurons that passed quality control from naive mice and mice
923 from each injury model. Cluster IDs that were assigned by Seurat are overlaid onto the
924 plot. Colors denote each cluster ID.

925 **(D)** Comparisons of the overlap between spinal nerve transection (SpNT) injury-induced
926 genes from our single-nucleus RNA-seq data (FDR < 0.01 and $\log_2FC > |1|$, injured state
927 nuclei after SpNT vs. nuclei from naive animals) and the gene modules identified from
928 microarrays of bulk DRG tissue (Chandran et al., 2016). The magenta module was the
929 predominant injury-induced gene module in the Chandran et al. dataset. Horizontal bars
930 show the \log_{10} transformed *P*-values from hypergeometric tests. Vertical dashed line is at
931 $P = 0.01$.

932 **(E)** UMAP plots displaying DRG neurons after sciatic nerve transection. Each time point
933 was randomly sampled to the number of nuclei at the time point with the fewest number
934 of nuclei sequenced (650 neuronal nuclei). Nuclei are colored by their \log_2 -normalized
935 expression of the injury-induced gene, *Sprr1a*.

936 cLTMR = C-fiber low threshold mechanoreceptor; PEP = peptidergic nociceptor; NP =
937 non-peptidergic nociceptor; NF = *Nefh*+ A-fiber low threshold mechanoreceptors; SST =
938 *Sst*+ pruriceptors.

939

940 **Figure S3, related to Figure 3. Classification of injured DRG neuronal subtypes after**
941 **spinal nerve transection (SpNT).**

942 **(A)** UMAP plots showing 7,000 naive neuronal nuclei and 7,000 randomly sampled SpNT
943 neuronal nuclei using all variable genes for clustering (left, same as Figure 1F) or after
944 removing injury-induced genes (FDR < 0.01, log₂FC > 0.5, injured state nuclei after SpNT
945 vs. nuclei from naive animals) from the variable genes prior to clustering (right). Colors
946 denote cell types/states.

947 **(B)** Pairwise clustering and projection strategy to classify the neuronal subtypes of injured
948 state nuclei after SpNT. Nuclei of known and unknown neuronal subtypes from each
949 SpNT time point were co-clustered with the subsequent time point collected (top row).
950 Nuclei of unknown neuronal subtype that co-clustered with clusters of marker-gene-
951 confirmed known neuronal subtypes (middle row), were then assigned the respective
952 neuronal subtype of that cluster (bottom row, see methods). The new injured neuronal
953 subtype assignments were projected forward to assist in the subtype assignment of
954 injured neurons at later time points after SpNT (long arrows). Each column shows co-
955 clustering of nuclei from two adjacent time points. Top row colors indicate neuronal
956 subtype with unknown injured nuclei colored gray. Middle row colors indicate cluster IDs
957 assigned by Seurat. Bottom row colors indicate the final subtype assignment after pair-
958 wise clustering and projection.

959 **(C)** UMAP plot showing 7,000 randomly sampled naive neuronal nuclei and 7,000
960 randomly sampled SpNT neuronal nuclei. Clustering was performed after regressing out
961 the injury-induced genes (FDR < 0.01, log₂FC > 0.5, injured state nuclei after SpNT vs.
962 nuclei from naive animals) from the mRNA counts tables (see methods). Colors denote
963 the independent neuronal subtype assignment using regression-based clustering (left) or
964 the concordance between injured neuronal subtype assignments using the two
965 complementary approaches: pairwise clustering and projection or regression-based
966 clustering (right).

967 **(D)** Lineage tracing to experimentally test neuronal subtype bioinformatic assignments of
968 non-peptidergic nociceptors (NP). UMAP plots of neurons from *Mrgprd-Cre^{ERT2}; Gcamp6f*
969 reporter mice after tamoxifen treatment. Nuclei are colored by their log₂-normalized
970 expression of *Gcamp6f* (left, nuclei with *Gcamp6f* expression ≤ median expression of are
971 colored grey), or by their assigned subtypes from pairwise clustering and projection
972 (middle). Fraction of nuclei expressing *Gcamp6f* greater than the median expression are
973 calculated for each naive/injured neuronal subtype (right). Median expression is
974 determined from nuclei with > 0 counts of *Gcamp6f* transcript.

975 **(E)** Fraction of each cell type within individual biological samples sequenced after
976 pairwise clustering and projection was used to classify the neuronal subtypes of nuclei in
977 the “injured state.” The number above of each bar shows total number of nuclei for each
978 sample that passed quality control.

979 cLTMR = C-fiber low threshold mechanoreceptor; PEP = peptidergic nociceptor; NP =
980 non-peptidergic nociceptor; NF = *Nefh*+ A-fiber low threshold mechanoreceptors; SST =
981 *Sst*+ pruriceptors.

982

983 **Figure S4, related to Figure 4. Cell-type specific transcriptional changes in DRG**
984 **neurons after spinal nerve transection (SpNT).**

985 **(A)** Number of significant differentially-expressed genes ($FDR < 0.01$, $\log_2FC > 1$) in each
986 neuronal subtype and time point after SpNT compared to naive nuclei of the respective
987 subtype. Lines: original = differential expression including all sequenced nuclei in a given
988 neuronal subtype (green). nUMI_1540 = prior to differential expression, nuclei from all
989 time points and neuronal subtypes are downsampled to an average of 1540 UMI (the
990 lowest average UMI in the SpNT time course, see methods). nUMI_1086 = prior to
991 differential expression, nuclei from all time points and neuronal subtypes are
992 downsampled to an average of 1086 UMI. nCell_30.1 and nCell_30.2 are two
993 independent downsamplings of each neuronal subtype to 30 nuclei prior to differential
994 expression. Solid circles = time points with ≥ 30 nuclei sequenced. Faded circles = time
995 points with < 30 nuclei sequenced.

996 **(B)** Summary of the number of significant differentially-expressed genes (left, positive
997 number indicates significantly upregulated genes with $FDR < 0.01$ and $\log_2FC > 1$, and
998 negative number denotes significantly down-regulated genes with $FDR < 0.01$ and \log_2FC
999 < -1) in each neuronal subtype and time point after SpNT compared to naive nuclei of the
1000 respective cell type, UMI per nucleus (middle \log_{10} transformed), and total number of
1001 nuclei (right) at each time point after SpNT. Boxes indicate quartiles and whiskers are
1002 1.5-times the interquartile range (Q1-Q3). Data outside 1.5-times the interquartile range
1003 are omitted for clarity. The median is a black line inside each box.

1004 **(C)** Heatmap of \log_2FC of significantly upregulated genes at both 3 and 7 days after
1005 SpNT compared to naive nuclei of the respective cell type (FDR < 0.01, $\log_2FC > 1$).
1006 Significantly regulated genes are grouped by cell type, and genes that are significantly
1007 regulated in multiple cell types are repeated. Genes that are not expressed in a cell type
1008 are colored gray.

1009 **(D)** Gene ontology analysis (topGO) of the 438 genes that are commonly induced in \geq
1010 5 neuronal subtypes after SpNT compared to naive neurons. The gene ontology terms
1011 displayed in the graph are terms that have > 10 annotated significant genes and P -value
1012 < 0.05.

1013 **(E)** Heatmap of the \log_2FC (3d and 7d SpNT nuclei compared to naive nuclei for each cell
1014 type) of select genes encoding ion channels. Genes shown on the heatmap are
1015 significantly regulated (FDR < 0.01, $\log_2FC > |1|$) in at least one cell type after SpNT.

1016 **(F)** Line plots showing regulation of the cell-type-specific genes within each cell type and
1017 time point after SpNT. Cell-type-specific genes are those genes that are expressed
1018 significantly higher in one naive cell type compared to all other naive cell types (see
1019 methods). For comparison, an equal number of expression-matched randomly-selected
1020 genes in each naive cell type are displayed. Bolded lines represent the average \log_2FC s
1021 of cell-type-specific genes (blue) or expression-matched random genes (orange).

1022 cLTMR = C-fiber low threshold mechanoreceptor; PEP = peptidergic nociceptor; NP =
1023 non-peptidergic nociceptor; NF = *Nefh*+ A-fiber low threshold mechanoreceptors; SST =
1024 *Sst*+ pruriceptors.

1025

1026 **Figure S5, related to Figure 5. Molecular characterization of DRG neurons after**
1027 **sciatic nerve crush.**

1028 **(A)** Sex differences in gene expression after sciatic nerve crush. Scatter plot displays the
1029 \log_2FC (1 week after sciatic nerve crush vs. naive controls) in male (on the x-axis) and
1030 female (on the y-axis) mice of the set of genes that are significantly regulated by sciatic
1031 nerve crush in either males or females ($FDR < 0.01$, $\log_2FC > |1|$, 1 week after sciatic
1032 nerve crush vs. naive) in each cell type. Pearson correlations are displayed. Venn
1033 diagrams of the above injury-regulated genes in male and female after sciatic nerve
1034 crush. Hypergeometric test P -values are displayed.

1035 **(B)** Recovery of sensory function after sciatic nerve crush as measured by the pinprick
1036 assay in C57/Bl6 mice. Pinprick responses recover to baseline 15 days after sciatic crush
1037 ($n=11$ female mice, 1-way repeated measured ANOVA, $F(1, 10) = 1180$, $P = 1 \times 10^{-11}$,
1038 Bonferroni post-hoc, $***P < 0.001$).

1039 **(C)** Diagram of the *Atf3* locus in the *Atf3-Cre^{ERT2}* transgenic mouse. An IRES_*Cre^{ERT2}*_pA
1040 cassette was inserted at the 3'UTR of the mouse *Atf3* locus to avoid interfering with
1041 endogenous *Atf3* expression.

1042 **(D-F)** Fluorescent *in situ* hybridization (FISH) images of an L4 *Atf3-Cre^{ERT2};Gcamp6f*
1043 mouse DRG 1 week after sciatic nerve crush stained with probes against *Gcamp6f*
1044 (green, D), *Atf3* (red, E), and colocalization of DAPI (blue), *Gcamp6f* (green) and *Atf3*
1045 (red) (F). There is a very high degree of colocalization of *Atf3* and the *Gcamp6f* reporter,
1046 suggesting this mouse is a reliable injury reporter.

1047 **(G)** Heatmap displaying the \log_2FC (sciatic crush compared to naive) of the 438 common
1048 injury-induced genes identified in Figure 4D (rows) in each neuronal subtype (columns).

1049 Differential expression for the neuronal subtypes in the “naive state” at any time point
1050 after sciatic crush was performed by comparing these nuclei to their respective naive
1051 neuronal subtype. Differential expression for the nuclei in the “injured state” at any time
1052 point sciatic crush was performed by comparing these nuclei to all naive nuclei. Gray color
1053 indicates a gene is not expressed in that cell type. Genes that have previously been
1054 described as regeneration-associated genes (Chandran et al., 2016) are labeled by the
1055 color of their gene module described in that study (e.g. magenta box denotes the gene is
1056 a member of the magenta cluster).

1057 **(H)** Time course of the number of significantly upregulated genes ($FDR < 0.01$, $\log_2FC >$
1058 1) in each neuronal subtype after sciatic nerve crush. Nuclei after sciatic nerve crush that
1059 were considered to be in the “naive state” were compared to naive neurons of the
1060 corresponding subtype. Neurons classified as injured after sciatic nerve crush were
1061 compared to all naive neurons. Colors of each line correspond to the cell type indicated
1062 in the legend.

1063 **(I-M)** FISH images of L4 mouse DRGs stained with probes against *Atf3* (I-M, red), *Tubb3*
1064 (I-M, blue) and *Mrgprd* (I, green), *Hapln4* (J, green), *Tac1* (K, green), *Th* (L, green) or *Sst*
1065 (M, green).

1066 **(N)** Quantification of FISH puncta from Figures S4I-M. DRG neurons were first identified
1067 by *Tubb3* fluorescence, then divided into *Atf3*-high (injured) and *Atf3*-low (naive)
1068 populations (see methods). On the box plot, each dot represents an individual cell, boxes
1069 indicate quartiles, and whiskers are 1.5-times the interquartile range (Q1-Q3). The
1070 median is a black line inside each box. Significance testing by 1-way ANOVAs were all P
1071 < 0.001 : *Th* ($n = 36$ [naive], 10 [7d *Atf3* low], 23 [7d *Atf3* high]), $F(2, 66) = 38.34$, *Atf3*(on

1072 Th slides), $F(2, 66) = 209.09$; *Tac1* (n = 68 [naive], 40 [7d *Atf3* low] , 45 [7d *Atf3* high]),
1073 $F(2, 150) = 85.03$, *Atf3*(on *Tac1* slides), $F(2, 150) = 420.46$; *Mrgprd* (n = 100 [naive], 41
1074 [7d *Atf3* low] , 209 [7d *Atf3* high]), $F(2, 347) = 899.72$, *Atf3*(on *Mrgprd* slides), $F(2, 347) =$
1075 780.13 ; *Hapln4* (n = 80 [naive], 32 [7d *Atf3* low] , 62 [7d *Atf3* high]), $F(2, 171) = 57.81$,
1076 *Atf3*(on *Hapln4* slides), $F(2, 171) = 235.85$; *Sst* (n = 26 [naive], 13 [7d *Atf3* low] , 26 [7d
1077 *Atf3* high]), $F(2, 62) = 29.31$, *Atf3*(on *Sst* slides), $F(2, 62) = 74.81$; Tukey HSD post-hoc
1078 testing (***: $p < 0.001$, **: $p < 0.01$, *: $p < 0.05$). Neurons expressing each marker gene
1079 are abundant in *Atf3*-low DRG neurons 1 week after sciatic crush, whereas *Atf3*-high DRG
1080 neurons contain significantly fewer marker gene puncta.

1081 cLTMR = C-fiber low threshold mechanoreceptor; PEP = peptidergic nociceptor; NP =
1082 non-peptidergic nociceptor; NF = *Nefh*+ A-fiber low threshold mechanoreceptors; SST =
1083 *Sst*+ pruriceptors.

1084

1085 **Figure S6, related to Figure 5. Comparison of transcriptional changes induced by**
1086 **axotomy and other animal models of pain in DRG neurons.**

1087 **(A)** Co-clustering of known injured neuronal subtypes after spinal nerve transection
1088 (SpNT) with sciatic crush and sciatic nerve transection (ScNT) “injured state” nuclei of
1089 unknown subtype. UMAP plots displaying 2,500 neurons randomly sampled from naive,
1090 and 2,500 neurons randomly sampled from each of the three injury models after they
1091 were clustered together. Nuclei of unknown neuronal subtype that co-clustered with
1092 clusters of known neuronal subtypes from SpNT (middle, nuclei colored by clusterID),
1093 were then assigned the respective neuronal subtype of that cluster (right, see methods).

1094 Nuclei are colored by their neuronal subtype (left, right) with “naive state” faded and
1095 “injured state” bolded.

1096 **(B, C, and G)** Summary of the number of significant differentially expressed genes (left,
1097 positive number indicates significantly upregulated genes with $FDR < 0.01$ and $\log_2FC >$
1098 1 , and negative number denotes significantly down-regulated genes with $FDR < 0.01$ and
1099 $\log_2FC < -1$), UMI (middle \log_{10} transformed), and total number of nuclei for cell type (right)
1100 at each time point in sciatic nerve crush (B), ScNT (C), and paclitaxel or Complete
1101 Freund’s Adjuvant (CFA) treatments (F). Boxes indicate quartiles and whiskers are 1.5-
1102 times the interquartile range (Q1-Q3). Data outside 1.5-times the interquartile range are
1103 omitted for clarity. The median is a black line inside each box.

1104 **(D)** Heatmap of the number of significant ($FDR < 0.01$, $\log_2FC > 1$) injury-induced genes
1105 for each cell type and injury model. Differential expression analyses were performed
1106 either by comparing all nuclei 3d and 7d after injury vs. nuclei from the respective neuronal
1107 subtype in naive animals (left) or by comparing only nuclei in the “injured state” 3d and
1108 7d after injury to the respective neuronal subtype from naive mice (right). The advantage
1109 of performing differential expression on all nuclei (left) is that we can identify cell-type-
1110 specific gene expression changes at early time points after injury prior to the emergence
1111 of the “injured state,” although these analyses are limited by the inclusion of
1112 unaxotomized neurons in the analysis. The advantage of performing differential
1113 expression specifically on injured nuclei is that it allows us to more directly compare gene
1114 expression programs between injury models without including unaxotomized neurons.
1115 Because the SpNT model axotomizes most neurons, while crush and ScNT only
1116 axotomize ~50% of neurons, the similar number of gene expression changes between

1117 “injured state” neurons across the three models suggest the gene expression program at
1118 the level of an individual injured neuron is quite similar between distal and proximal axonal
1119 injury. The number of nuclei used for differential expression analysis in each neuronal
1120 subtype was equal across injury models and set to the number of nuclei in the injury
1121 model with the fewest number of nuclei sequenced.

1122 **(E)** Von Frey behavioral measurement of mechanical sensitivity in C57/Bl6 mice at
1123 baseline or 1 week after every-other-day treatment with 4mg/kg paclitaxel. Paclitaxel
1124 treatment causes a significant mechanical allodynia 1 week after start of treatment (n=7
1125 mice, paired two-tailed Student’s t-test, $**P = 0.006$).

1126 **(F)** Von Frey behavioral measurement of mechanical sensitivity in C57/Bl6 mice after
1127 hindpaw injection of 20 μ L CFA. CFA treatment causes significant mechanical allodynia
1128 24 hours after treatment that persists for at least 7 days after treatment (n=10 mice, 1-
1129 way repeated measured ANOVA, $F(4, 36) = 12.3$, $p=0.005$, Bonferroni post-hoc $**P <$
1130 0.01 , $*** P < 0.001$).

1131 cLTMR = C-fiber low threshold mechanoreceptor; PEP = peptidergic nociceptor; NP =
1132 non-peptidergic nociceptor; NF = *Nefh*+ A-fiber low threshold mechanoreceptors; SST =
1133 *Sst*+ pruriceptors.

1134

1135 **Figure S7, related to Figure 7. Transcription factor analysis of the injury-induced**
1136 **gene expression program.**

1137 **(A)** Log₂FC (spinal nerve transection [SpNT] compared to naive) of *Atf3* mRNA (red line)
1138 and ATF3 target genes (light blue lines) at each time point and DRG cell type. Each line

1139 represents regulation of one gene over time. A break in the line occurs if the gene is below
1140 the expression threshold at a specific time point.

1141 **(B)** Representative Western Blot (top) and quantification (bottom) of ATF3 protein in DRG
1142 protein extract from ipsilateral and contralateral L3-L5 DRG neurons from *Brn3a-*
1143 *Cre^{ERT2};Atf3f/f* mice 1 week after sciatic nerve crush. ATF3 is significantly induced in
1144 ipsilateral injured but not in uninjured contralateral DRG neurons in *Brn3a-Cre^{ERT2};Atf3f/f*
1145 mice treated with vehicle (retaining Atf3) ($p=0.04$, $n=2$, two-tailed Student's t-test). In
1146 *Brn3a-Cre^{ERT2};Atf3f/f* mice treated with tamoxifen (which causes loss of Atf3), Atf3 is not
1147 significantly induced in ipsilateral L3-L5 DRG neurons 1 week after sciatic nerve crush
1148 ($p=0.23$, $n=2$, two-tailed Student's t-test). For quantification (bottom), the ratio of
1149 ATF3/GAPDH protein levels was calculated from the Western Blot data. Data are
1150 mean \pm SEM.

1151 **(C)** Recovery of sensory function as measured by the pinprick assay in vehicle and
1152 tamoxifen treated *Brn3a-Cre^{ERT2};Atf3f/f* mice after sciatic nerve crush. Sciatic nerve crush
1153 causes a loss of sensory responses in the ipsilateral hindpaw, followed by a recovery
1154 over time associated with sensory neuron regeneration. The pinprick responses of vehicle
1155 treated *Brn3a-Cre^{ERT2};Atf3f/f* mice ($n=8$, black line) recover to baseline within 16 days
1156 after sciatic nerve crush (1-way repeated measures within subjects ANOVA, lower bound
1157 $F(1,7) = 343$, $P = 3.3 \times 10^{-7}$). The pinprick responses of tamoxifen treated *Brn3a-*
1158 *Cre^{ERT2};Atf3f/f* DRG mice ($n=7$, red line) show a significant delay in the time course of
1159 sensory function recovery (2-way repeated measures between subjects ANOVA, $F(1, 13)$
1160 $= 40.2$, $P = 2.6 \times 10^{-5}$, Bonferroni post-hoc, $*** P < 0.001$), suggesting a slower rate of
1161 sensory neuron regeneration.

1162 **(D)** Dot plot of neuronal subtype-specific marker genes (rows) in neuronal subtypes
1163 (columns) from naive *Atf3f/f* (WT, orange circles) or *Vglut2-Cre;Atf3f/f* (cKO, purple
1164 circles) DRGs. The fraction of nuclei expressing a marker gene is calculated as the
1165 number of nuclei in each cell type that express a gene (> 0 counts) divided by the total
1166 number of naive nuclei in the respective cell type. Expression in each cell type is
1167 calculated as the mean scaled counts of the marker gene relative to the highest mean-
1168 scaled counts of that gene across cell types.

1169 **(E)** Bar plot showing the percent of nuclei 7 days after sciatic crush [$100 * \text{crush nuclei} /$
1170 (naive + crush nuclei)] within each neuronal cluster (top row) and violin plots showing
1171 \log_2 -normalized expression of selected injury-induced genes in each cluster (second to
1172 fourth rows). Note that sciatic crush only injures approximately 50% of lumbar DRG
1173 neurons sequenced. Cluster ID (x-axis) corresponds to cluster number assignment from
1174 Seurat (see methods). Clusters are classified as “injured state” (red) if they are comprised
1175 of > 95% nuclei from sciatic crush mice and have a median normalized *Atf3* expression >
1176 0.8 SD from mean (corresponding to > \log_2 -normalized expression of 2). All other clusters
1177 are classified as “naive state” (green).

1178 **(F)** Quantification of Nissl+ DRG neurons in L4 DRG sections from *Vglut2-Cre;Atf3f/f* cKO
1179 (n=4 sections, red) and *Atf3f/f* WT (n=4 sections, black) mice 1 week after SpNT. There
1180 is no significant difference in DRG neuron density ($P = 0.71$, two-tailed Student’s t-test),
1181 suggesting there is no DRG neuron death at this time point. Data are mean \pm SEM.

1182 **(G)** Violin plot of ATF3 regulon enrichment (AUCell score, see methods). All neuronal
1183 nuclei are grouped by genotype (WT or cKO) and injury (naive or crush). Lines in the
1184 violins indicate the lower quartile, median, and upper quartile. One-way ANOVA: $F(3,$

1185 11737) = 1391.28, $P < 0.001$; Tukey HSD post-hoc testing $P > 0.05$ for naive cKO vs.
1186 naive WT, $p < 0.001$ for all other pair-wise comparisons.

1187 **(H)** Regulation of the 438 common injury-induced genes (rows, from Figure 4C) after
1188 SpNT, crush, ScNT, and embryonic development. Heatmap shows the \log_2FC from
1189 differential expression analysis of “injured state” nuclei in each injury model compared to
1190 all naive nuclei as well as the \log_2FC between RET+ DRG neurons at 3 embryonic time
1191 points (E12.5, E14.5, E18.5) compared to adult RET+ DRG neurons (see methods).

1192 **(I)** Heatmap displays the transcription factors (rows) identified by SCENIC analysis (see
1193 methods) as having their consensus binding sites enriched within expressed genes in
1194 naive and SpNT cell types at all time points (columns). Colors on the heatmap represent
1195 row-normalized average AUCell scores for nuclei in each cell type and time point. AUCell
1196 scores are a SCENIC metric of the activity of a transcription factor in each cell; higher
1197 AUCell scores indicate greater predicted activity of a transcription factor on its target
1198 genes in a given cell. The horizontal bar plots for each transcription factor indicates the
1199 mean AUCell score (not row-normalized) across all cell types and time points.

1200 cLTMR = C-fiber low threshold mechanoreceptor; PEP = peptidergic nociceptor; NP =
1201 non-peptidergic nociceptor; NF = *Nefh*+ A-fiber low threshold mechanoreceptors; SST =
1202 *Sst*+ pruriceptors.

1203

1204 **Methods**

1205 **Animals**

1206 Male and female 8-12-week-old C57 mice were obtained from Jackson Labs (strain
1207 #000667) and used in most behavioral and snRNA-seq experiments. Unless stated

1208 otherwise, male mice were used in all experiments. *The Atf3-Cre^{ERT2}* mice were
1209 generated by inserting an IRES_Cre^{ERT2}_pA cassette at the 3'UTR of the mouse *Atf3*
1210 locus in order to preserve endogenous *Atf3* expression. CRISPR guide RNAs were
1211 designed to produce a defined double-strand break (DSB) at the 3'UTR in order to enable
1212 homology-directed repair (HDR). The HDR donor sequence consisted of
1213 IRES_Cre^{ERT2}_pA cassette flanked by two homologous arms 1 kb (left-arm) and 4 kb
1214 (right-arm) in length. We mixed synthetic sgRNA targeting at 3'UTR of mouse *Atf3*, Cas9
1215 protein and HDR donor, and then injected the mixture directly into single-cell mouse
1216 embryos. *Atf3-Cre^{ERT2};Gcamp6f f/f* mice were generated by crossing the *Atf3-Cre^{ERT2}*
1217 transgenic mice with *Gcamp6f f/f* mice from Jackson Labs (strain #024105) and bred to
1218 homozygosity for both alleles. *Gcamp6f* reporter expression was induced in injured *Atf3-*
1219 *Cre^{ERT2};Gcamp6f f/f* mice 24 hrs after injury by intraperitoneal (i.p.) tamoxifen injection at
1220 the same time as in naive *Atf3-Cre^{ERT2};Gcamp6f f/f* mice. *Atf3f/f* mice were generated by
1221 inserting loxP sites around exon 3 of the mouse *Atf3* gene. *Vglut2-Cre;Atf3f/f* and *Brn3a-*
1222 *Cre^{ERT2};Atf3f/f* mice were generated by crossing the *Atf3f/f* mice with *Vglut2-ires-Cre*
1223 (strain #016963) or *Brn3a-Cre^{ERT2}* (strain #032594) mice from Jackson Labs. These mice
1224 were bred as homozygotes for *Atf3f/f* and heterozygotes for *Vglut2-Cre* or *Brn3a-Cre^{ERT2}*.
1225 Littermate controls were used for experiments involving transgenic mice. Injured *Vglut2-*
1226 *Cre;Atf3f/f* cKO DRG neurons express *Atf3* mRNA as measured by FISH (data not shown)
1227 and snRNA-seq (Table S8), but do not express nuclear ATF3 protein in sensory neurons
1228 (Figure 7B). *Mrgprd-Cre^{ERT2};Gcamp6f* mice were generated by crossing the *Mrgprd-*
1229 *Cre^{ERT2}* transgenic mice from Jackson Labs (strain #031286) with *Gcamp6f f/f* mice (strain
1230 #024105) and bred to homozygosity for both alleles. All animal experiments were

1231 conducted according to institutional animal care and safety guidelines at Boston
1232 Children's Hospital and Harvard Medical School.

1233

1234 **Surgical Procedures**

1235 Sciatic nerve crush and ScNT were performed as previously described (Ma et al., 2011),
1236 and the SpNT protocol was modified from previous reports (Ogawa et al., 2014; Vilceanu
1237 et al., 2010). Briefly, mice were anesthetized by administration of 2.5% isoflurane. Sciatic
1238 nerve crush and ScNT were performed by exposing the left sciatic nerve at the mid-thigh
1239 level and crushing with smooth forceps for 30 s or cutting a 2mm segment with a pair of
1240 scissors followed by a tight ligation of the proximal end to prevent regeneration,
1241 respectively. SpNT was performed by making a midline incision of mouse back skin,
1242 exposing the left L3 and L4 spinal nerves on the visual field and cutting them with a pair
1243 of scissors. These two ganglia were selected in order to maximize the number of
1244 transected sensory axons in the sciatic nerve. Intraperitoneal injections of 4mg/kg
1245 paclitaxel every other day for 6 days (total of 4 injections) were performed as previously
1246 described (Toma et al., 2017). A single intraplantar injection of 20 μ l CFA was performed
1247 into the left hindpaw as previously described (Ghasemlou et al., 2015). Naive and treated
1248 mice were euthanized by CO₂ asphyxiation and decapitation. Ipsilateral lumbar L3-L5
1249 ganglia from naive, crush, ScNT, paclitaxel or CFA-treated mice and ipsilateral L3-L4
1250 ganglia from SpNT mice were collected at various time points after treatment. Ganglia
1251 were from 3-5 mice per sample were immediately frozen on dry ice, then pooled for
1252 subsequent snRNA-seq profiling or histology. There were 2-7 biological replicates of each
1253 pooled condition, as indicated in Figure S1. Two biological replicates were used in

1254 snRNA-seq experiments of *Atf3* cKO mice. Each replicate of a specific condition (naive
1255 or crush) or genotype (*Atf3* cKO; *Vglut2-Cre;Atf3f/f* or littermate WT controls; *Atf3f/f*)
1256 contained L3-L5 DRGs pooled from 1 male mouse and 1 female mouse.

1257

1258 **Single-nuclei isolation from mouse DRG**

1259 Single-nuclei suspensions of lumbar DRGs from naive or injured/treated mice were
1260 collected using a modified protocol from that described previously (Renthal et al., 2018).
1261 Briefly, DRGs were removed from dry ice and placed into homogenization buffer (0.25 M
1262 sucrose, 25 mM KCl, 5 mM MgCl₂, 20 mM tricine-KOH, pH 7.8, 1 mM DTT, 5 µg/mL
1263 actinomycin, and 0.04% BSA). After a brief incubation on ice, the samples were briefly
1264 homogenized using a tissue tearer and transferred to a Dounce homogenizer for an
1265 additional ten strokes with a tight pestle in a total volume of 5mL homogenization buffer.
1266 After ten strokes with a tight pestle, a 5% IGEPAL (Sigma) solution was added to a final
1267 concentration of 0.32% and five additional strokes with the tight pestle were formed. The
1268 tissue homogenate was then passed through a 40-µm filter, and diluted 1:1 with OptiPrep
1269 (Sigma) and layered onto an OptiPrep gradient as described previously (Mo et al., 2015).
1270 After ultracentrifugation, nuclei were collected between the 30 and 40% OptiPrep layers.
1271 This layer contains DRG nuclei as well as some membrane fragments likely from
1272 Schwann cells that have the same density as nuclei. We diluted this layer in 30% OptiPrep
1273 to a final concentration of 80-90,000 nuclei+fragments/mL for loading into the inDrops
1274 microfluidic device. All buffers and gradient solutions for nuclei extraction contained
1275 RNAsin (Promega) and 0.04% BSA.

1276

1277 **Single-nucleus RNA sequencing (inDrops)**

1278 Single-nuclei suspensions were encapsulated into droplets and the RNA in each droplet
1279 was reverse transcribed using a unique oligonucleotide barcode for each nucleus as
1280 described previously (Klein et al., 2015). Nuclei encapsulation was performed in a blinded
1281 fashion and the order of sample processing was randomized. After encapsulation, the
1282 sample was divided into pools of approximately 3,000 droplets and library preparation
1283 was performed as described previously (Hrvatin et al. 2017). Libraries were sequenced
1284 on an Illumina Nextseq 500 to a depth of 500 million reads per 30,000 droplets collected,
1285 resulting in at least 5 reads per UMI on average per sample. Sequencing data was
1286 processed and mapped to the mouse genome GRCm38 (modified by the addition of 3'
1287 regions of *Gcamp6f*-WPRE and *Cre*) using the pipeline described in
1288 <https://github.com/indrops/indrops> (Klein et al., 2015). Counts tables from each library
1289 were then combined and processed as described below.

1290

1291 **Initial quality control, clustering and visualization of snRNA-seq**

1292 To be included for analysis, nuclei were required to contain counts for greater than 600
1293 unique genes, fewer than 15,000 total UMI, and fewer than 10% of the counts deriving
1294 from mitochondrial genes. There were 171,827 nuclei that met these criteria. We used
1295 the Seurat package (version 2.3.4) in R to perform clustering of these nuclei as previously
1296 described (Satija et al., 2015). Raw counts were scaled to 10,000 transcripts per nucleus
1297 to control the sequencing depth between nuclei. Counts were centered and scaled for
1298 each gene. The effects of total UMI and percent of mitochondrial genes in each nucleus,
1299 as well as the batch in which the library was prepared were regressed out using a linear

1300 model in `Scaledata()` function. Highly variable genes were identified using the
1301 `MeanVarPlot()` with default settings. The top 20 principal components were retrieved with
1302 the `RunPCA()` function using default parameters. Nuclei clustering was performed using
1303 `FindClusters()` based on the top 20 principal components, with resolution at 1.5 for the
1304 initial clustering of all nuclei and the sub-clustering of non-neuronal nuclei except where
1305 otherwise specified. For dimension reduction and visualization, Uniform Manifold
1306 Approximation and Projection (UMAP) coordinates were calculated in the PCA space by
1307 using the implemented function `runUMAP()` in Seurat.

1308

1309 **Doublet identification and classification of neuronal and non-neuronal nuclei**

1310 After clustering all DRG nuclei that passed initial quality control metrics as above, we next
1311 excluded nuclei from downstream analysis that were likely to be doublets. Specifically,
1312 nuclei that expressed marker genes (> 0.5 standard deviations away from the mean of
1313 the nuclei included for clustering) from multiple cell types were classified as doublets and
1314 excluded from downstream analysis. After doublet removal, 145,338 nuclei were included
1315 for downstream analysis (97,137 neuronal nuclei and 48,201 non-neuronal nuclei). The
1316 marker genes used to make doublet calls were neurons = *Rbfox3*, endothelial = *Cldn5*,
1317 macrophages = *Mrc1*, glia = *Mbp*, and meninges = *Mgp*). A nucleus was also classified
1318 as a doublet if it expressed multiple neuronal subtype marker genes (peptidergic
1319 nociceptors (PEP) = *Tac1*, non-peptidergic nociceptors (NP) = *Cd55*, pruriceptors (SST)
1320 = *Sst*, cLTMR = *Fam19a4*, A-LTMR (NF) = *Nefh*). Clusters enriched for the expression of
1321 the neuronal marker gene *Rbfox3* were classified as neuronal clusters, and clusters

1322 enriched for the expression of the non-neuronal marker genes *Cldn5*, *Mrc1*, *Mbp*, or *Mgp*
1323 were classified as non-neuronal clusters.

1324

1325 **Annotation of non-neuronal DRG cell types**

1326 Non-neuronal subtypes (defined by low *Rbfox3* expression and expression of any non-
1327 neuronal marker) were clustered separately as described above to facilitate classification
1328 of non-neuronal subtypes. Doublet removal was performed again with higher stringency
1329 to remove nuclei from downstream analysis that expressed marker genes from multiple
1330 cell types (marker gene expression > 1 standard deviation away from the mean of non-
1331 neuronal nuclei). The same genes were used as above to make doublet calls. Significant
1332 enrichment (FDR < 0.01, $\log_2FC > 0.5$) of known non-neuronal marker genes within a
1333 cluster of nuclei compared to all other nuclei was used to assign the respective non-
1334 neuronal cell type to each cluster (satellite glia = *ApoE*, Schwann cells = *Mpz*, meninges
1335 = *Mgp*, endothelial cells = *Cldn5*, and pericytes/endothelial = *Flt1*). The final non-neuronal
1336 dataset after quality control contains 34,108 nuclei, with 33 clusters corresponding to 6
1337 cell types.

1338

1339 **Annotation of neuronal DRG subtypes**

1340 Neuronal nuclei (classified as above) were clustered separately as described above to
1341 facilitate neuronal subtype classification. Doublet removal was performed again with
1342 higher stringency to remove nuclei from downstream analysis that expressed marker
1343 genes from multiple neuronal subtypes (marker gene expression > 1 standard deviation
1344 away from the mean of the neuronal nuclei). The same neuronal subtype marker genes

1345 were used as above to make doublet calls. Significant enrichment (FDR < 0.01, log₂FC >
1346 0.5) of known neuronal subtype marker genes within a cluster of nuclei compared to all
1347 other neuronal nuclei was used to assign the neuronal subtype to each cluster.
1348 Specifically, peptidergic nociceptors (PEP)1 = *Tac1, Gpx3*; PEP2 = *Tac1, Hpca*; non-
1349 peptidergic nociceptors (NP) = *Cd55*; non-peptidergic/itch receptors (SST) = *Sst*; cLTMR1
1350 = *Fam19a4, Th+*; p_cLTMR2 = *Fam19a4, Th-*; A-LTMR (NF1) = *Nefh, Cadps2*;
1351 proprioceptors (NF2) = *Nefh, Pvalb*; A-LTMR (NF3) = *Nefh, Cplx2*. Each of these
1352 subtypes was confirmed by FISH (see Figure S1). We removed 4 neuronal clusters that
1353 were significantly enriched for *Rgs11* after being unable to confirm this cell population by
1354 FISH. The final neuronal dataset after quality control contains 73,433 high-quality nuclei,
1355 with 37 clusters corresponding to 9 neuronal subtypes and “injured state” neurons (see
1356 below).

1357

1358 **Classification of naive and injured transcriptional states**

1359 To quantitatively classify neurons as being in either a transcriptionally “naive state” or
1360 “injured state,” we calculated the percent of nuclei that were derived from naive mice or
1361 SpNT mice within each neuronal cluster. Percentages were calculated with all 7,742 naive
1362 neuronal nuclei and 6,482 SpNT neuronal nuclei > 1 day after injury. Clusters of neuronal
1363 nuclei were classified as in the “injured state” if >95% of the nuclei in that cluster were
1364 derived from SpNT mice and median log₂-normalized expression of injury induced genes
1365 *Atf3* greater than 2. All other clusters were classified as “naive,” which on average had
1366 ~7% (roughly the percent of un-axotomized neurons after SpNT) of their nuclei from SpNT
1367 mice and a median *Atf3* expression of 0.

1368

1369 **Classification of injured neuronal subtypes**

1370 The “injured state” neurons lose most of the distinguishing gene expression features used
1371 for classifying neuronal subtypes (e.g. *Tac1* expression for PEP). Thus, to classify “injured
1372 state” neuronal subtypes, we aimed to identify more subtle gene expression signatures
1373 that could be used to distinguish between neuronal subtypes after injury. To do this, we
1374 co-clustered nuclei from two consecutive time points after SpNT, reasoning that if we had
1375 sufficient temporal resolution of the transition states between “naive” and “injured”
1376 neurons, we could project remaining neuronal subtype-specific transcriptional signatures
1377 from one time point to the next even after the primary marker genes are downregulated.
1378 Each pairwise co-clustering was pairwise as follows: naive and 6h after SpNT, 6h and
1379 12h 6h after SpNT, 12h and 1d 6h after SpNT, 1d and 1.5d 6h after SpNT, 1.5d and 2d
1380 6h after SpNT, 2d and 3d 6h after SpNT, and 3d and 7d 6h after SpNT. The neuronal
1381 subtype classifications of naive neuronal clusters were then projected onto
1382 “injured”/unknown neuronal nuclei from 6h after SpNT that were present in the same
1383 cluster. We then used the new neuronal subtype classifications of 6h SpNT nuclei to guide
1384 the classification of “injured”/unknown nuclei 12h after SpNT, and continued in this
1385 fashion until nuclei from all SpNT time points were classified.

1386

1387 For each pairwise clustering and projection step, if > 50% of the total nuclei (classified +
1388 unknown) in a cluster were already assigned to a specific neuronal subtype, either from
1389 the initial clustering above using marker gene expression or projection from an earlier
1390 pairwise clustering step, this subtype classification was projected to all nuclei in the same

1391 cluster. If $\leq 50\%$ of the total nuclei in a cluster had a known subtype classification, we
1392 determined whether the classified nuclei in these clusters were all from the same subtype
1393 or multiple subtypes. If they were from the same subtype, we next used the FindMarkers()
1394 function in Seurat to identify cluster-specific gene expression patterns as described
1395 previously. If known subtype-specific marker genes were significantly enriched in a
1396 specific cluster ($FDR < 0.01$, $\log_2FC > 0.5$), we assigned this cluster the corresponding
1397 subtype as described above (e.g. *Tac1+* clusters are peptidergic nociceptors). If multiple
1398 previously-classified neuronal subtypes were present in a cluster, we re-clustered these
1399 nuclei separately to maximize the potential to separate neuronal subtypes into biologically
1400 meaningful clusters. After re-clustering, the FindMarkers() function in Seurat was
1401 performed on each cluster as described previously to identify cluster-specific gene
1402 expression patterns. If known subtype-specific marker genes were significantly enriched
1403 in a specific cluster ($FDR < 0.01$, $\log_2FC > 0.5$), we assigned this cluster the corresponding
1404 subtype as described above. If known marker genes were not enriched in a cluster even
1405 after re-clustering, we classified these clusters as unknown (1.9% of SpNT nuclei).

1406

1407 To assign the neuronal subtypes of “injured state” nuclei from crush, ScNT, paclitaxel,
1408 CFA, naive, and the “unknown” SpNT nuclei above, we clustered all “injured state”
1409 neuronal nuclei in the study together. Having classified most SpNT nuclei previously, we
1410 were able to project those neuronal subtypes onto the “injured state” nuclei from other
1411 models. We assigned clusters to the neuronal subtype of the most abundant SpNT
1412 neuronal subtype in that cluster if it was more than 3X more abundant than the next most
1413 abundant subtype in that cluster (88.5% of nuclei classified this way). Otherwise, nuclei

1414 from the remaining clusters were separately clustered and each new cluster was assigned
1415 to a neuronal subtype depending on the number proportion of previously classified
1416 neurons in that cluster. A neuronal subtype was then assigned to the new cluster if > 80%
1417 of previously-classified SpNT nuclei in the new cluster were of the same neuronal subtype
1418 (on average ~1/3 of the nuclei within a cluster were previously-classified SpNT nuclei and
1419 ~2/3 were of unknown subtype) (7.5% of nuclei classified this way). If $\leq 80\%$ of the
1420 previously-classified SpNT nuclei in the new cluster were of the same neuronal subtype,
1421 we assigned the new cluster to the most abundant subtype in that cluster (4% of nuclei
1422 classified this way).

1423

1424 We also used an independent bioinformatic approach in which injury-induced gene
1425 expression within each cell is regressed out prior to subtype. To do this, we used the
1426 FindMarkers() function in Seurat to identify differential gene expression (FDR<0.01 and
1427 $\log_2FC > 1$) between “injured state” clusters and “naive state” clusters across all injury
1428 models. Seventy-five genes were identified, and a score was generated with these genes
1429 using the AddModuleScore() function in Seurat. This function calculates the mean
1430 normalized expression of the specified gene set, subtracted by the mean normalized
1431 expression of a random gene set for each single nucleus. We then scaled the counts
1432 matrix using the Scaledata() function in Seurat, including the injury score along with UMI,
1433 % mitochondrial genes, and batch to the linear regression. The regressed counts matrix
1434 was then clustered with default settings described above. Regressing out the injury score
1435 resulted in “injured state” nuclei clustering with their “naive state” counterparts, which
1436 enabled cell types to be assigned to each cluster based on their marker gene expression

1437 as described above. Neuronal subtypes assigned by the regression method were
1438 compared to the neuronal subtypes assigned by pairwise clustering and projection, and
1439 the concordance rate was 99% for naive nuclei and 91% for injured nuclei.

1440

1441 **Lineage tracing of injured non-peptidergic neurons**

1442 Neuronal DRG nuclei from tamoxifen-treated *Mrgprd-Cre^{ERT2}* mice (naive and 7d after
1443 crush) were co-clustered with neuronal nuclei from our injury time course with default
1444 clustering settings in Seurat. Neuronal subtypes were identified by pairwise clustering and
1445 projection described above. We then calculated the fraction of nuclei in each neuronal
1446 subtype that expresses the *Gcamp6f* reporter of *Mrgprd*⁺ NP neurons greater than the
1447 threshold. The threshold was set as the median *Gcamp6f* expression of all *Gcamp6f*-
1448 expressing nuclei from *Mrgprd-Cre^{ERT2}* mice. The error rate (1.88 for “naive state” nuclei,
1449 2.93% for “injured state” nuclei), for neuronal classification by pairwise clustering and
1450 projection was reported as the fraction of non-NP neuronal nuclei expressing *Gcamp6f*
1451 greater than the threshold.

1452

1453 **Differential expression analysis**

1454 Differential expression analysis was done with edgeR (version 3.24.3) similar to that
1455 described for single-cell analysis in (Soneson and Robinson, 2018). Briefly, edgeR uses
1456 the raw counts as input, and genes detected in fewer than 5% of nuclei selected for each
1457 comparison were excluded from analysis. Counts within each nucleus were normalized
1458 by the trimmed mean of M-values (TMM) method to adjust for total RNA differences
1459 between nuclei. Dispersion was estimated by fitting a quasi-likelihood negative binomial

1460 generalized log-linear model (glmQLFit) with the conditions being analyzed. The QL F-
1461 test was used to determine statistical significance between differentially expressed genes
1462 in the experimental and control groups. For each experimental condition (e.g. NP neurons
1463 6h after SpNT), the control group used for each comparison was the corresponding cell
1464 type from naive animals, unless otherwise specified. Differentially regulated genes are
1465 defined as genes with $FDR < 0.01$ and $\log_2FC > |1|$.

1466

1467 **Cell-type-specificity score**

1468 “Cell-type-specific” genes in naive animals were identified using the FindMarkers()
1469 function in Seurat to compare gene expression in nuclei of each cell type to all other nuclei
1470 ($FDR < 0.01$ and $\log_2FC > 1$). These “cell-type-specific” genes for each cell type were used
1471 to generate cell-type-specificity scores using the AddModuleScore() function in Seurat,
1472 which resulted in a distinct cell-type-specificity score for each cell type. Each nucleus was
1473 assigned to the cell-type-specificity score of its respective cell type.

1474

1475 **Common injury score**

1476 The 438 injury-induced genes that are present in ≥ 5 neuronal subtypes (see common
1477 genes in Figure 4D, Table S3) are used to generate the common injury score. The injury
1478 score was calculated for each nucleus by using the AddModuleScore() function in Seurat
1479 as described above.

1480

1481 **Random gene selection**

1482 To generate expression-matched control gene lists, genes in each cell type were first
1483 ranked by their level of expression, and then for each cell-type-specific gene, the gene
1484 either above or below it was selected randomly. Random gene lists for motif enrichment
1485 analysis were generated as described in that section.

1486

1487 **Gene ontology (GO) analysis**

1488 GO analysis was performed using topGO (version 2.34.0) in R. Expressed genes ($\geq 5\%$
1489 of SpNT+naive nuclei with the mean \log_2 -normalized expression > 0.1 from edgeR
1490 analysis in any neuronal subtype) were used as the background list. The common injury-
1491 induced genes described above were used as the input gene list. R package
1492 org.Mm.eg.db (version 3.7.0) was used as the genome wide annotation database for *Mus*
1493 *musculus*. Genes were annotated for their biological process and associated gene
1494 ontology terms with > 10 annotated genes and enrichment P -value < 0.05 were returned.
1495 Enrichment is defined as the number of annotated genes observed in the input list divided
1496 by the number of annotated genes expected from the background list.

1497

1498 PANTHER was used to categorize the molecular function of cell-type-specific genes
1499 (Figure S2A) using default settings for *Mus musculus*. Genes containing the molecular
1500 function of transcription factors, ion channels, and GPCRs were selected and used for
1501 plotting. Neuropeptide gene lists were obtained from
1502 <http://www.neuropeptides.nl/tabel%20neuropeptides%20linked.htm>.

1503

1504 **Transcription factor analysis**

1505 We used SCENIC package (version 1.1.1-9) (Aibar et al., 2017) to conduct gene
1506 regulatory network analysis and transcription factor assessment. For inclusion in this
1507 analysis, genes needed to be detected in at least 5% of nuclei and have a mean log₂-
1508 normalized expression > 0.1. To identify potential transcription factor targets, SCENIC
1509 first performs a co-expression network analysis to identify the genes whose expression is
1510 positively correlated (Pearson's $r > 0.01$) with each transcription factor expressed in the
1511 dataset. For each transcription factor and its corresponding module of genes that are
1512 positively correlated with it, SCENIC uses RcisTarget to perform motif enrichment
1513 analysis to identify the putative regulon for each transcription factor. RcisTarget was run
1514 with default settings and motif enrichment was calculated based on regions 500 bp
1515 upstream and 20 kb centered (10 kb upstream + 10kb downstream) around the
1516 transcription start site of each gene. Once a regulon is assigned for each transcription
1517 factor, SCENIC then calculates a score (AUC_{cell}) that represents the "activity" of each
1518 transcription factor within each cell based on the expression of the transcription factor
1519 and its target genes. Only transcription factors that were identified by SCENIC and also
1520 present in the list of annotated mouse transcription factors from AnimalTFDB database
1521 (<http://bioinfo.life.hust.edu.cn/AnimalTFDB/>) were included in the study.

1522

1523 **Gene set motif enrichment analysis**

1524 To identify motifs that are significantly enriched in a gene set, motif enrichment analysis
1525 was run with RcisTarget (version 1.3.5). Motif analysis was performed for 20 kb regions
1526 centered (10 kb upstream + 10kb downstream) around the transcription start site of each
1527 gene. RcisTarget assigns an enrichment score for each motif based on its frequency near

1528 the transcription start site of our input gene list compared to its average frequency in the
1529 genome. Enrichment scores for each motif were then normalized and motifs with
1530 normalized enrichment scores $> 3SD$ are considered enriched. The relative activity of the
1531 injury-induced transcription factors (see Figure 6B) was predicted by counting the motifs
1532 they are known to bind within the set of enriched motifs within a given input gene list (e.g.
1533 438 common injury-induced genes). Motif enrichment was performed on the set of
1534 common injury-induced genes (see Table S3) and cell-type-specific genes (see Table S6)
1535 as well as random gene sets. To calculate motif enrichment for random gene sets, motif
1536 analysis was averaged across 1000 sets of either 438 randomly selected expressed
1537 genes (to compare with common injury-induced genes) or 1240 randomly selected
1538 expressed genes (to compare with cell-type-specific genes).

1539

1540 **Bulk RNA-seq library preparation and sequencing**

1541 Total RNA was extracted from DRG tissue samples using TRIzol (ThermoFisher), and
1542 then purified using total RNA mini kit (Qiagen). Quality control assessment of these
1543 purified RNA samples was conducted using Bioanalyzer (Agilent) and the RNA integrity
1544 numbers (RIN) of all RNA samples submitted for sequencing were > 7 . RNA-sequencing
1545 was carried out using the NuGEN Ovation RNA Ultra Low Input kit and TruSeq Nano.
1546 Libraries were indexed and sequenced by HiSeq2500/HiSeq4000 with 69-bp paired end
1547 reads. Quality control (QC) was performed on base qualities and nucleotide composition
1548 of sequences, to identify problems in library preparation or sequencing. Reads were
1549 trimmed if necessary after the QC before input to the alignment stage. Reads were
1550 aligned to the Mouse mm10 reference genome (GRCm38.75) using the STAR spliced

1551 read aligner (ver 2.4.0). Average input read counts were 63.7M per sample and average
1552 percentage of uniquely aligned reads were 76.5%. Total counts of read-fragments aligned
1553 to known gene regions within the mouse (mm10) refSeq (refFlat ver 07.24.14) reference
1554 annotation are used as the basis for quantification of gene expression. Fragment counts
1555 were derived using HTSeq program (ver 0.6.0). Batch effect was removed using
1556 Bioconductor package ComBat and RUV (removal of unwanted variation). Differentially
1557 expressed genes were identified using the Bioconductor package edgeR (FDR \leq 0.1).
1558 Scripts used in the RNA sequencing analyses are available at
1559 <https://github.com/icnn/RNAseq-PIPELINE.git>.

1560

1561 **Behavioral Experiments**

1562 Mouse behavior experiments were performed as previously described (Ghasemlou et al.,
1563 2015; Latremoliere et al., 2018; Sakuma et al., 2016). Briefly, von Frey filaments were
1564 used to measure the mechanical sensitivity of ipsilateral mouse hindpaws by blinded
1565 experimenters. 50% von Frey thresholds were calculated using the Up-Down Reader
1566 (Gonzalez-Cano et al., 2018). Responses to pinprick stimulation of different parts of the
1567 ipsilateral hindpaw were recorded in the same animals by blinded experimenters at
1568 different time points following sciatic nerve crush as previously described (Sakuma et al.,
1569 2016).

1570

1571 **RNAScope *in situ* histochemistry**

1572 RNAScope fluorescence *in situ* hybridization (FISH) experiments were performed
1573 according to the manufacturer's instructions, using the RNAScope Multiplex Fluorescent

1574 kit (Advanced Cell Diagnostics (ACD)) for fresh frozen tissue, as previously described
1575 (Zeisel et al., 2018). Briefly, fresh frozen ipsilateral naive or injured L4 lumbar DRGs were
1576 dissected at various points after injury, fresh frozen and sectioned into 12 μm sections
1577 using a cryostat. *In situ* probes were ordered from ACD and multiplexed in the same
1578 permutations across quantified sections. Following FISH, some sections were imaged
1579 using a 20x widefield objective on an Olympus Slide Scanner microscope. In order to
1580 quantify marker gene expression, high resolution images of a single z-plane were
1581 obtained using a 60x oil immersion objective on a Perkin Elmer UltraView Spinning Disk
1582 confocal microscope.

1583

1584 **Fluorescence *in situ* hybridization quantification**

1585 L4 DRG section images from 3-6 mice per probe were used for quantification. All in-focus
1586 neurons were manually segmented by blinded scorers using *Tubb3* fluorescence. Images
1587 were then thresholded, puncta were automatically quantified using ImageJ and puncta
1588 counts per μm^2 per neuron compared across conditions. For sciatic crush sections (Fig
1589 S5N), cutoffs were set to the mean of *Atf3* puncta density in naive neurons plus 2 standard
1590 deviations, and neurons after crush are divided into *Atf3* high (injured, *Atf3* puncta density
1591 > cutoff) and *Atf3* low (uninjured, *Atf3* puncta density \leq cutoff) populations; for SpNT slides
1592 (Fig 2H), neurons were analyzed as one population. Then neurons with the most marker
1593 puncta density in each condition were selected for visualization and statistical tests in
1594 accordance with the relative abundance of naive neuronal cell types in the snRNA-seq
1595 data (top 9.28% of neurons were selected for marker *Th* (cLTMR), top 18.33% for *Tac1*
1596 (PEP), top 22.43% for *Mrgprd* (NP), top 21.51% for *Hapln4* (NF), and top 4.25% for *Sst*

1597 (SST). One-way analysis of variance (ANOVA) was carried out by calling `anova()` function
1598 in R to compare means in different conditions. As the ANOVA test is significant, Tukey
1599 Multiple Comparisons are conducted to compare between conditions by calling
1600 `TukeyHSD()` function in R.

1601

1602 **Western Blot**

1603 *Brn3a-Cre^{ERT2};Atf3f/f* mice were injected intraperitoneally with tamoxifen or vehicle. Two
1604 weeks after induction, the mice underwent sciatic nerve crush. Ipsilateral L3-5 DRGs were
1605 harvested from 4 mice (12 DRGs/mouse) 1 week after crush and pooled for protein
1606 extraction. The protein lysates were extracted in presence of a protease cocktail tablet
1607 (Roche Diagnostics) using Cell Lysis buffer (ThermoFisher). Cell debris was removed by
1608 centrifugation (4°C, 10 min) after homogenization. Protein concentrations were
1609 determined using the BCA protein assay kit (ThermoFisher). Equivalent amounts of
1610 protein were loaded and separated by 4-12% gradient SDS-PAGE and subsequently
1611 transferred to an Immobilon-P PVDF transfer membrane (EMD Millipore). Blots were
1612 blocked in 5% blotting-grade blocker (Bio-rad) in PBS for 20 min at room temperature
1613 (RT) and incubated with rabbit polyclonal antibodies against ATF3 (Santa Cruz, 1:500,
1614 RRID: AB_1078233), and Horseradish peroxidase (HRP)-conjugated mouse monoclonal
1615 antibody against GAPDH (Cell Signaling, 1:5000, RRID:AB_1642205) overnight. After
1616 washing 3 times with TBST (1% Tween-20), HRP-conjugated secondary antibody (anti-
1617 rabbit, ThermoFisher, 1: 20,000), a SuperSignal West Femto Maximum Sensitivity
1618 chemiluminescence ECL kit (ThermoFisher), and Amersham Hyperfilm ECL (GE

1619 Healthcare Life Sciences) were used for signal detection. Image signals were analyzed
1620 and quantified using ImageJ software (NIH).

1621

1622 **Immunohistochemistry**

1623 *Vglut2-Cre;Atf3f/f* and *Atf3f/f* mice underwent SpNT. Ipsilateral L4 DRGs were harvested
1624 1 week after SpNT from injured mice, immediately fixed with 4% PFA for 1 hr at 25°C and
1625 cryoprotected with 30% sucrose in PBS overnight. DRGs were sectioned into 12µm
1626 sections, which were blocked and permeabilized with 5% normal goat serum in 0.25%
1627 Triton X-100 in PBS (Roche Diagnostics) for 30 min at 25°C. Sections were incubated
1628 with rabbit polyclonal antibody against ATF3 (Sigma Aldrich; HPA001562; 1:1000) at 4°C
1629 overnight and then incubated with Alexa Fluor 488 goat antibody against rabbit IgG and
1630 Alexa Fluor 488 goat antibody against chicken IgG for 40 min at 25°C. Sections were then
1631 stained with 1:200 NeuroTrace 640/660 Deep-Red Fluorescent Nissl Stain (Thermo
1632 Fisher, N21483, RRID: AB_2572212) for 10 min and mounted with ProLong Gold Antifade
1633 Mountant with DAPI (Thermo Fisher, P36931). Slides were imaged using a 20x widefield
1634 objective on an Olympus Slide Scanner microscope. Images were thresholded and
1635 ATF3+ neurons quantified in ImageJ. Nissl+ DRG neurons were manually counted by
1636 blinded scorers. To quantify Nissl+ DRG neuron density, representative 360000 µm²
1637 sections of each *Vglut2-Cre;Atf3f/f* and *Atf3f/f* DRG image were selected for
1638 quantification.

1639

1640 **Data obtained from other sources**

1641 Embryonic DRG development data were obtained from GEO Accessions GSE98592,
1642 GSE77892, GSE77891, deposited by the GUDMAP Database Group. We performed
1643 differential expression analysis similar to that described above in edgeR to compare the
1644 expression profiles of RET+ E12.5, E14.5, E18.5 DRG neurons to adult RET+ DRGs.
1645 Briefly, genes with counts <10 were removed from differential expression. Differential
1646 expression was otherwise performed using the default settings (calcNormFactors,
1647 estimateCommonDisp(y), and estimateTagwiseDisp(y), and exactTest("adult DRG",
1648 "each embryonic time point"). Regeneration associated gene modules were obtained from
1649 (Chandran et al., 2016). Gene names were cleaned up by removing suffix, and genes not
1650 detected in our snRNA-seq data were excluded.

1651

1652 **Data Visualization**

1653 Plots were generated using R version 3.5.0 with ggplot2 package (version 3.2.0).
1654 Heatmaps were generated using gplots package (version 3.0.1.1).

1655

1656 **Statistics**

1657 Statistics were performed using R version 3.5.0. Hypergeometric tests were used to test
1658 the significance of overlap between two gene sets. It was conducted by calling phyper()
1659 function in R version 3.5.0. Permutation tests were used to estimate a *P* value for
1660 transcription factor motif enrichment by calculating the number of times out of 1000 the
1661 ATF3 motif enrichment was greater in a random set of genes than the experimental set
1662 of genes divided by 1000.

1663

1664 **Data availability**

1665 Processed data are available at www.painseq.com. Raw and processed data were also
1666 deposited within the Gene Expression Omnibus (GEO) repository
1667 (www.ncbi.nlm.nih.gov/geo) with an accession number (GSExxxxx). Custom R scripts are
1668 available upon request.

1669

1670 **Supplemental Tables:**

- 1671 - Table S1: Cell-type-specific gene expression in naive DRG nuclei.
- 1672 - Table S2: Differential expression analysis between injury/neuropathy models
1673 and naive nuclei at each time point after injury.
- 1674 - Table S3: Genes that are commonly upregulated across ≥ 5 neuronal subtypes
1675 after spinal nerve transection compared to their respective naive cell types.
- 1676 - Table S4: Genes that are upregulated in only 1 neuronal subtype after spinal
1677 nerve transection compared to their respective naive cell types.
- 1678 - Table S5: Common and cell-type-specific gene induction after spinal nerve
1679 transection, corresponding to heatmap in Figure 4D.
- 1680 - Table S6: Genes that are enriched in specific DRG neuronal subtypes in naive
1681 mice. These genes are used for cell-type-specificity score.
- 1682 - Table S7: *Atf3*-dependent gene regulation after sciatic nerve crush
- 1683 - Table S8: Differential gene expression between embryonic (E12.5, E14.5,
1684 E18.5) and adult DRG neurons

1685

1686

1687 **References**

- 1688 Abe, N., and Cavalli, V. (2008). Nerve injury signaling. *Current opinion in neurobiology*
1689 *18*, 276-283.
- 1690 Aguilera, C., Nakagawa, K., Sancho, R., Chakraborty, A., Hendrich, B., and Behrens, A.
1691 (2011). c-Jun N-terminal phosphorylation antagonises recruitment of the Mbd3/NuRD
1692 repressor complex. *Nature* *469*, 231-235.
- 1693 Aibar, S., Gonzalez-Blas, C.B., Moerman, T., Huynh-Thu, V.A., Imrichova, H.,
1694 Hulselmans, G., Rambow, F., Marine, J.C., Geurts, P., Aerts, J., *et al.* (2017). SCENIC:
1695 single-cell regulatory network inference and clustering. *Nature methods* *14*, 1083-1086.
- 1696 Bangash, M.A., Alles, S.R.A., Santana-Varela, S., Millet, Q., Sikandar, S., de Clauser, L.,
1697 Ter Heegde, F., Habib, A.M., Pereira, V., Sexton, J.E., *et al.* (2018). Distinct
1698 transcriptional responses of mouse sensory neurons in models of human chronic pain
1699 conditions. *Wellcome open research* *3*, 78.
- 1700 Berta, T., Perrin, F.E., Pertin, M., Tonello, R., Liu, Y.-C., Chamesian, A., Kato, A.C., Ji,
1701 R.-R., and Decosterd, I. (2017). Gene Expression Profiling of Cutaneous Injured and Non-
1702 Injured Nociceptors in SNI Animal Model of Neuropathic Pain. *Scientific Reports* *7*, 9367.
- 1703 Brouwer, M., Zhou, H., and Nadif Kasri, N. (2016). Choices for Induction of Pluripotency:
1704 Recent Developments in Human Induced Pluripotent Stem Cell Reprogramming
1705 Strategies. *Stem Cell Reviews and Reports* *12*, 54-72.
- 1706 Cattin, A.L., and Lloyd, A.C. (2016). The multicellular complexity of peripheral nerve
1707 regeneration. *Current opinion in neurobiology* *39*, 38-46.

1708 Chandran, V., Coppola, G., Nawabi, H., Omura, T., Versano, R., Huebner, E.A., Zhang,
1709 A., Costigan, M., Yekkirala, A., Barrett, L., *et al.* (2016). A Systems-Level Analysis of the
1710 Peripheral Nerve Intrinsic Axonal Growth Program. *Neuron* 89, 956-970.

1711 Chang, I.A., and Namgung, U. (2013). Induction of Regenerative Responses of Injured
1712 Sciatic Nerve by Pharmacopuncture Therapy in Rats. *Journal of Acupuncture and*
1713 *Meridian Studies* 6, 89-97.

1714 Chapman, C.R., and Vierck, C.J. (2017). The Transition of Acute Postoperative Pain to
1715 Chronic Pain: An Integrative Overview of Research on Mechanisms. *The journal of pain*
1716 *: official journal of the American Pain Society* 18, 359.e351-359.e338.

1717 Chen, H., Hu, Y., Xie, K., Chen, Y., Wang, H., Bian, Y., Wang, Y., Dong, A., and Yu, Y.
1718 (2018). Effect of autophagy on allodynia, hyperalgesia and astrocyte activation in a rat
1719 model of neuropathic pain. *Int J Mol Med* 42, 2009-2019.

1720 Chiu, I.M., Barrett, L.B., Williams, E.K., Strohlic, D.E., Lee, S., Weyer, A.D., Lou, S.,
1721 Bryman, G.S., Roberson, D.P., Ghasemlou, N., *et al.* (2014). Transcriptional profiling at
1722 whole population and single cell levels reveals somatosensory neuron molecular
1723 diversity. *eLife* 3.

1724 Collins, K.L., Russell, H.G., Schumacher, P.J., Robinson-Freeman, K.E., O'Connor, E.C.,
1725 Gibney, K.D., Yambem, O., Dykes, R.W., Waters, R.S., and Tsao, J.W. (2018). A review
1726 of current theories and treatments for phantom limb pain. *The Journal of clinical*
1727 *investigation* 128, 2168-2176.

1728 Colloca, L., Ludman, T., Bouhassira, D., Baron, R., Dickenson, A.H., Yarnitsky, D.,
1729 Freeman, R., Truini, A., Attal, N., Finnerup, N.B., *et al.* (2017). Neuropathic pain. *Nature*
1730 *Reviews Disease Primers* 3, 17002.

1731 Costigan, M., Befort, K., Karchewski, L., Griffin, R.S., D'Urso, D., Allchorne, A., Sitarski,
1732 J., Mannion, J.W., Pratt, R.E., and Woolf, C.J. (2002). Replicate high-density rat genome
1733 oligonucleotide microarrays reveal hundreds of regulated genes in the dorsal root
1734 ganglion after peripheral nerve injury. *BMC neuroscience* 3, 16.

1735 Duan, J., Li, B., Bhakta, M., Xie, S., Zhou, P., Munshi, N.V., and Hon, G.C. (2019).
1736 Rational Reprogramming of Cellular States by Combinatorial Perturbation. *Cell reports*
1737 27, 3486-3499.e3486.

1738 Frey, E., Valakh, V., Karney-Grobe, S., Shi, Y., Milbrandt, J., and DiAntonio, A. (2015).
1739 An in vitro assay to study induction of the regenerative state in sensory neurons. *Exp*
1740 *Neurol* 263, 350-363.

1741 Fukuoka, T., Yamanaka, H., Kobayashi, K., Okubo, M., Miyoshi, K., Dai, Y., and Noguchi,
1742 K. (2012). Re-evaluation of the phenotypic changes in L4 dorsal root ganglion neurons
1743 after L5 spinal nerve ligation. *Pain* 153, 68-79.

1744 Gatto, G., Smith, K.M., Ross, S.E., and Goulding, M. (2019). Neuronal diversity in the
1745 somatosensory system: bridging the gap between cell type and function. *Current opinion*
1746 *in neurobiology* 56, 167-174.

1747 Gey, M., Wanner, R., Schilling, C., Pedro, M.T., Sinske, D., and Knoll, B. (2016). Atf3
1748 mutant mice show reduced axon regeneration and impaired regeneration-associated
1749 gene induction after peripheral nerve injury. *Open biology* 6.

1750 Ghasemlou, N., Chiu, I.M., Julien, J.-P., and Woolf, C.J. (2015). CD11b+Ly6G- myeloid
1751 cells mediate mechanical inflammatory pain hypersensitivity. *Proc Natl Acad Sci U S A*
1752 112, E6808-E6817.

1753 Gonzalez-Cano, R., Boivin, B., Bullock, D., Cornelissen, L., Andrews, N., and Costigan,
1754 M. (2018). Up–Down Reader: An Open Source Program for Efficiently Processing 50%
1755 von Frey Thresholds. *Frontiers in Pharmacology* 9.

1756 Gosselin, R.-D., Suter, M.R., Ji, R.-R., and Decosterd, I. (2010). Glial cells and chronic
1757 pain. *The Neuroscientist* 16, 519-531.

1758 Harel, N.Y., and Strittmatter, S.M. (2006). Can regenerating axons recapitulate
1759 developmental guidance during recovery from spinal cord injury? *Nature Reviews*
1760 *Neuroscience* 7, 603-616.

1761 Haroutounian, S., Nikolajsen, L., Bendtsen, T.F., Finnerup, N.B., Kristensen, A.D.,
1762 Hasselstrom, J.B., and Jensen, T.S. (2014). Primary afferent input critical for maintaining
1763 spontaneous pain in peripheral neuropathy. *Pain* 155, 1272-1279.

1764 Hart, A.M., Brannstrom, T., Wiberg, M., and Terenghi, G. (2002). Primary sensory
1765 neurons and satellite cells after peripheral axotomy in the adult rat. *Experimental brain*
1766 *research* 142, 308-318.

1767 He, Z., and Jin, Y. (2016). Intrinsic Control of Axon Regeneration. *Neuron* 90, 437-451.

1768 Herdegen, T., Fiallos-Estrada, C.E., Schmid, W., Bravo, R., and Zimmermann, M. (1992).
1769 The transcription factors c-JUN, JUN D and CREB, but not FOS and KROX-24, are
1770 differentially regulated in axotomized neurons following transection of rat sciatic nerve.
1771 *Molecular brain research* 14, 155-165.

1772 Hrvatin, S., Hochbaum, D.R., Nagy, M.A., Cicconet, M., Robertson, K., Cheadle, L.,
1773 Zilionis, R., Ratner, A., Borges-Monroy, R., Klein, A.M., *et al.* (2018). Single-cell analysis
1774 of experience-dependent transcriptomic states in the mouse visual cortex. *Nature*
1775 *neuroscience* 21, 120-129.

- 1776 Hunt, D., Raivich, G., and Anderson, P.N. (2012). Activating transcription factor 3 and the
1777 nervous system. *Frontiers in molecular neuroscience* 5, 7-7.
- 1778 Jager, S.B., Pallesen, L.T., and Vaegter, C.B. (2018). Isolation of satellite glial cells for
1779 high-quality RNA purification. *Journal of neuroscience methods* 297, 1-8.
- 1780 Jaggi, A.S., Jain, V., and Singh, N. (2011). Animal models of neuropathic pain.
1781 *Fundamental & Clinical Pharmacology* 25, 1-28.
- 1782 Jessen, K., and Mirsky, R. (2016). The repair Schwann cell and its function in
1783 regenerating nerves. *The Journal of physiology* 594, 3521-3531.
- 1784 Ji, R.-R., Chamesian, A., and Zhang, Y.-Q. (2016). Pain regulation by non-neuronal cells
1785 and inflammation. *Science* 354, 572.
- 1786 Jia, L., Chopp, M., Wang, L., Lu, X., Zhang, Y., Szalad, A., and Zhang, Z.G. (2018). MiR-
1787 34a Regulates Axonal Growth of Dorsal Root Ganglia Neurons by Targeting FOXP2 and
1788 VAT1 in Postnatal and Adult Mouse. *Mol Neurobiol* 55, 9089-9099.
- 1789 Jing, X., Wang, T., Huang, S., Glorioso, J.C., and Albers, K.M. (2012). The transcription
1790 factor Sox11 promotes nerve regeneration through activation of the regeneration-
1791 associated gene *Sprr1a*. *Exp Neurol* 233, 221-232.
- 1792 Kataoka, K., Kanje, M., and Dahlin, L.B. (2007). Induction of activating transcription factor
1793 3 after different sciatic nerve injuries in adult rats. *Scandinavian Journal of Plastic and*
1794 *Reconstructive Surgery and Hand Surgery* 41, 158-166.
- 1795 Kim, K.K., Adelstein, R.S., and Kawamoto, S. (2009). Identification of neuronal nuclei
1796 (NeuN) as Fox-3, a new member of the Fox-1 gene family of splicing factors. *The Journal*
1797 *of biological chemistry* 284, 31052-31061.

1798 Klein, A.M., Mazutis, L., Akartuna, I., Tallapragada, N., Veres, A., Li, V., Peshkin, L.,
1799 Weitz, D.A., and Kirschner, M.W. (2015). Droplet barcoding for single-cell transcriptomics
1800 applied to embryonic stem cells. *Cell* 161, 1187-1201.

1801 Kupari, J., Haring, M., Agirre, E., Castelo-Branco, G., and Ernfors, P. (2019). An Atlas of
1802 Vagal Sensory Neurons and Their Molecular Specialization. *Cell reports* 27, 2508-
1803 2523.e2504.

1804 Lacar, B., Linker, S.B., Jaeger, B.N., Krishnaswami, S.R., Barron, J.J., Kelder, M.J.E.,
1805 Parylak, S.L., Paquola, A.C.M., Venepally, P., Novotny, M., *et al.* (2016). Nuclear RNA-
1806 seq of single neurons reveals molecular signatures of activation. *Nature Communications*
1807 7, 11022.

1808 LaCroix-Fralish, M.L., Austin, J.S., Zheng, F.Y., Levitin, D.J., and Mogil, J.S. (2011).
1809 Patterns of pain: meta-analysis of microarray studies of pain. *Pain* 152, 1888-1898.

1810 Laedermann, C.J., Pertin, M., Suter, M.R., and Decosterd, I. (2014). Voltage-gated
1811 sodium channel expression in mouse DRG after SNI leads to re-evaluation of projections
1812 of injured fibers. *Mol Pain* 10, 19.

1813 Latremoliere, A., Cheng, L., DeLisle, M., Wu, C., Chew, S., Hutchinson, E.B., Sheridan,
1814 A., Alexandre, C., Latremoliere, F., Sheu, S.H., *et al.* (2018). Neuronal-Specific TUBB3
1815 Is Not Required for Normal Neuronal Function but Is Essential for Timely Axon
1816 Regeneration. *Cell reports* 24, 1865-1879.e1869.

1817 Le Pichon, C.E., and Chesler, A.T. (2014). The functional and anatomical dissection of
1818 somatosensory subpopulations using mouse genetics. *Frontiers in neuroanatomy* 8, 21.

1819 Lee, B., Cho, H., Jung, J., Yang, Y.D., Yang, D.-J., and Oh, U. (2014). Anoctamin 1
1820 contributes to inflammatory and nerve-injury induced hypersensitivity. *Mol Pain* 10, 5.

- 1821 Lindwall, C., Dahlin, L., Lundborg, G., and Kanje, M. (2004). Inhibition of c-Jun
1822 phosphorylation reduces axonal outgrowth of adult rat nodose ganglia and dorsal root
1823 ganglia sensory neurons. *Molecular and Cellular Neuroscience* 27, 267-279.
- 1824 Lisi, V., Singh, B., Giroux, M., Guzman, E., Painter, M.W., Cheng, Y.C., Huebner, E.,
1825 Coppola, G., Costigan, M., Woolf, C.J., *et al.* (2017). Enhanced Neuronal Regeneration
1826 in the CAST/Ei Mouse Strain Is Linked to Expression of Differentiation Markers after
1827 Injury. *Cell reports* 20, 1136-1147.
- 1828 Liu, X., Eschenfelder, S., Blenk, K.-H., Jänig, W., and Häbler, H.-J. (2000). Spontaneous
1829 activity of axotomized afferent neurons after L5 spinal nerve injury in rats. *PAIN®* 84, 309-
1830 318.
- 1831 Ma, C.H.E., Omura, T., Cobos, E.J., Latrémolière, A., Ghasemlou, N., Brenner, G.J., van
1832 Veen, E., Barrett, L., Sawada, T., Gao, F., *et al.* (2011). Accelerating axonal growth
1833 promotes motor recovery after peripheral nerve injury in mice. *The Journal of clinical*
1834 *investigation* 121, 4332-4347.
- 1835 Mahar, M., and Cavalli, V. (2018). Intrinsic mechanisms of neuronal axon regeneration.
1836 *Nat Rev Neurosci* 19, 323-337.
- 1837 Michaelevski, I., Segal-Ruder, Y., Rozenbaum, M., Medzihradzky, K.F., Shalem, O.,
1838 Coppola, G., Horn-Saban, S., Ben-Yaakov, K., Dagan, S.Y., Rishal, I., *et al.* (2010).
1839 Signaling to transcription networks in the neuronal retrograde injury response. *Science*
1840 *signaling* 3, ra53.
- 1841 Mo, A., Mukamel, E.A., Davis, F.P., Luo, C., Henry, G.L., Picard, S., Urich, M.A., Nery,
1842 J.R., Sejnowski, T.J., Lister, R., *et al.* (2015). Epigenomic Signatures of Neuronal
1843 Diversity in the Mammalian Brain. *Neuron* 86, 1369-1384.

1844 Navarro, X., Verdú, E., and Butí, M. (1994). Comparison of Regenerative and
1845 Reinnervating Capabilities of Different Functional Types of Nerve Fibers. *Exp Neurol* 129,
1846 217-224.

1847 Nguyen, M.Q., Le Pichon, C.E., and Ryba, N. (2019). Stereotyped transcriptomic
1848 transformation of somatosensory neurons in response to injury. *eLife* 8.

1849 Ogawa, N., Kawai, H., Terashima, T., Kojima, H., Oka, K., Chan, L., and Maegawa, H.
1850 (2014). Gene therapy for neuropathic pain by silencing of TNF-alpha expression with
1851 lentiviral vectors targeting the dorsal root ganglion in mice. *PLoS one* 9, e92073.

1852 Parsadanian, A., Pan, Y., Li, W., Myckatyn, T.M., and Brakefield, D. (2006). Astrocyte-
1853 derived transgene GDNF promotes complete and long-term survival of adult facial
1854 motoneurons following avulsion and differentially regulates the expression of transcription
1855 factors of AP-1 and ATF/CREB families. *Exp Neurol* 200, 26-37.

1856 Patel, R., Montagut-Bordas, C., and Dickenson, A.H. (2018). Calcium channel modulation
1857 as a target in chronic pain control. *Br J Pharmacol* 175, 2173-2184.

1858 Patodia, S., and Raivich, G. (2012). Role of transcription factors in peripheral nerve
1859 regeneration. *Frontiers in molecular neuroscience* 5, 8.

1860 Perkins, J.R., Antunes-Martins, A., Calvo, M., Grist, J., Rust, W., Schmid, R., Hildebrandt,
1861 T., Kohl, M., Orengo, C., McMahon, S.B., *et al.* (2014). A comparison of RNA-seq and
1862 exon arrays for whole genome transcription profiling of the L5 spinal nerve transection
1863 model of neuropathic pain in the rat. *Mol Pain* 10, 7-7.

1864 Raivich, G., Bohatschek, M., Da Costa, C., Iwata, O., Galiano, M., Hristova, M., Nateri,
1865 A.S., Makwana, M., Riera-Sans, L., Wolfer, D.P., *et al.* (2004). The AP-1 transcription
1866 factor c-Jun is required for efficient axonal regeneration. *Neuron* 43, 57-67.

1867 Renthall, W., Boxer, L.D., Hrvatin, S., Li, E., Silberfeld, A., Nagy, M.A., Griffith, E.C.,
1868 Vierbuchen, T., and Greenberg, M.E. (2018). Characterization of human mosaic Rett
1869 syndrome brain tissue by single-nucleus RNA sequencing. *Nature neuroscience* 21,
1870 1670-1679.

1871 Renthall, W., Carle, T.L., Maze, I., Covington, H.E., 3rd, Truong, H.T., Alibhai, I., Kumar,
1872 A., Montgomery, R.L., Olson, E.N., and Nestler, E.J. (2008). Delta FosB mediates
1873 epigenetic desensitization of the c-fos gene after chronic amphetamine exposure. *The*
1874 *Journal of neuroscience : the official journal of the Society for Neuroscience* 28, 7344-
1875 7349.

1876 Rigaud, M., Gemes, G., Barabas, M.-E., Chernoff, D.I., Abram, S.E., Stucky, C.L., and
1877 Hogan, Q.H. (2008). Species and strain differences in rodent sciatic nerve anatomy:
1878 implications for studies of neuropathic pain. *Pain* 136, 188-201.

1879 Ronquist, S., Patterson, G., Muir, L.A., Lindsly, S., Chen, H., Brown, M., Wicha, M.S.,
1880 Bloch, A., Brockett, R., and Rajapakse, I. (2017). Algorithm for cellular reprogramming.
1881 *Proceedings of the National Academy of Sciences* 114, 11832.

1882 Sakuma, M., Gorski, G., Sheu, S.H., Lee, S., Barrett, L.B., Singh, B., Omura, T.,
1883 Latremoliere, A., and Woolf, C.J. (2016). Lack of motor recovery after prolonged
1884 denervation of the neuromuscular junction is not due to regenerative failure. *The*
1885 *European journal of neuroscience* 43, 451-462.

1886 Satija, R., Farrell, J.A., Gennert, D., Schier, A.F., and Regev, A. (2015). Spatial
1887 reconstruction of single-cell gene expression data. *Nature biotechnology* 33, 495-502.

1888 Scheib, J., and Höke, A. (2013). Advances in peripheral nerve regeneration. *Nature*
1889 *Reviews Neurology* 9, 668.

1890 Schmid, D., Zeis, T., Sobrio, M., and Schaeren-Wiemers, N. (2014). MAL overexpression
1891 leads to disturbed expression of genes that influence cytoskeletal organization and
1892 differentiation of Schwann cells. *ASN Neuro* 6, 1759091414548916.

1893 Seiffers, R., Allchorne, A.J., and Woolf, C.J. (2006). The transcription factor ATF-3
1894 promotes neurite outgrowth. *Molecular and cellular neurosciences* 32, 143-154.

1895 Seiffers, R., Mills, C.D., and Woolf, C.J. (2007). ATF3 increases the intrinsic growth state
1896 of DRG neurons to enhance peripheral nerve regeneration. *The Journal of neuroscience*
1897 : the official journal of the Society for Neuroscience 27, 7911-7920.

1898 Serra, J., Bostock, H., Sola, R., Aleu, J., Garcia, E., Cokic, B., Navarro, X., and Quiles,
1899 C. (2012). Microneurographic identification of spontaneous activity in C-nociceptors in
1900 neuropathic pain states in humans and rats. *Pain* 153, 42-55.

1901 Shortland, P.J., Baytug, B., Krzyzanowska, A., McMahon, S.B., Priestley, J.V., and
1902 Averill, S. (2006). ATF3 expression in L4 dorsal root ganglion neurons after L5 spinal
1903 nerve transection. *The European journal of neuroscience* 23, 365-373.

1904 Sonesson, C., and Robinson, M.D. (2018). Bias, robustness and scalability in single-cell
1905 differential expression analysis. *Nature methods* 15, 255-261.

1906 Stavoe, A.K., Gopal, P.P., Gubas, A., Tooze, S.A., and Holzbaur, E.L. (2019). Expression
1907 of WIPI2B counteracts age-related decline in autophagosome biogenesis in neurons.
1908 *eLife* 8, e44219.

1909 Stevens, A.R., Ahmed, U., Vigneswara, V., and Ahmed, Z. (2019). Pigment Epithelium-
1910 Derived Factor Promotes Axon Regeneration and Functional Recovery After Spinal Cord
1911 Injury. *Molecular Neurobiology*.

- 1912 Swett, J.E., Hong, C.Z., and Miller, P.G. (1995). Most dorsal root ganglion neurons of the
1913 adult rat survive nerve crush injury. *Somatosensory & motor research* *12*, 177-189.
- 1914 Tandrup, T., Woolf, C.J., and Coggeshall, R.E. (2000). Delayed loss of small dorsal root
1915 ganglion cells after transection of the rat sciatic nerve. *Journal of Comparative Neurology*
1916 *422*, 172-180.
- 1917 Toma, W., Kyte, S.L., Bagdas, D., Alkhlaif, Y., Alsharari, S.D., Lichtman, A.H., Chen, Z.J.,
1918 Del Fabbro, E., Bigbee, J.W., Gewirtz, D.A., *et al.* (2017). Effects of paclitaxel on the
1919 development of neuropathy and affective behaviors in the mouse. *Neuropharmacology*
1920 *117*, 305-315.
- 1921 Tsantoulas, C., and McMahon, S.B. (2014). Opening paths to novel analgesics: the role
1922 of potassium channels in chronic pain. *Trends in neurosciences* *37*, 146-158.
- 1923 Tsujino, H., Kondo, E., Fukuoka, T., Dai, Y., Tokunaga, A., Miki, K., Yonenobu, K., Ochi,
1924 T., and Noguchi, K. (2000). Activating Transcription Factor 3 (ATF3) Induction by
1925 Axotomy in Sensory and Motoneurons: A Novel Neuronal Marker of Nerve Injury.
1926 *Molecular and Cellular Neuroscience* *15*, 170-182.
- 1927 Tuszynski, M.H., and Steward, O. (2012). Concepts and methods for the study of axonal
1928 regeneration in the CNS. *Neuron* *74*, 777-791.
- 1929 Usoskin, D., Furlan, A., Islam, S., Abdo, H., Lonnerberg, P., Lou, D., Hjerling-Leffler, J.,
1930 Haeggstrom, J., Kharchenko, O., Kharchenko, P.V., *et al.* (2015). Unbiased classification
1931 of sensory neuron types by large-scale single-cell RNA sequencing. *Nature neuroscience*
1932 *18*, 145-153.
- 1933 Velasco, R., and Bruna, J. (2015). Taxane-Induced Peripheral Neurotoxicity. *Toxics* *3*,
1934 152-169.

- 1935 Vilceanu, D., Honore, P., Hogan, Q.H., and Stucky, C.L. (2010). Spinal Nerve Ligation in
1936 Mouse Upregulates TRPV1 Heat Function in Injured IB4-Positive Nociceptors. *The*
1937 *Journal of Pain* 11, 588-599.
- 1938 Vogelaar, C.F., Vrinten, D.H., Hoekman, M.F.M., Brakkee, J.H., Burbach, J.P.H., and
1939 Hamers, F.P.T. (2004). Sciatic nerve regeneration in mice and rats: recovery of sensory
1940 innervation is followed by a slowly retreating neuropathic pain-like syndrome. *Brain*
1941 *Research* 1027, 67-72.
- 1942 Woolf, C.J., Reynolds, M.L., Molander, C., O'Brien, C., Lindsay, R.M., and benowitz, L.I.
1943 (1990). The growth-associated protein gap-43 appears in dorsal root ganglion cells and
1944 in the dorsal horn of the rat spinal cord following peripheral nerve injury. *Neuroscience*
1945 34, 465-478.
- 1946 Wu, Y.E., Pan, L., Zuo, Y., Li, X., and Hong, W. (2017). Detecting Activated Cell
1947 Populations Using Single-Cell RNA-Seq. *Neuron* 96, 313-329.e316.
- 1948 Xiao, H.-S., Huang, Q.-H., Zhang, F.-X., Bao, L., Lu, Y.-J., Guo, C., Yang, L., Huang, W.-
1949 J., Fu, G., Xu, S.-H., *et al.* (2002). Identification of gene expression profile of dorsal root
1950 ganglion in the rat peripheral axotomy model of neuropathic pain. *Proceedings of the*
1951 *National Academy of Sciences* 99, 8360.
- 1952 Xie, W., Strong, J.A., and Zhang, J.M. (2017). Active Nerve Regeneration with Failed
1953 Target Reinnervation Drives Persistent Neuropathic Pain. *eNeuro* 4.
- 1954 Zeisel, A., Hochgerner, H., Lonnerberg, P., Johnsson, A., Memic, F., van der Zwan, J.,
1955 Haring, M., Braun, E., Borm, L.E., La Manno, G., *et al.* (2018). Molecular Architecture of
1956 the Mouse Nervous System. *Cell* 174, 999-1014.e1022.

1957 Zhang, H., and Dougherty, P.M. (2014). Enhanced excitability of primary sensory neurons
1958 and altered gene expression of neuronal ion channels in dorsal root ganglion in paclitaxel-
1959 induced peripheral neuropathy. *Anesthesiology* 120, 1463-1475.

1960 Zheng, Y., Liu, P., Bai, L., Trimmer, J.S., Bean, B.P., and Ginty, D.D. (2019). Deep
1961 Sequencing of Somatosensory Neurons Reveals Molecular Determinants of Intrinsic
1962 Physiological Properties. *Neuron*.

1963

1964

Figure 1

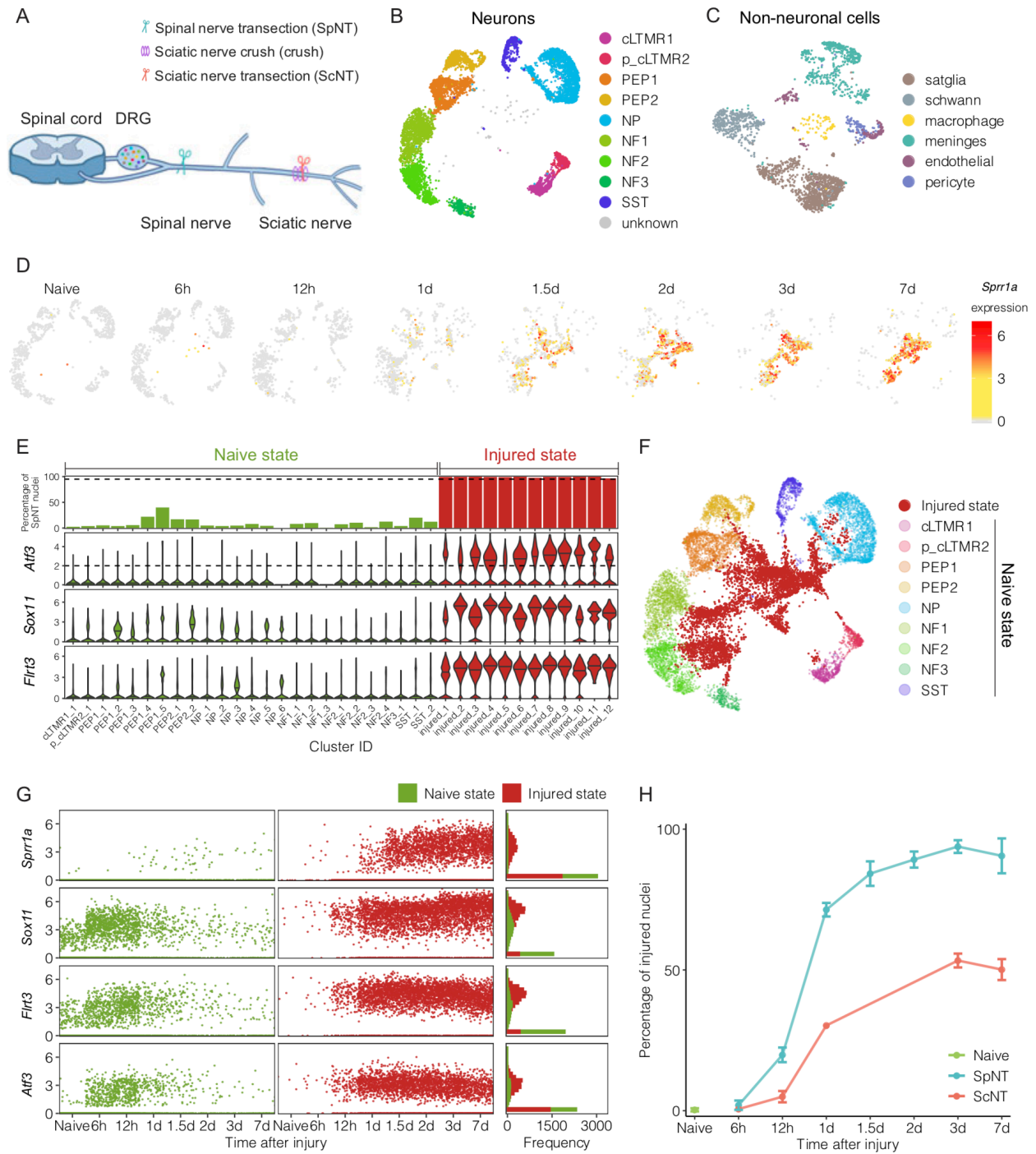


Figure 2

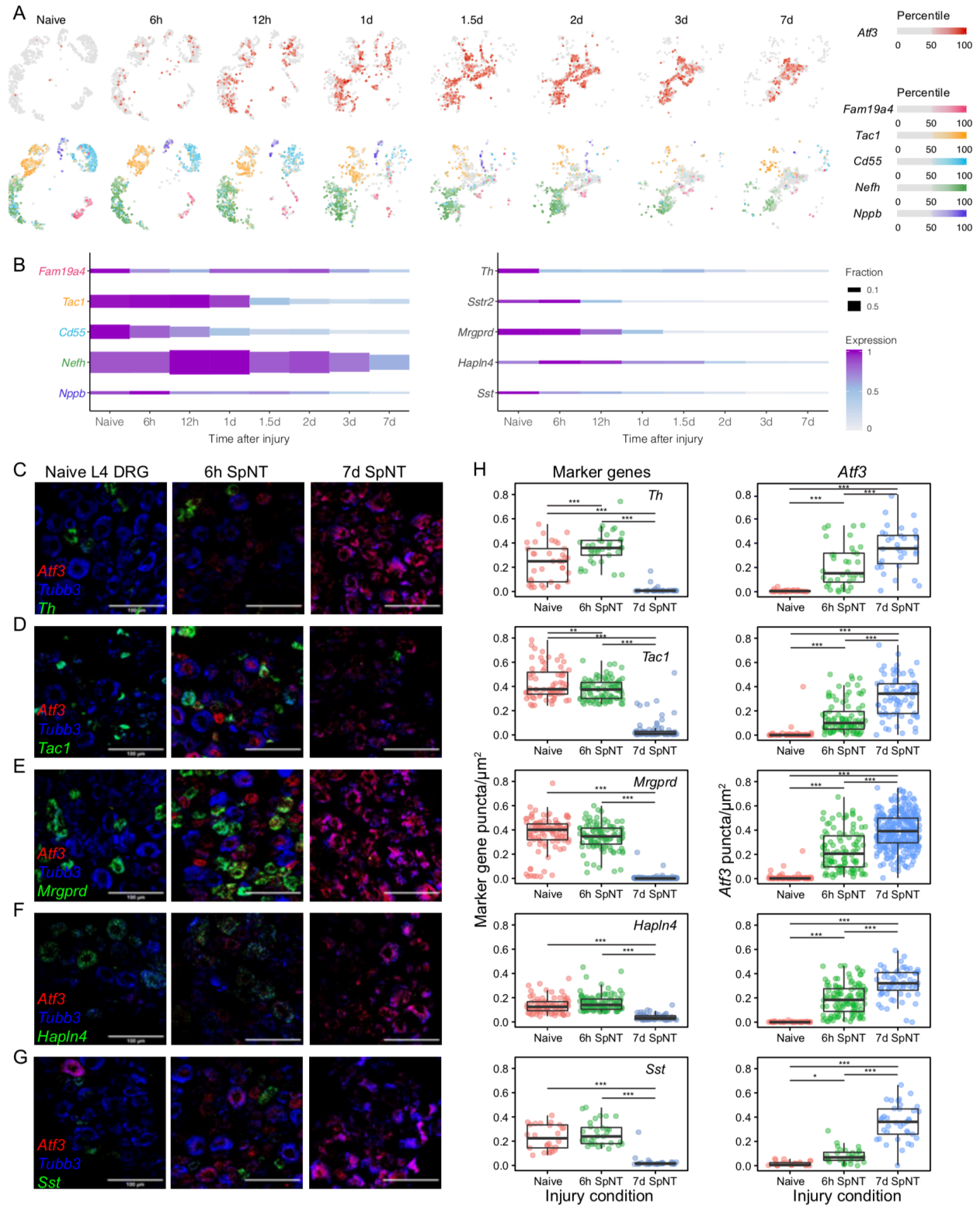


Figure 3

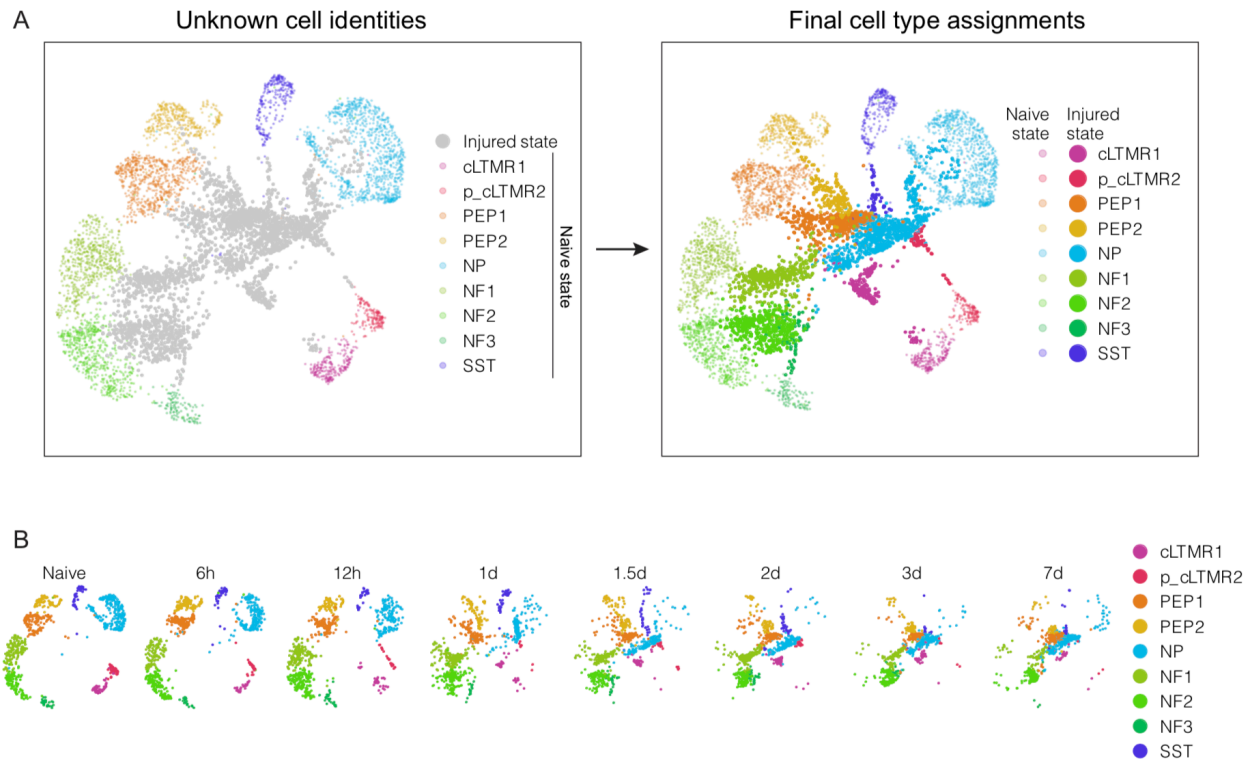


Figure 4

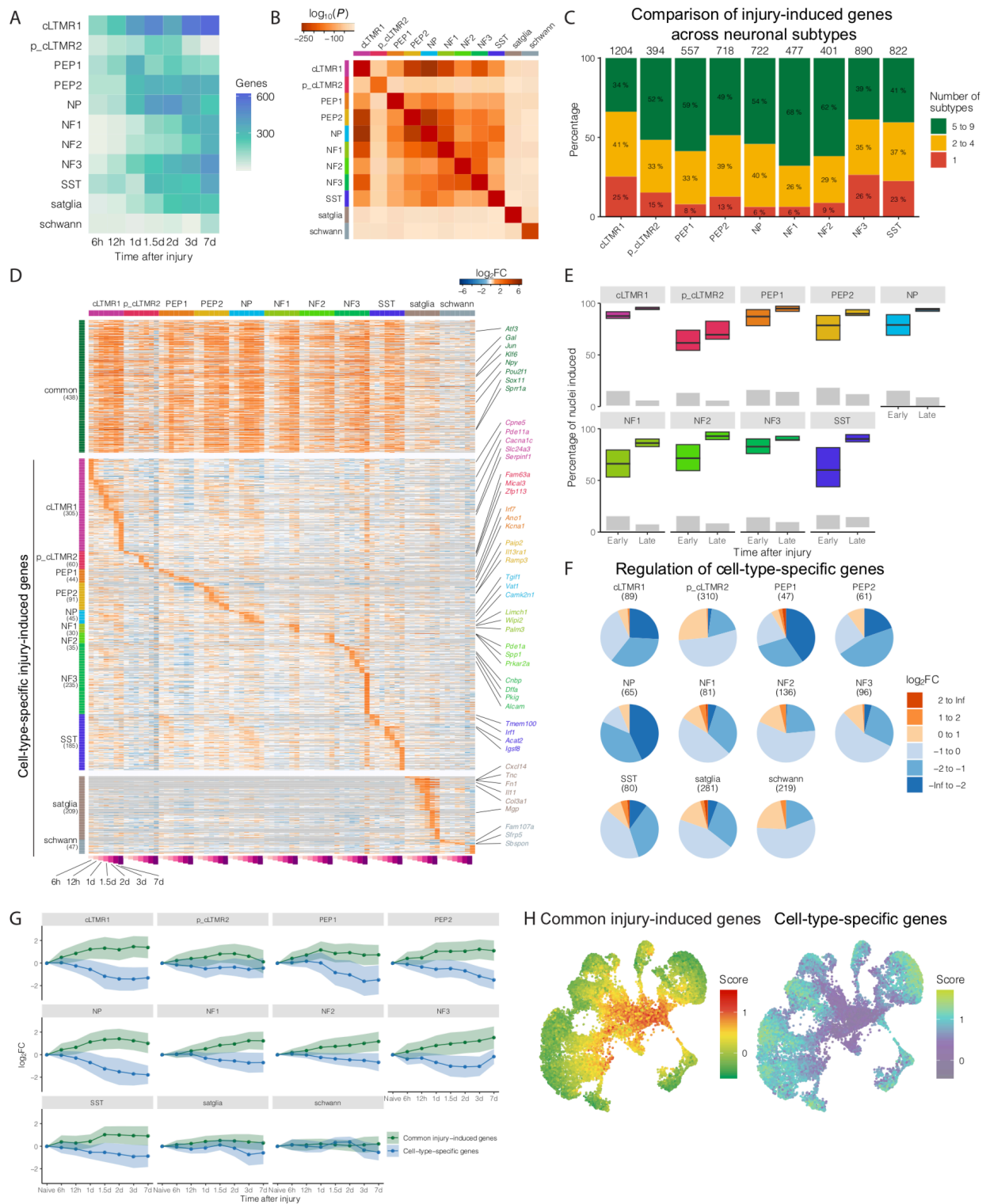


Figure 5

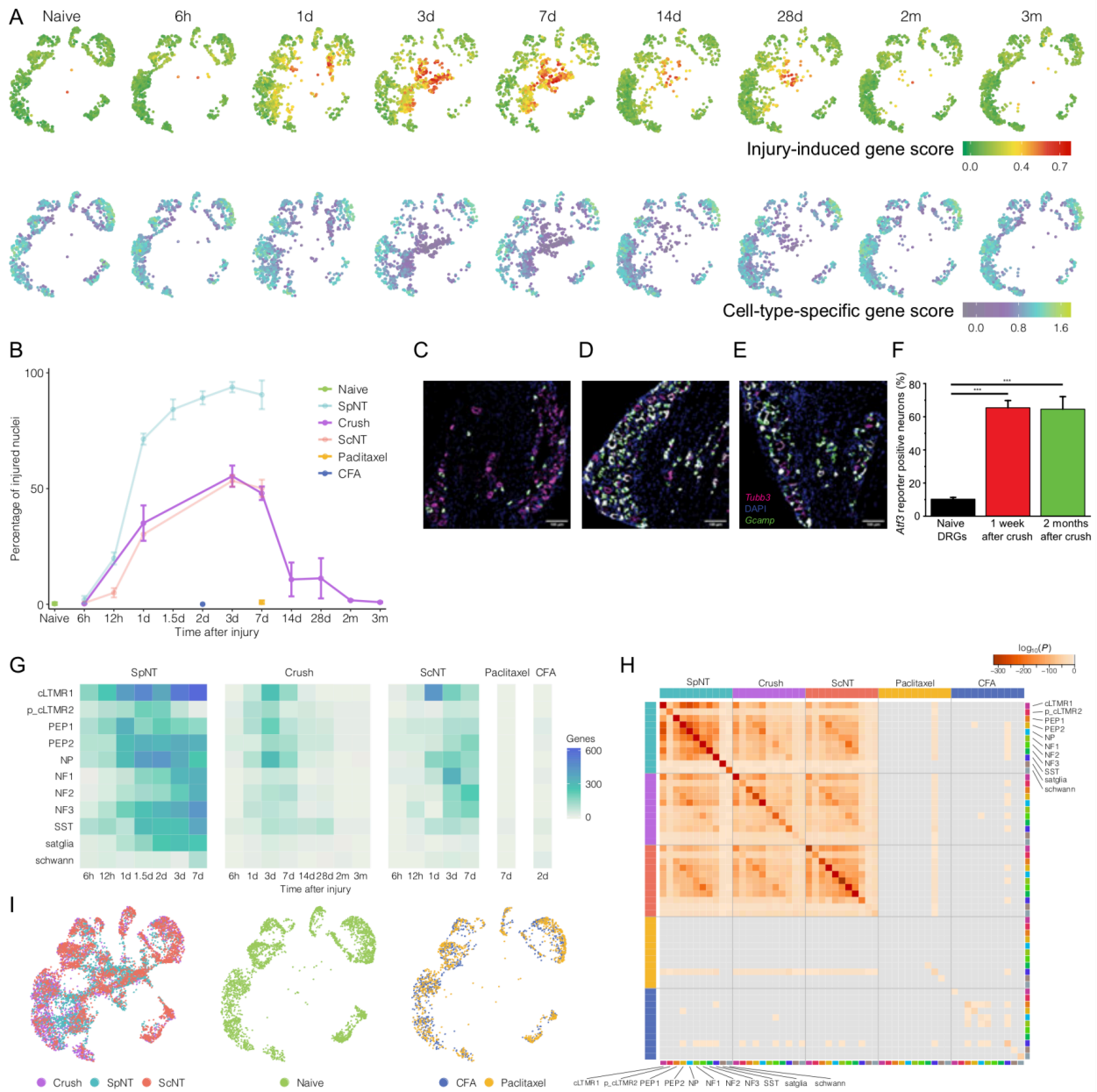


Figure 6

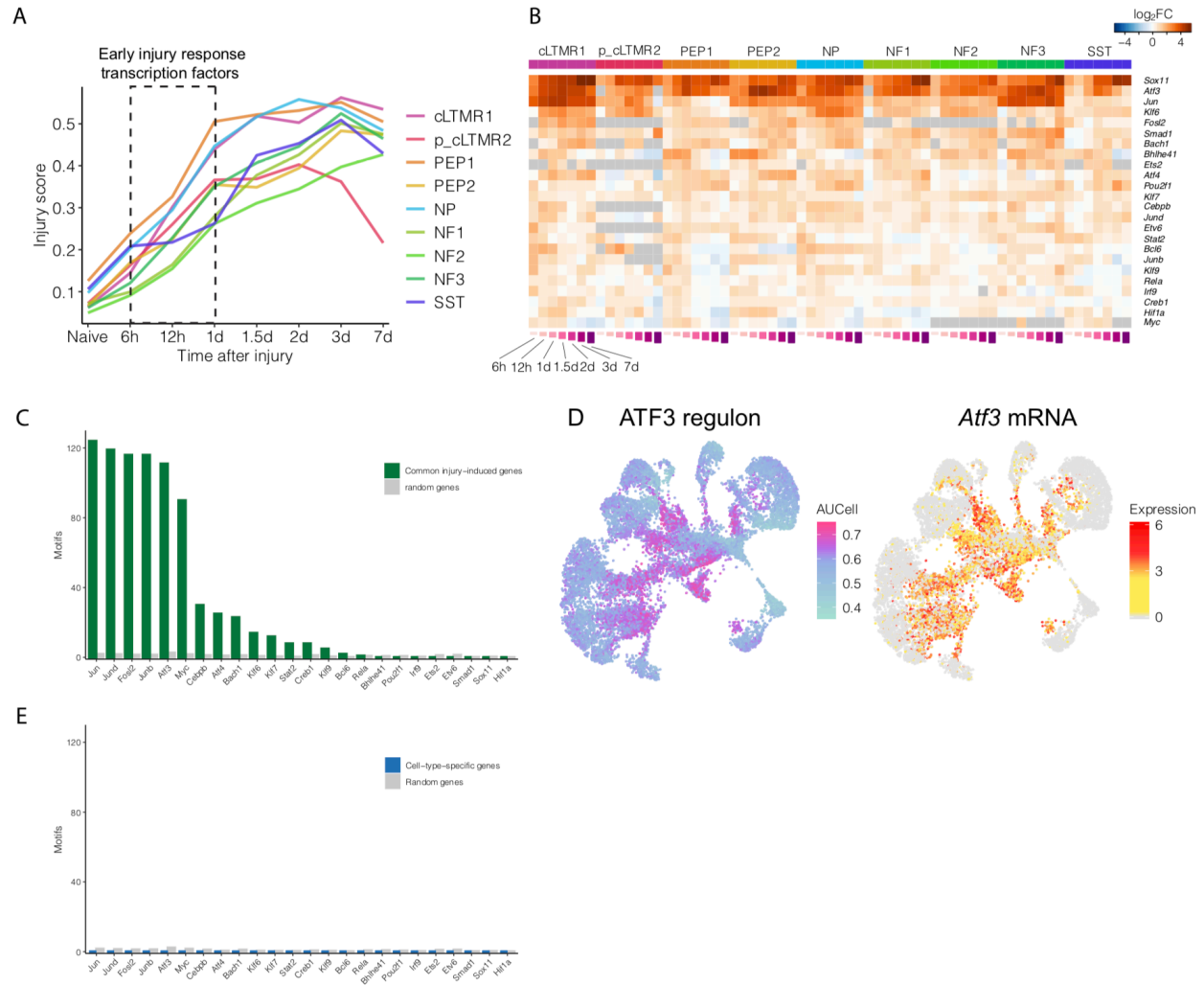
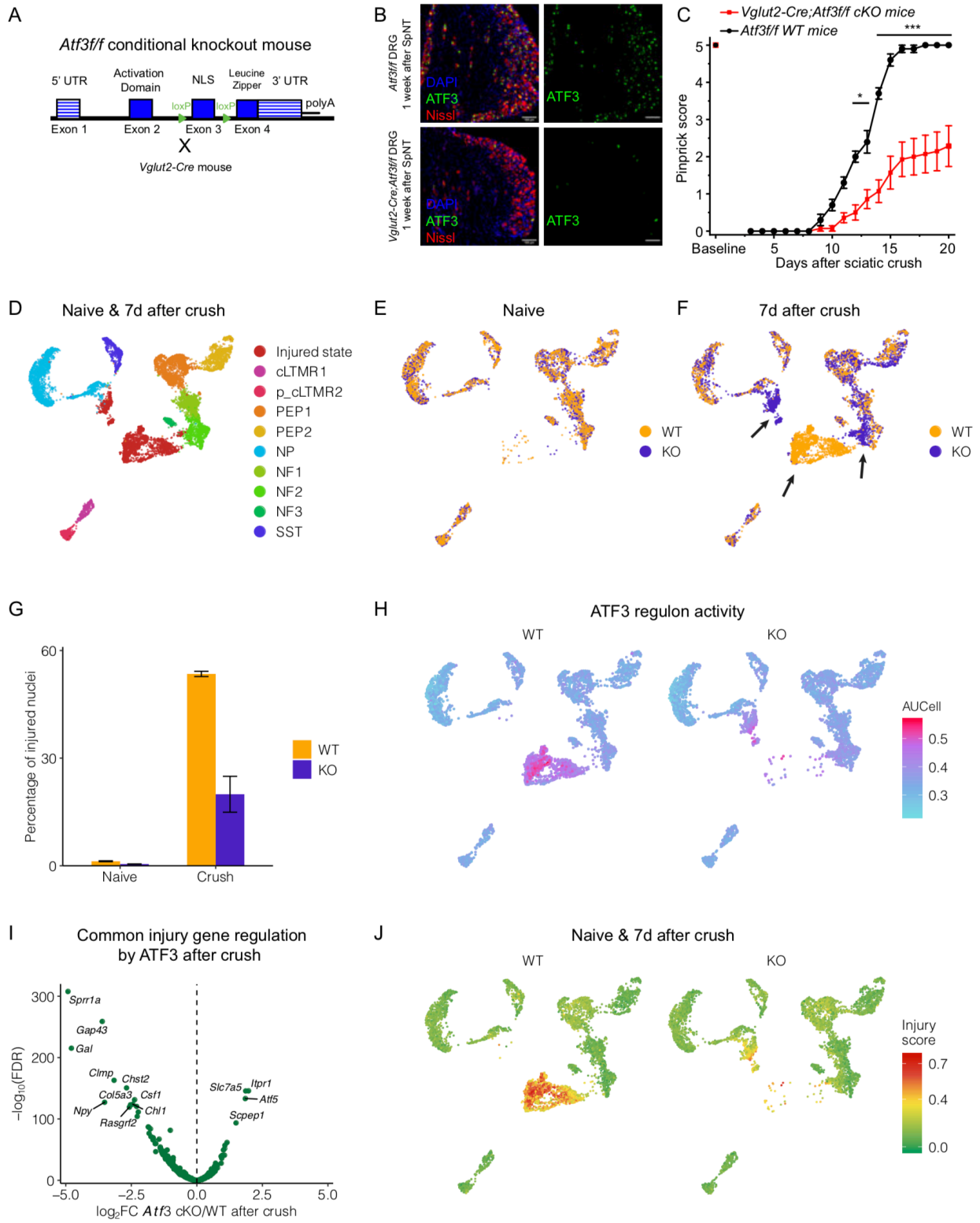
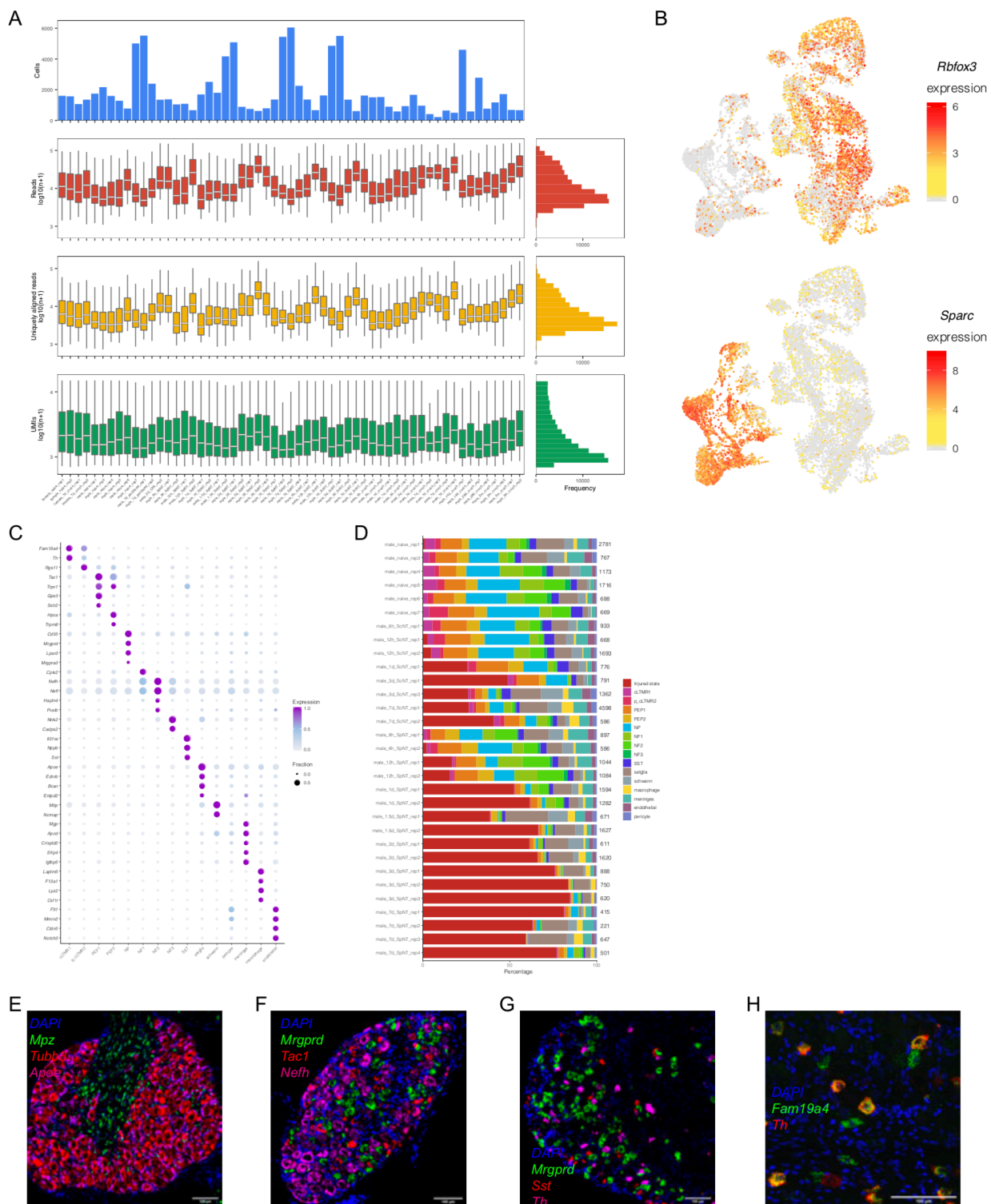


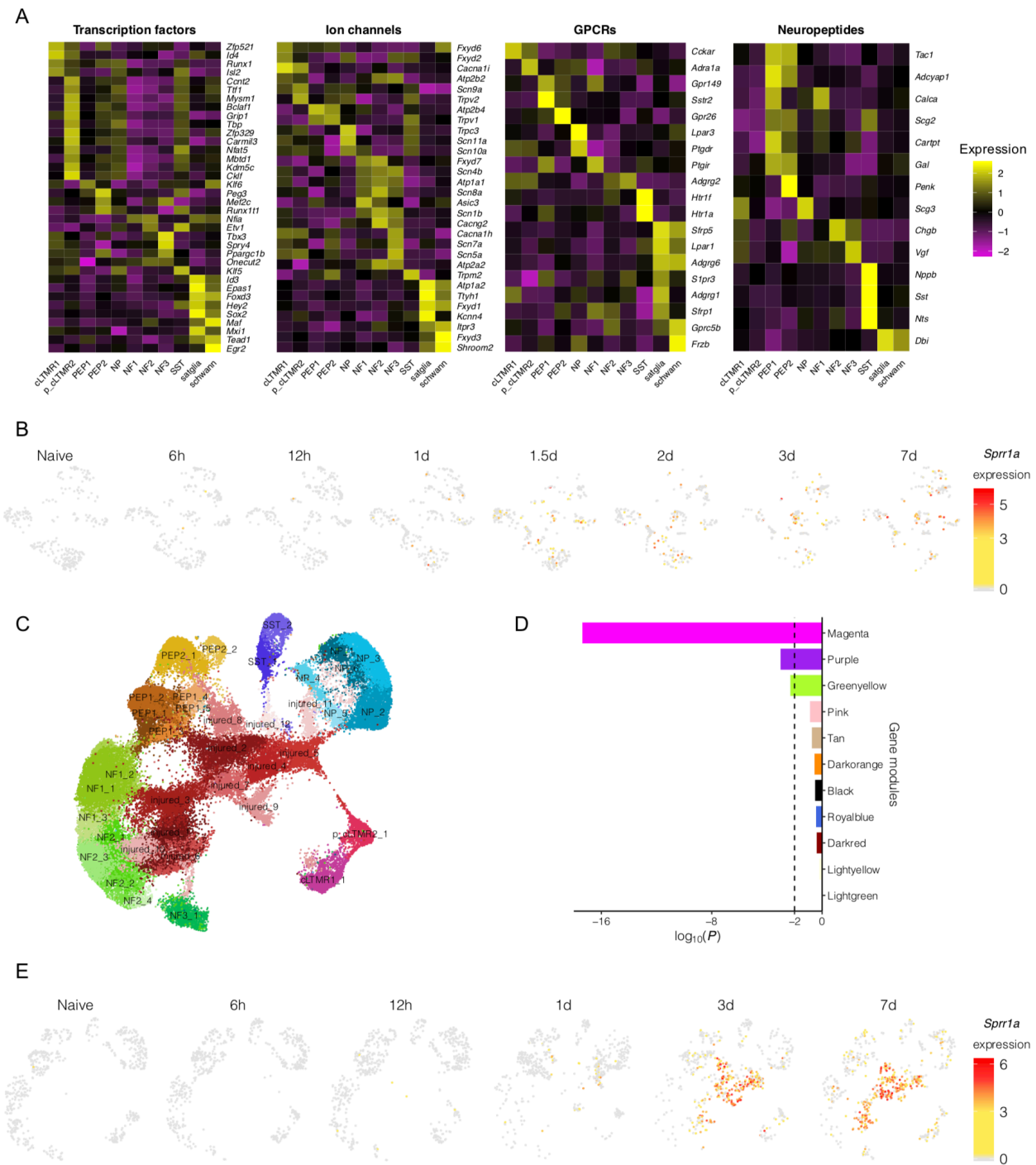
Figure 7



Supplementary Figure 1 -- related to Figure 1

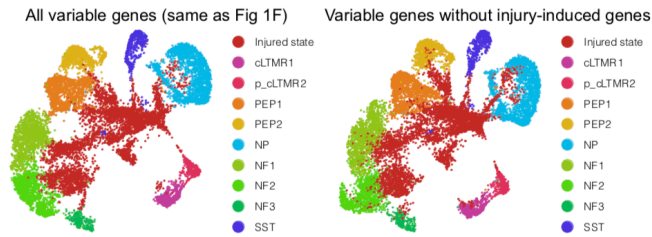


Supplementary Figure 2 -- related to Figure 1

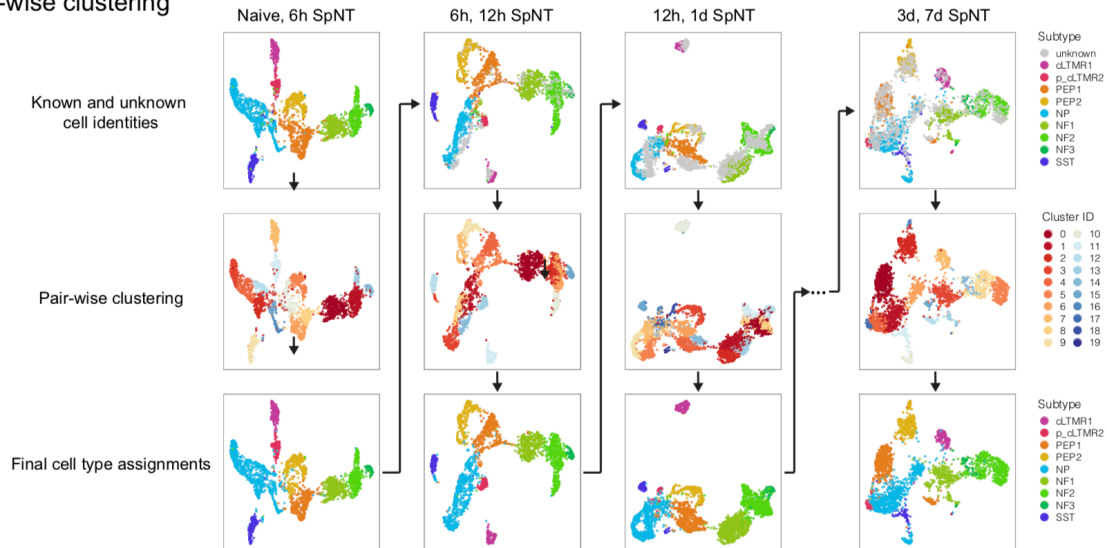


Supplementary Figure 3 -- related to Figure 3

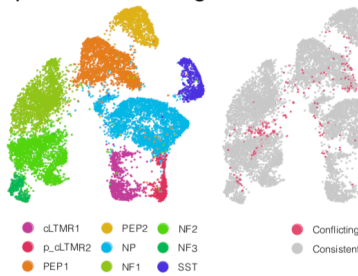
A Removal of injury-induced genes prior to clustering



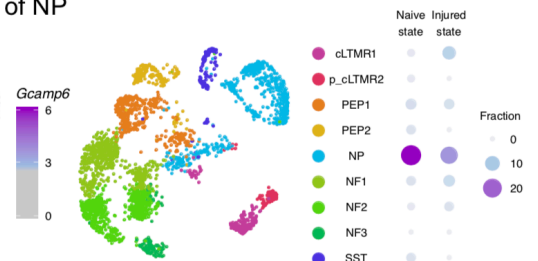
B Pair-wise clustering



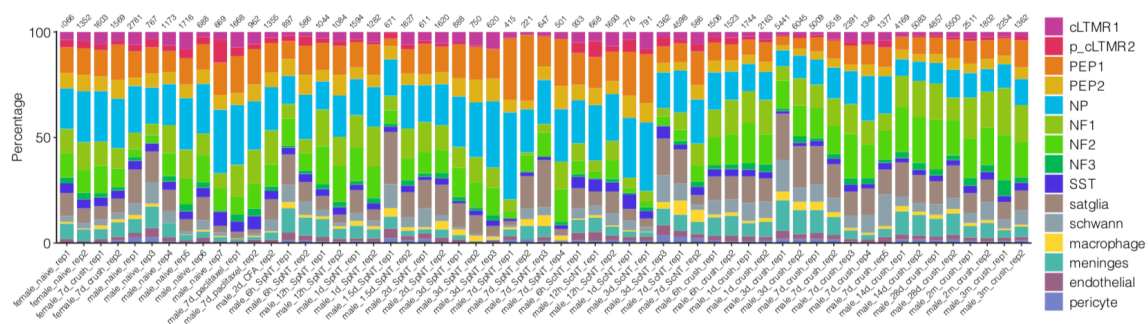
C Regress out injury-induced genes prior to clustering



D Lineage tracing of NP

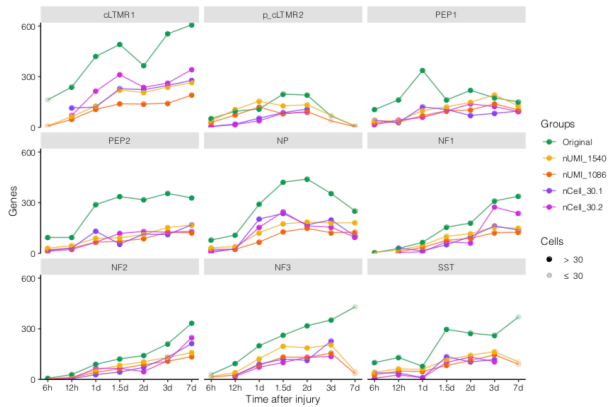


E

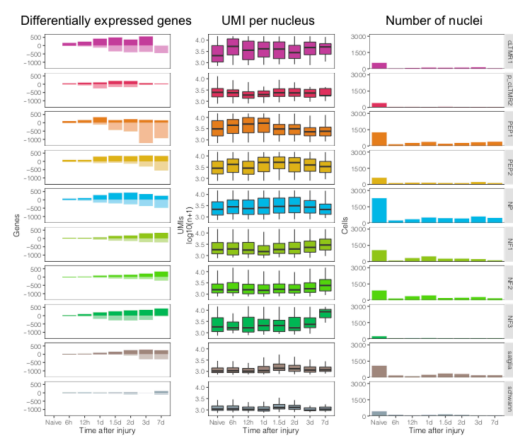


Supplementary Figure 4 -- related to Figure 4

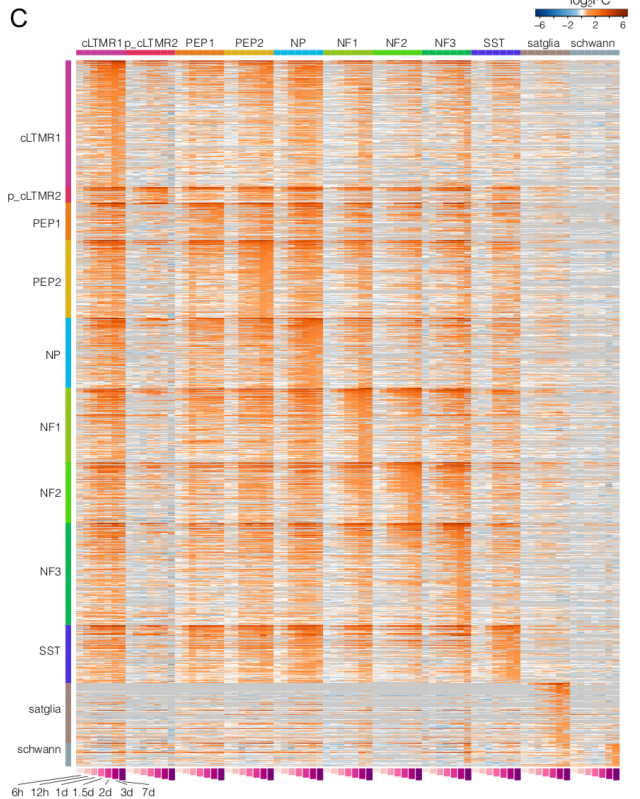
A



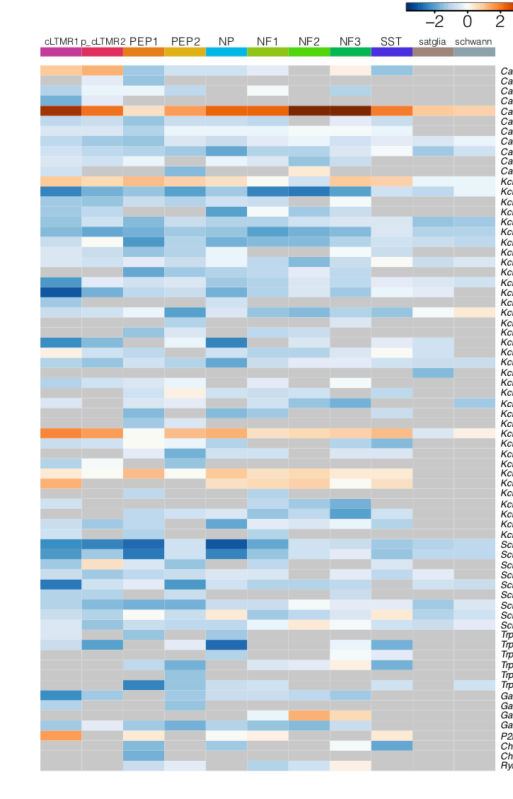
B



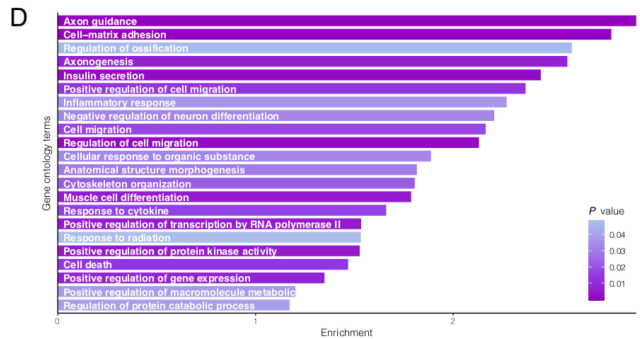
C



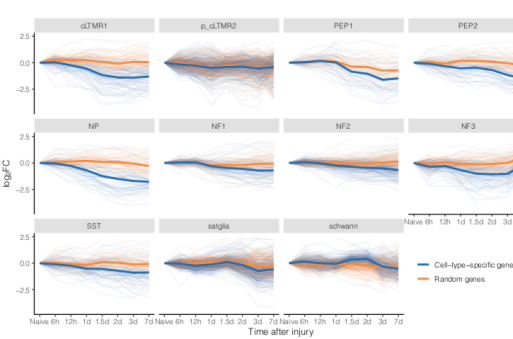
E



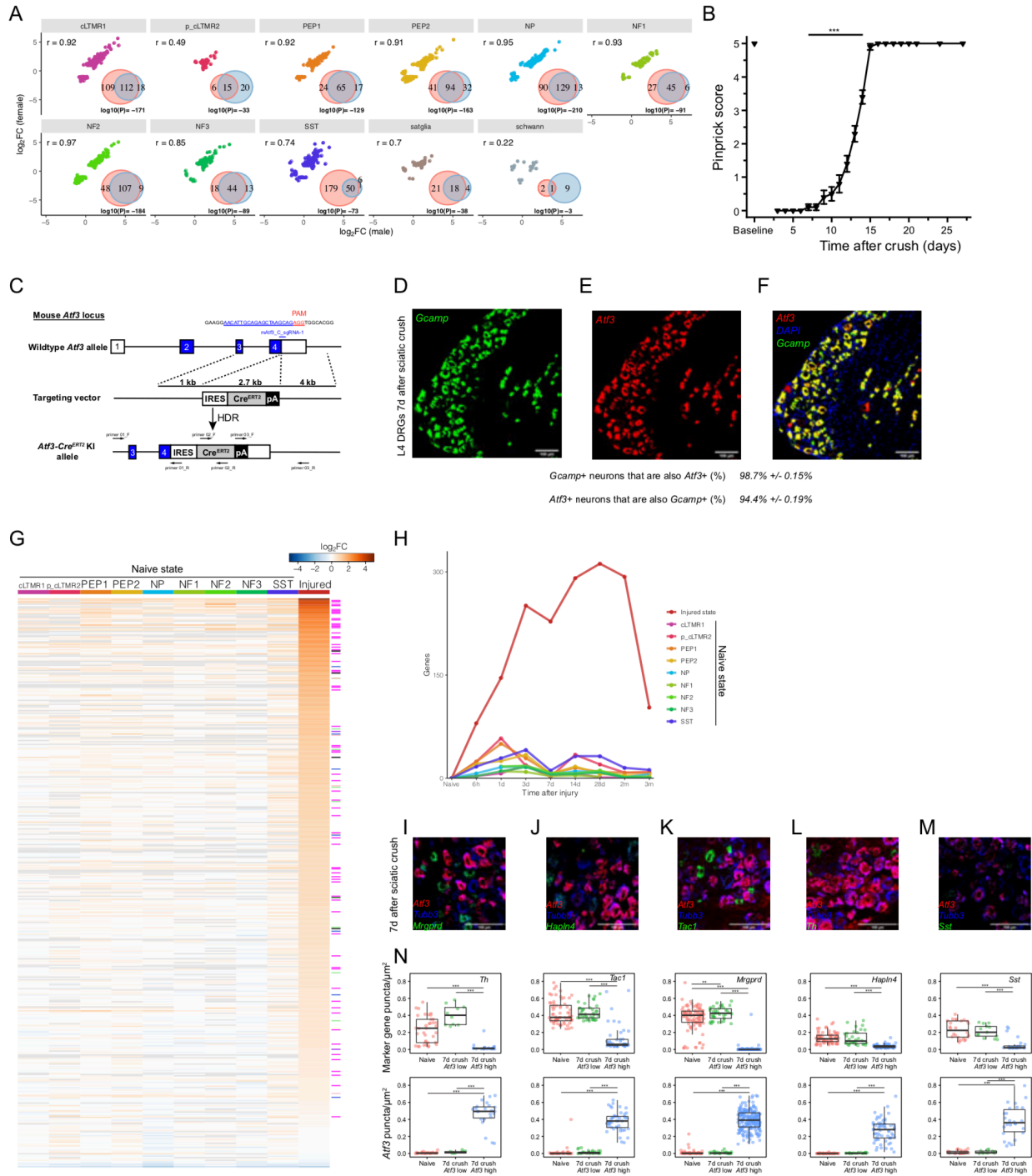
D



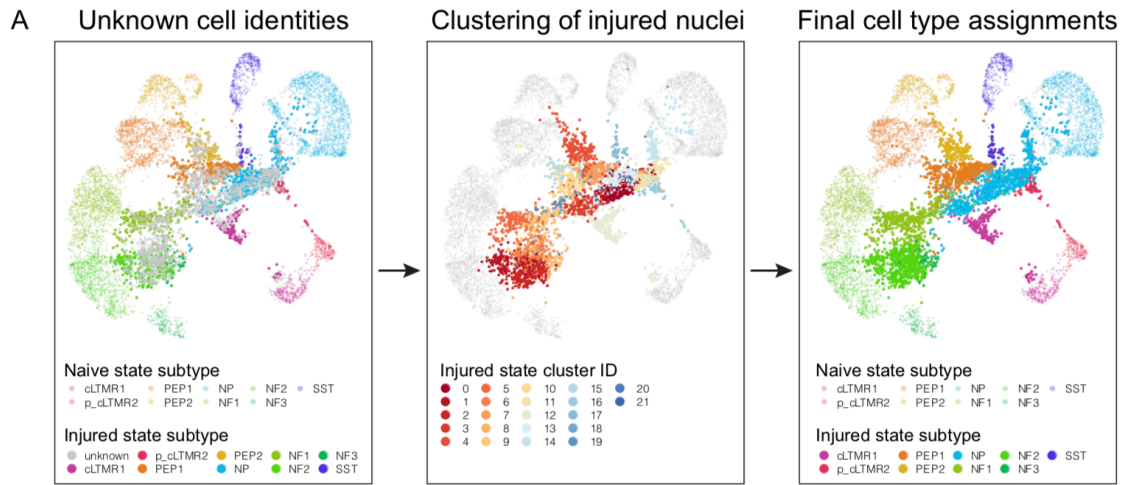
F



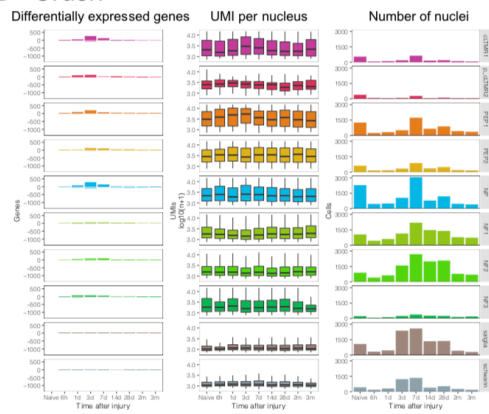
Supplementary Figure 5 -- related to Figure 5



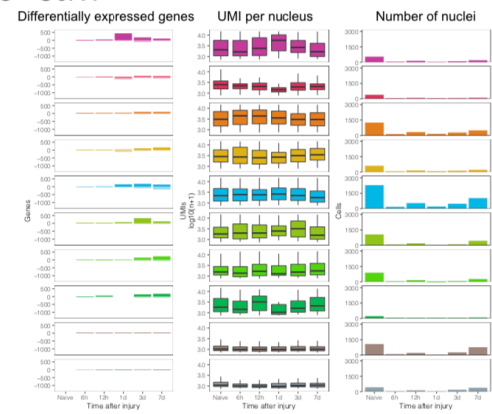
Supplementary Figure 6 -- related to Figure 5



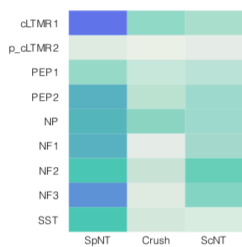
B Crush



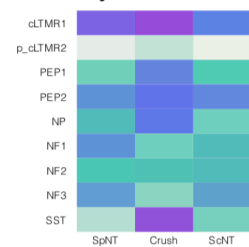
C ScNT



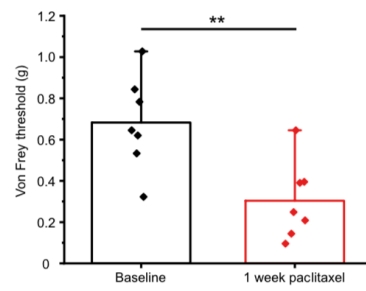
D All nuclei



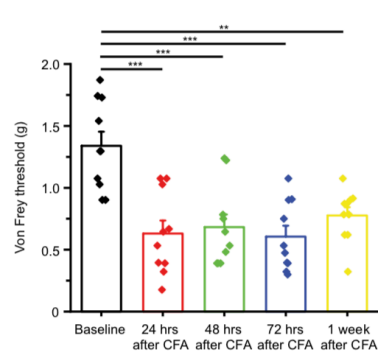
Injured nuclei



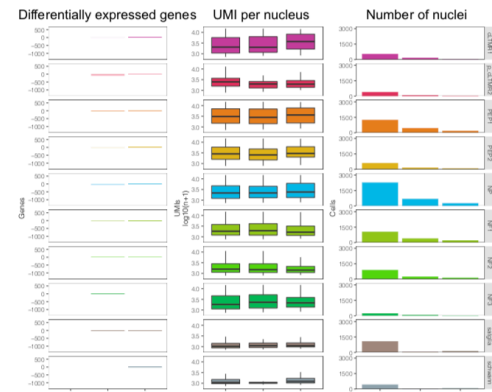
E



F



G Paclitaxel/CFA



Supplementary Figure 7 -- related to Figures 6 and 7

A *Atf3* mRNA and its target genes

